NASA Technical Memorandum 81365

ANALYTIC STUDY OF ORBITER LANDING PROFILES

Harold J. Walker

September 1981

NASA

NASA Technical Memorandum 81365

ANALYTIC STUDY OF ORBITER LANDING PROFILES

Harold J. Walker
Dryden Flight Research Center
Edwards, California

National Aeronautics and
Space Administration

1981

ANALYTIC STUDY OF ORBITER LANDING PROFILES

Harold J. Walker
Dryden Flight Research Vehicle

INTRODUCTION

The shuttle orbiter is the first aerodynamic vehicle designed to be routinely landed without power. Many other nonoperational vehicles, such as the early rocket research aircraft and the lifting bodies, have been landed without power numerous times, but generally these landings were made under good, if not ideal, conditions. The shuttle must routinely make unpowered landings under even the worst conditions. Thus a more thorough understanding of its landing capabilities is highly desirable.

The present analysis has two principal goals: (1) the determination of the trajectory limits where vehicle maneuverability or the piloting task may be marginal, and (2) the estimation of limits where power-off landings of a low L/D vehicle could be made in a more or less routine manner. Since analytical methods are employed, the results should be interpreted as trends rather than accurate predictions, although a correlation with actual flight experience (that is, approach and landing test flight number 5 with tail cone off) is included as an indicator of the validity of the method.

Trajectories are calculated from an initial steady-state glide approach at various angles to touchdown at 180 knots airspeed for eight combinations of speed brake deployment and two vehicle loadings, namely 56 and 70.6 pounds per square foot (corresponding respectively to total vehicle weights of 150,800 and 190,000 pounds). The speed brake configurations are identified in terms of three phases of the landing maneuver (fig. 1): the flare (phase I), gear deployment (phase II), and final glide to touchdown (phase III). Any combination of fixed speed brake deflections is allowed for these three phases. Each configuration is designated by three speed brake angles in sequence; each speed brake angle represents an <u>average</u> value for that landing phase. Aerodynamic data were obtained for four speed brake angles, namely 0°, 25°, 55°, and 87°. The analysis covers the following eight combinations of these angles.

Speed brake angle, deg, during -		
Flare	Gear deployment	Final glide
0	0	0
0	25	55
25	25	25
25	0	0
55	55	55
55	25	0
87	87	87
87	55	25

These combinations are referred to in the rest of this report as 0°-0°-0°, and so forth. The gear deployment interval is assumed to be the 7 seconds immediately after flare, and the vehicle center of gravity is held fixed at 66.25 percent of the body length. A fixed glide slope of -1° from the end of flare to touchdown is assumed. The average speed brake angles for phases II and III are, of course, only rough approximations of what might be obtained in flight.

METHOD OF ANALYSIS

Flare

The principal terms involved in the flare and glide analyses are given in figure 2 for wings-level unpowered flight. The symbols used are defined in appendix A. In general, the balance of forces in unsteady curvilinear flight (such as the flare) is given by:

$$\frac{W}{g}\dot{V} = -D - W \sin \gamma \tag{1}$$

in the tangential direction, and

$$\frac{W}{g}V\dot{\gamma} = L - W \cos \gamma \tag{2}$$

in the direction normal to the flightpath.

These expressions are nonlinear in the time relationships for velocity and flightpath angle. However, an approximate solution may be obtained by eliminating the time element as follows:

$$dt = \frac{W\,dV}{g(-D - W\sin\gamma)} = \frac{W\,V d\gamma}{g(L - W\cos\gamma)} \tag{3}$$

from which

$$\frac{dV}{V} = -\frac{\frac{n}{L/D} + \sin\gamma}{n - \cos\gamma}\,d\gamma \tag{4}$$

where $n = L/W$ and $D/W = \frac{n}{L/D}$.

This relationship is linear and solvable only if the terms n and $\frac{n}{L/D}$ are assumed to be constant. In reality only one term can be held constant, however, and in the present analysis the flare is assumed to be made at constant load factor such that n is fixed. It is then necessary to use an average value for L/D, which is found by a rapidly convergent iteration method using a desk calculator. If L/D were held constant, as in a flare at constant angle of attack, then an average value for n must be found. Under the assumption of constant load factor, the velocity becomes a function of flightpath angle as follows:

$$V = V_0 \frac{n - \cos\gamma_0}{n - \cos\gamma} e^{a(\lambda - \lambda_0)} \tag{5}$$

where

$$a = \frac{2n}{(L/D)_{av}\sqrt{n^2 - 1}}$$

$$\lambda = \tan^{-1}\sqrt{\frac{n+1}{n-1}}\tan\frac{\gamma}{2}$$

Once velocity has been determined by this approximation, the other flare properties of interest may be obtained from the following expressions:

$$dt = \frac{V}{g}\,\frac{d\gamma}{n - \cos\gamma} \tag{6}$$

$$dh = -\frac{V^2}{g}\,\frac{\sin\gamma}{n - \cos\gamma}\,d\gamma \tag{7}$$

$$ds = \frac{V^2}{g}\,\frac{\cos\gamma}{n - \cos\gamma}\,d\gamma \tag{8}$$

The solutions to these equations are given in appendix B. The term $(L/D)_{av}$, it is noted, must first be obtained by iterating the velocity equation in conjunction with the lift-drag polars for the configuration of interest. Integration of the above equations is then straightforward.

Flare Approach

The flare is assumed to be preceded by a steady-state glide (that is, $\dot{V} = \dot{\gamma} = 0$), as shown in figure 2. It follows then (for a given slope) that:

$$\tan \gamma_0 = - \frac{1}{(L/D)_0} \tag{9}$$

$$n_0 = \cos \gamma_0 \tag{10}$$

$$V_0 = \sqrt{\frac{2}{\rho} \frac{n_0 \, (W/S)}{C_{L_0}}} \tag{11}$$

where corresponding values of C_{L_0} and $(L/D)_0$ are obtained from the aerodynamic polars.

Postflare Glide

After the flare the vehicle is held to a constant glide slope (-1°) until touchdown. The gear is deployed during the first 7 seconds of this period of decelerating flight. Touchdown is assumed to occur at an airspeed of 180 knots. During this phase $\dot{\gamma} = 0$ and

$$\dot{V} = -g\left[\frac{n}{(L/D)_{av}} + \sin \gamma_F\right] \tag{12}$$

where $n \sim 1$ and $\gamma_L = -1°$. During gear deployment, $(L/D)_{av}$ is assumed to be the average of the gear-retracted and gear-down values at the average lift coefficient during the 7 second period.

If C_{L_1} and C_{L_2} correspond to velocities V_1 and V_2 in figure 1,

then:

$$C_{L_{av}} = \frac{1}{2}\left(C_{L_1} + C_{L_2}\right) = \frac{C_{L_1}}{2}\left(1 + \frac{V_1^2}{V_2^2}\right) \tag{13}$$

Letting $V_2 = V_1 + \Delta V_g$, and neglecting ΔV_g^2

$$\left(\frac{V_2}{V_1}\right)^2 \sim 1 + \frac{2\Delta V_g}{V_1} \tag{14}$$

and

$$C_{L_{av}} = C_{L_1} \frac{V_1 + \Delta V_g}{V_1 + 2\Delta V_g} \tag{15}$$

Noting (as an approximation) that

$$\Delta V_g \sim -g\left[\frac{1}{(L/D)_1} - 0.01745\right]\Delta t_g \tag{16}$$

then

$$C_{L_{av}} = C_{L_1} \frac{V_1 - g\Delta t_g\left[\frac{1}{(L/D)_1} - 0.01745\right]}{V_1 - 2g\Delta t_g\left[\frac{1}{(L/D)_1} - 0.01745\right]} \tag{17}$$

where $\Delta t_g = 7$ seconds.

It follows that

$$\Delta S_g \sim V_{av}\,\Delta t_g = V_1\left(1 + \frac{1}{2}\frac{\Delta V_g}{V_1}\right)\Delta t_g \tag{18}$$

$$\Delta h_g = \Delta S_g \tan(-1°) \tag{19}$$

Between the gear down and touchdown points, $\Delta V_L = V_{TD} - V_2$ such that:

$$\Delta t_L = \frac{-\Delta V_F}{g\left[\frac{1}{(L/D)_{av}} - 0.01745\right]} \tag{20}$$

and

$$\Delta S_L = V_{av}\,\Delta t_F \tag{21}$$

$$\Delta h_L = -0.01745\,\Delta S_F$$

In these expressions, $(L/D)_{av}$ is obtained from the average lift coefficient in the final glide phase. The above approximations are consistent with those made in the flare analysis.

AERODYNAMIC DATA

The lift and drag characteristics for the shuttle in trimmed flight with the center of gravity fixed at 66.25 percent of the body length were obtained from the Rockwell International Space Division Aerodynamic Design Data Book (Volume I) for the orbiter vehicle. Curves of L/D versus C_L for speed brake positions of 0°, 25°, 55°, and 87°, gear retracted and deployed, are shown in figure 3 for Mach numbers of 0.25 and 0.60. The lower body flap was fixed at zero deflection. The variation of Mach number was assumed to be linear between 0.25 and 0.60.

METHOD VERIFICATION

The landing profile for orbiter approach and landing test flight number 5 (with tail cone off) was chosen for assessing the accuracy of the foregoing method. The conditions for comparing the actual and calculated profiles, however, were less than ideal due to differences in speed brake deflection and gear deployment that were not accommodated in the analytical approach. Figure 4 shows a comparison of the two profiles and includes details of configuration differences. For convenience, the origin is located at the end of the flare. Two factors the profiles have in common during the flare are initial steady-state glide slope

(-25.1°) and normal acceleration (1.32g's). The flare entry speeds differ slightly due to the noted difference in speed brake deflection. Differences are also noted in the times of gear deployment and the speed brake angles during the first half of the flare. These discrepancies, however, are relatively minor, and the two flare profiles are in fairly good agreement.

Between flare termination and touchdown the profiles differ noticeably. The cause of this disagreement is generally consistent with the differences noted in landing gear and speed brake deployment, touchdown velocities, and glide slopes, which could not be adjusted in the computerized analysis. Since the methods used for this portion of the profile are quite simple, the disagreement is not particularly significant.

Figure 5 shows a comparison of the flare profile from orbiter flight number 5 with two calculated profiles, one by the previously described method (integrated solution) and the other by step integration in 2° increments. The overall agreement is considered to be adequate for purposes of this study. As a matter of interest, figure 6 illustrates the (calculated) flare profile differences that would occur if flight number 5 were conducted at a typically higher landing weight (190,000 lbs).

CRITICAL LANDING PROFILES

Two aspects of the piloting task during landings are considered to be critical: (1) the time available for final adjustment of the flightpath for landing after completion of the flare and gear deployment, and (2) the pilot's judgment of the proper conditions for initiating the flare for a potential wide range of unpowered approach trajectories. With these limitations in mind, a set of landing profile boundaries will be sought beyond which the piloting task is likely to be precarious. These boundaries will be refined further by considerations of possible backside L/D conditions and the total landing time available to the pilot. The boundaries will in turn be of assistance in determining the optimal paths for the aircraft in various configurations.

Landing Maneuver Time

The available time in phase III between gear deployment (phase II) and touchdown was obtained for a series of combinations of approach angle (γ_0) and flare load factor (n) for each of the eight configurations mentioned earlier at the two vehicle loadings of 56.0 psf and 70.6 psf. The results are presented in figures 7 and 8, respectively, in which available time (Δt_F) is

shown in terms of preflare glide slope (γ_0). A maximum usable load factor of 2.0 is assumed. Particularly noteworthy in these figures is the rapid reduction in available time as the limiting glide slope angles are approached, especially for the clean configurations. Thus, little margin of error is allowed in establishing a proper set of preflare conditions.

Two bounds of available time are indicated in figures 7 and 8: (1) a lower bound of 5 seconds, representing a minimal requirement for safe landings, and (2) a more realistic interval of 10 seconds, which is believed to be more typical of prior low-L/D landing experience. The intercepts of these bounds with the lines of constant load factor for the eight speed brake configurations are presented in figures 9 and 10, respectively, for the 5- and 10-second intervals. The form of the boundaries defined by these intercepts is hyperbolic, and the hyperbola becomes more acute as speed brake angle decreases. As the lower limits of γ_0 are approached the load factor requirement rises sharply. At the lower limits of load factor, the required preflare glide slope increases abruptly. Obviously, the flare maneuver must be performed above and to the right of these boundaries to accomplish a landing within the two time constraints and at 180 knots.

Several configurations with high speed brake angles are missing from the figures. In these cases it was impossible to reach the 5- or 10-second bounds. One of those ruled out is 87°-87°-87° for the 10-second limit for both vehicle loadings and for the 5-second limit at a loading of 56.0 pounds per square foot. Also ruled out are both 55°-55°-55° and 87°-55°-25° for the 10-second limit at 56.0 pounds per square foot.

Additional Landing Constraints

The regions within the boundaries in figures 8 and 9 still allow extremely wide ranges of glide slope and load factor to perform landings with increasing maneuver times in phase III; hence, additional constraints are needed. Other constraints that should be examined as noted earlier are (1) the altitude range within which the pilot can accurately judge the point of flare initiation, (2) the avoidance of flight on the back side of the L/D curves, and (3) the overall time available for performing the entire landing maneuver from flare initiation to touchdown. Possible restrictions in these areas are considered next.

Altitude and L/D constraints. - The altitude change from flare initiation to touchdown (Δh_T) is shown in terms of preflare glide angle in figures 11 and 12 for aircraft loadings of 56.0 psf and 70.6 psf. These figures show variations for the 5- and 10-second

time constraints and the full range of load factors for the eight selected configurations. Pilot judgment of the altitude for flare initiation was considered to be practical in the range from about 800 feet for high load factors to about 3000 feet for low load factors. These altitude constraints were then used to define a more restrictive set of limits for the vertical and lateral arms of the boundaries shown in figures 9 and 10. The new set was further checked for avoidance of backside L/D flight by reference to the average L/D levels, reached in the flare, as summarized in figures 13 and 14, which show $(L/D)_{av}$ versus γ_0 for the full range of load factors and configurations and the two vehicle loadings. In these figures load factor points on the right side of the peak levels correspond to normal aircraft response on the front side of the L/D curves. Backside operation was found for only a limited number of cases, principally at high load factors for the heavier vehicle loading. In general, these cases lay outside the two altitude constraints, and little correction was necessary. The resultant effect of these constraints on the earlier bounds for load factor and initial glide angle is shown in figures 15 and 16 for the vehicle loadings of 56.0 and 70.6 psf, respectively. The new set of constraints is seen to form corridors through the original boundaries which confine substantially the range of conditions in which power off landings should be carried out. The 5-second boundaries would, of course, be considered marginal for routine operations.

A comparison of the 5- and 10-second boundaries for several paired configurations is given in figure 17 for the two vehicle loadings. The corridors for the two time periods are similar in form and size, but those for the 10-second period are slightly higher on the load factor scale.

Total time constraint. - Figures 18 and 19 show the total time to complete the landing maneuver from flare initiation to touchdown as a function of γ_0 for the two vehicle loadings. Based on piloting experience with the X-15 and lifting bodies, a period of 20 to 30 seconds between flare initiation and touchdown is required to perform a satisfactory landing maneuver. For this study a midpoint value of 25 seconds is used. This requirement, based on the results from figures 18 and 19, introduces an additional upper constraint on the n, γ_0 boundaries, as shown in figures 20 and 21 (shaded dashed lines) for the two vehicle loadings. The effect of this requirement is seen to be most pronounced on the 5-second time constraint for both vehicle loadings. The 800-foot altitude constraint is overriding at the lower glide angles for the 10-second constraint at the higher vehicle loading.

A summary of these various constraints on the n, γ_0 boundaries is presented in figures 22(a) and 22(b) for the 56.0 and 70.6 psf loadings and the various configurations that fall within the 5- and 10-second landing constraints. The corridors for regular landing operations are seen to be substantially reduced as compared with the original set defined only by the 5- and 10-second landing intervals. Those for the 10-second interval, although shown open ended on the right side, are likely to be limited, even under emergency conditions, by entry glide slopes more than about -45°.

Other Landing Characteristics

Ground distance. - The horizontal (ground) distance traversed in the landing maneuver from the aim point (fig. 1) to touchdown is usually not a constraining factor. A summary of this characteristic for all of the combinations of configuration, load factor and time constraint, is given in figures 23 and 24, respectively, for the two basic vehicle loadings. These distances are roughly the same for both vehicle loadings and range from 6200 to 16000 feet for the 5-second touchdown time and from 8000 to 13,000 feet for the 10-second time, within the corriders shown in figure 22. The variations of horizontal distance, however, may be more clearly observed in the bar diagrams in figures 25(a) and 25(b), respectively, for the two vehicle loadings. It is generally observed that cleaner configurations give shorter landing distances at the same flare load factors, and that increased speed brake angles in phases II and III result in increased landing distance at the same load factor. Also noted in figures 25(a) and 25(b) are the near constant glide distance (s_1) in phases II and III, and the height at the end of the flare ($h_1 = S_1 \tan 1°$), for each set of vehicle loading and landing time constraints. These characteristics are seen to be approximately constant for each set, that is, independent of configuration and load factor. Comparison of the notation in both figures shows that they are also essentially independent of vehicle loading. The reasons for near constant distance in the final glide will become more apparent after first reviewing the velocity changes along the landing trajectory.

Velocity variations. - Aircraft velocities at various points along the 5- and 10-second landing profiles (fig. 1) are summarized in figures 26 and 27, respectively, for the two vehicle loadings and all configurations. For each configuration in phase I, the initial steady velocity (V_0) varies identically with γ_0 and, as would be expected, diminishes with increasing speed brake angle

or reduced vehicle weight at the same glide slope (γ_0). The load factors corresponding to each value of γ_0 are indicated by the vertical lines between V_0 and V_1 (velocity at the end of the flare). It is noted that the variation of V_1 for each landing time interval is quite small (230 to 240 knots for 5 seconds and 250 to 270 knots for 10 seconds) and is more or less independent of vehicle loading. Similarly, the velocities at the completion of gear deployment (V_2) fall within a small range for each loading. These results are attributable mainly to the fixed constraint on touchdown velocity. On the other hand, the velocity change in the flare decreases gradually with increasing load factor in a similar manner for both loadings.

With reference to the near constant distance along the final glide slope from flare to touchdown (preceding paragraph), it can be shown as an approximation that:

$$S_1 \sim \frac{1}{2g} (L/D)_{av} \left(V_1^2 - V_{TD}^2 \right) \tag{22}$$

For nearly all cases, the ranges of V_1 and $(L/D)_{av}$ during phases II and III have been small for the two landing time intervals at both vehicle weights. Also, the levels of $(L/D)_{av}$ are on the low side when V_1 is on the high side and vice versa. The result is that S_1 (hence h_1) is near constant for all configurations and flare load factors for each vehicle loading.

COMPARATIVE LANDING TRAJECTORIES

The previous section dealt largely with defining the boundaries for more or less marginal and normal landing maneuvers, but gave little, if any, impression of how the many possible trajectories would compare in a more graphic form. In the following sections representative sets of trajectories will be considered to illustrate particular effects, such as touchdown time (phase III), vehicle loading, extreme points on the corridors, speed brake settings, and so forth. In order to magnify differences in altitude, the vertical scale of the trajectories has been stretched by a factor of 5 over the horizontal scale, and the trajectories will therefore appear in a distorted form.

Orbiter Flight Number 5

Figure 28(a) shows two points on the lower corridor boundaries for the 5- and 10-second touchdown times at 56 psf loading, which were thought to be most appropriate for the comparison of computed trajectories with the trajectory of flight number 5. The two points are located approximately on the centerlines between the upper and lower boundaries of the two corridors. Figure 28(b) shows the trajectory comparison. Although the actual trajectory more nearly resembles that for the 5-second touchdown boundary, the flare entry speed, glide slope, and normal acceleration in flight number 5 are closer to those of the 10-second boundary. Actually, the flare entry point of flight number 5 in figure 28(a) is more conservative than the two selected points and thus is reflected as a steeper landing approach in figure 28(b). Other previously mentioned differences in gear deployment and touchdown glide slope also contribute to the disparities between the actual and calculated profiles. The total times, however, are nearly the same.

Effect of Landing Weight

To illustrate the effect of vehicle loading, centerline points for the clean configuration on the 5- and 10-second boundaries were chosen, as shown in figures 29(a) and 29(b), for loadings of 56.0 and 70.6 psf. As shown by figure 29(c), the heavier landing weight obviously exhibits a flatter landing maneuver with shallower glide slopes, although the entry velocities are about the same for the two landing time intervals. The order of the differences between the two loadings is generally consistent, but it is interesting to observe that the total landing maneuver times are roughly the same.

Boundary Extremities

Comparisons of the landing profiles at the bottom centerlines of the corridors with those at extreme points on the boundaries are compared in figures 30 and 31 for the two vehicle loadings. Part (a) in each figure shows the selected points for the 5- and 10-second touchdown intervals, and part (b) shows the trajectory comparisons. The extremes were chosen only for configurations for which aerodynamic data were available (without interpolation). Details of entry conditions and the total maneuver times under each configuration notation are included with the trajectories. The flattest profiles represent the lower extremes, and the steepest profiles the upper extremes. The corridor centerline profiles are intermediate. The lower and intermediate profiles have zero speed brake deflections in both cases. In general, the profiles for the three sets (centerline and two extremes) do not differ substantially for the two loadings.

Entry speeds are correspondingly similar. However, entry slopes and flare load factors vary considerably, although consistently, between corresponding sets. The midcorridor profiles, although appearing to be closer to those for the lower bounds, are initiated at much lower altitudes. Those for the upper bounds require much steeper entry slopes and higher flare load factors.

Speed Brake Effects

The speed brakes, of course, provide a wide range of trajectories for reaching a given touchdown point and speed. Figures 32 to 35 illustrate the range available for the two vehicle loadings and landing time intervals (56 psf in figs. 32 and 33, for t_F = 5 and 10 seconds, respectively, and 70.6 psf in figs. 34 and 35, for t_F = 5 and 10 seconds, respectively). An overview of the four figures (where corridor points are shown in part (a) in each case) shows an overall flare entry angle range from around -20° to over -40° as well as a general similarity and consistency of trajectory variations with speed brake settings. Flare entry angle and speed and flare normal acceleration naturally increase with speed brake opening, whereas the overall touchdown maneuver time slowly decreases. For each of the two loadings, the higher landing time interval (t_L) at each speed brake configuration also requires increased flare entry angle and speed, as well as a higher flare load factor (by comparing figs. 32(b), 33(b), and 34(b), 35(b)). Although the differences in total landing time for the same configuration do not show a consistent pattern for the two loadings, they are generally small.

The effect of increased vehicle loading at the same touchdown maneuver time for each configuration (figs. 32(b), 34(b), and 33(b), 35(b), respectively) is to diminish both the flare entry angle and flare load factor. However, it has little effect on entry speed. Total landing time (t_T) tends to be higher for the heavier loading.

Fixed Configuration Limits

The point selections for the 0°-0°-0° configuration and two touchdown maneuver times are shown in figures 36(a) and 37(a), and the trajectories at the boundary limits are shown in figures 36(b) and 37(b) for vehicle loadings of 56.0 and 70.6 psf, respectively. The trajectories for the lower limits are considerably longer than those for the upper limits and require steeper flare entry angles and higher approach speeds. The flare entry altitudes due to small errors in the boundary fairings are near - but not exactly on - the 800 foot and 3000 foot limits used to estab-

lish the boundaries. Thus, in general, a wide range of trajectories is available for the landing maneuver with a fixed speed brake setting.

SUMMARY OF RESULTS

1. A relatively simple integrated solution to the equations of motion for the landing maneuver was derived which provides a fairly accurate prediction of landing trajectory characteristics of low L/D aircraft.

2. The method was applied to the orbiter both to establish a set of flare entry boundaries for marginal and normal landing capability and to illustrate typical landing profiles at points of interest relative along the boundaries.

3. The method gave a good representation of the flare maneuver of orbiter flight number 5 for the same entry glide angle and normal load factor.

4. Predicted flare entry angles for satisfactory landings (time from gear down to touchdown, t_L, equals 10 seconds)

ranged from -20° for a landing weight of 150,800 pounds and -16° for a weight of 190,000 pounds to over -40°, in each case depending upon the sequence of speed brake settings. The minimum load factor to complete the maneuver was found to be about 1.25g's for a landing weight of 150,800 pounds and 1.15g's for 190,000 pounds.

5. A landing could not be safely made with the speed brakes fully opened at the lower landing weight (t_L > 5 seconds).

6. For a given flare load factor, the minimum distance from the glide aim point to touchdown is obtained with the cleanest configuration due to the low approach speeds required to complete landing.

7. The height above (h_1) and distance from the end of the

flare to touchdown (s_1) is dependent only upon the time requirement

from gear deployment to touchdown; that is, it is essentially independent of flare entry conditions, load factor, speed brake angle, and vehicle weight.

8. The orbiter speeds at the end of the flare and gear deployment also are dependent only on the required time interval from gear down to touchdown.

9. Higher landing weights in general result in flatter flare trajectories with longer distances from the aim point to touchdown, and slightly reduced load factors, but little change in flare entry speed.

10. Extreme points on the landing boundaries provide a wide range of trajectories for successful landings, depending principally on the speed brake settings. Also, speed brake variations along the centerlines of the landing corridors allow the variation of approach angles from about -22° to -36° for the 150,800 pound landing weight, and -18° to -40° for the 190,000 pound weight (t_L > 10 seconds).

11. For fixed speed brake angles, substantial variations of the landing profile are also obtained with relatively small changes (4° to 6°) in approach angle.

CONCLUDING REMARKS

It has been the intent of this report to conduct a broad survey of possible orbiter landing configurations and entry conditions with specific goals of defining boundaries (or corridors) within which the landing task would be marginal on one hand and somewhat routine on the other. The results of the survey suggest that the centerline of the routine corridors represent more or less optimal preflare entry conditions for regular operations, depending upon space position at the start of the flare and the required speed brake configuration, to arrive at the desired touchdown point and speed. The various constraints used to define the boundaries are based largely on qualitative judgments from earlier flight experience with the X-15 aircraft and lifting bodies, and thus would be subject to possible adjustment as more information is gained from orbiter simulation and flight tests. During the interim, the study results should serve as useful background for expanding and validating ongoing landing simulation programs. The analytic approach offers a particular advantage in identifying trends due to the systematic variations of specific factors, such as vehicle weight, flare load factor, approach speed, aim point, and so forth.

There are, of course, limitations in the method used in this study, such as constant load factor during the flare and fixed gear deployment interval at the termination of the flare. These, can, however, be removed by adding more flexibility (and complexity) to the computer program. It is noteworthy also that the flare maneuver could also have been readily programmed for constant L/D (that is, constant angle of attack) with varying load factor instead of constant load factor. A short iterative computation would then have been required to determine the average

load factor for subsequent calculations of flare time, altitude loss, and ground distance covered.

More configurations may also have been included in the study (time permitting), such as increasing the speed brake deflection during the last two landing phases beyond the case studied (25° and 53°). Also, more comparisons of landing profiles should be made, such as fixed versus varied speed brake configurations and for points within and beyond, as well as on, the corridor boundaries. This attempt at an analytic definition of the landing profiles of the orbiter thus may suggest additional studies for more complete coverage or analysis of particular problems.

Dryden Flight Research Center
National Aeronautics and Space Administration
Edwards, California 93523
August 11, 1981

APPENDIX A - SYMBOLS

a	nondimensional term, $\frac{2n}{(L/D)_{av}\sqrt{n^2 - 1}}$
b	$\sqrt{\frac{n + 1}{n - 1}}$
C_L	lift coefficient, $\frac{W}{gS}$
D	drag
g	gravitational acceleration, 32.2 ft/sec/sec
h	altitude
Δh	change in altitude
K_h	constant term, $\frac{V_0^2}{g}(n - \cos \gamma_0)^2 e^{2a\lambda_0}$ (eq. (34))
K_s	constant term, $\frac{V_0^2}{g}(n - \cos \gamma_0)^2 e^{2a\lambda_0}$ (eq. (39))
K_t	constant term, $\frac{V_0}{g}(n - \cos \gamma_0) e^{a\lambda_0}$ (eq. (28))
L	lift
M	Mach number
n	load factor, $\frac{L}{W}$
q	dynamic pressure, $0.5\rho V^2$
S	orbiter reference area, 2690 ft^2
s	ground distance
Δs	change in ground distance
s_T	ground distance from aim point to touchdown point (fig. 1)
t	time
Δt	increment of time

V	vehicle velocity
$\dot{V}$	vehicle deceleration, $\frac{dV}{dt}$
W	orbiter weight
γ	flightpath slope
$\dot{\gamma}$	rate of change of flightpath slope, $\frac{d\gamma}{dt}$
δ_{BF}	body flap angle (fixed at 0°)
δ_{SB}	speed brake angle
λ	angle defined by $\tan^{-1}\sqrt{\frac{n+1}{n-1}}\tan\frac{\gamma}{2}$
ρ	air density

Subscripts:

av	average
f	flare portion of landing (phase I)
g	gear deployment interval (phase II)
L	final landing interval between gear deployment and touchdown
T	total maneuver from flare initiation to touchdown
TD	touchdown
0	initiation of flare
1	end of flare
2	end of gear deployment

APPENDIX B - INTEGRATION OF FLARE EQUATIONS

The following is a brief outline of the procedures for integrating equations (6), (7), and (8) in the section entitled METHOD OF ANALYSIS. The solutions require the substitution of the expression for velocity variation in the flare (eq. (3)), namely :

$$V = V_0 \frac{n - \cos \gamma_0}{n - \cos \gamma} e^{a(\lambda - \lambda_0)} \tag{23}$$

where

$$a = \frac{2n}{(L/D)_{av} \sqrt{n^2 - 1}}$$

$$\lambda = \tan^{-1} \sqrt{\frac{n + 1}{n - 1}} \tan \frac{\gamma}{2}$$

In the following integrals the upper limit λ_1 for simplicity will be assumed to be zero rather -1° (the final glide slope).

Flare Time

From equations (5) and (6) it is apparent that

$$\Delta t_f = \frac{V_0}{g}(n - \cos \gamma_0) e^{a\lambda_0} \int_{\gamma_0}^{\gamma_1} \frac{e^{-a\lambda} \, d\gamma}{(n - \cos \gamma)^2} \tag{24}$$

Solution of equation (24) requires the substitution of λ for γ, noting that

$$\gamma = 2 \tan^{-1} \frac{1}{b} \tan \lambda \tag{25}$$

$$d\gamma = 2b \frac{1 + \tan^2 \lambda}{b^2 + \tan^2 \lambda} d\lambda \tag{26}$$

where $b = \sqrt{\frac{n+1}{n-1}}$. Also

$$n - \cos \gamma = n - \frac{1 - \tan^2(\tan^{-1} \frac{1}{b} \tan \lambda)}{1 + \tan^2(\tan^{-1} \frac{1}{b} \tan \lambda)}$$

$$= n - \frac{b^2 - \tan^2 \lambda}{b^2 + \tan^2 \lambda} \tag{27}$$

With the above substitutions,

$$\Delta t_f = K_t \frac{2}{b^3 (n-1)^2} \int_{\lambda_0}^{0} \frac{b^2 + \tan^2 \lambda}{1 + \tan^2 \lambda} e^{-a\lambda} d\lambda \tag{28}$$

where $K_t = \frac{V_0}{g} (n - \cos \gamma_0) e^{a\lambda_0}$

This expression can be further simplified by substituting $\tan \lambda = \sin \lambda / \cos \lambda$, leading to

$$\Delta t_f = \frac{2K_t}{b^3 (n-1)^2} \int_{\lambda_0}^{0} (b^2 \cos^2 \lambda + \sin^2 \lambda) e^{-a\lambda} d\lambda \tag{29}$$

where further

$$b^2 \cos^2 \lambda + \sin^2 \lambda = \frac{b^2}{2} (1 + \cos 2\lambda) + \frac{1}{2} (1 - \cos 1\lambda)$$

Further simplification results in

$$\Delta t_f = \frac{2K_t}{(n^2 - 1)^{3/2}} \int_{\lambda_0}^{0} e^{-a\lambda} (n - \cos 2\lambda) d\lambda \tag{30}$$

The solution to this equation is as follows (see "A Short Table of Integrals" by B. O. Peirce and R. M. Foster, Ginn and Company, 1956, eqs. 411 and 431):

$$\Delta t_f = \frac{2V_0}{g} \frac{n - \cos \gamma_0}{(n^2 - 1)^{3/2}} e^{a\lambda_0} \left\{ -e^{-a\lambda} \left[\frac{n}{a} + \frac{1}{a^2 + 4} (a \cos 2\lambda - 2 \sin 2\lambda) \right] \right\}_{\lambda_0}^{0} \tag{31}$$

Substitution of the limits gives

$$\Delta t_f = \frac{2V_0}{g} \frac{n - \cos \gamma_0}{(n^2 - 1)^{3/2}} e^{a\lambda_0} \left\{ -\frac{n}{a} - \frac{a}{a^2 + 4} + e^{-a\lambda_0} \left[\frac{n}{a} + \frac{1}{a^2 + 4} (a \cos 2\lambda_0 - 2 \sin 2\lambda_0) \right] \right\} \tag{32}$$

Flare Altitude Change

The expression for altitude change from equations (5) and (7) becomes

$$\Delta h_f = \frac{V_0^2}{g} (n - \cos \gamma_0)^2 e^{2a\lambda} \int_{\gamma_0}^{\gamma_1} \frac{\sin \delta}{(n - \cos \gamma)^3} e^{-2a\lambda} \, d\gamma \tag{33}$$

Substitution of

$$\sin \gamma = \frac{2 \tan \frac{\gamma}{2}}{1 + \tan^2 \frac{\gamma}{2}} = \frac{2b \tan \lambda}{b^2 + \tan^2 \lambda}$$

in addition to equations (26) and (27) leads to

$$\Delta h_f = \frac{4K_h}{b^4 (n - 1)^3} \int_{\lambda_0}^{0} \frac{\tan \lambda (b^2 + \tan^2 \lambda)}{(1 + \tan^2 \lambda)^2} e^{-2a\lambda} \, d\lambda \tag{34}$$

where

$$K_h = \frac{V_0^2}{g} (n - \cos \gamma_0)^2 e^{2a\lambda}$$

Replacing tan λ by (sin λ)/(cos λ) and simplifying gives

$$\Delta h_f = \frac{K_h}{b^4(n-1)^3} \int_{\lambda_0}^{0} \left[(b^2 + 1) \sin 2\lambda + \frac{1}{2}(b^2 - 1) \sin 4\lambda \right] e^{-2a\lambda} d\lambda \qquad (35)$$

Using the previously mentioned reference handbook for a solution (eq. 430) results in

$$\Delta h_f = - \frac{K_h}{2b^4(n-1)^3} \left\{ e^{-2a\lambda} \left[\frac{b^2 + 1}{a^2 + 1} (a \sin 2\lambda + \cos 2\lambda) + \frac{b^2 - 1}{2(a^2 + 4)} (a \sin 4\lambda + 2 \cos 4\lambda) \right] \right\}_{\lambda_0}^{0} \qquad (36)$$

Substituting for K_h and b and the limits gives

$$\Delta h_f = \frac{V_0^2}{2g} \frac{(n - \cos \gamma_0)^2}{(n^2 - 1)^2} e^{2a\lambda_0} \left\{ - \frac{2n}{a^2 + 1} - \frac{2}{a^2 + 4} + e^{-2a\lambda_0} \left[\frac{2n}{a^2 + 1} (a \sin 2\lambda_0 + \cos 2\lambda_0) + \frac{1}{a^2 + 4} (a \sin 4\lambda_0 + 2 \cos 4\lambda_0) \right] \right\} \qquad (37)$$

Flare Ground Distance

The solution to the expression for ground distance covered in the flare (eq. (8)) begins with

$$\Delta S_f = \frac{V_0^2}{g}(n - \cos \gamma_0)^2 e^{2a\lambda_0} \int_{\gamma_0}^{\gamma_1} \frac{\cos \gamma}{(n - \cos \gamma)^3} e^{-2a\lambda} d\lambda \qquad (38)$$

Following the procedures used in the previous section gives

$$\Delta S_f = \frac{2 K_s}{b^5 (n - 1)^3} \int_{\lambda_0}^{0} \frac{(b^2 - \tan^2 \lambda)(b^2 + \tan^2 \lambda)}{(1 + \tan^2 \lambda)} e^{-2a\lambda} d\lambda \qquad (39)$$

where $K_s = \frac{V_0^2}{g} (n - \cos \gamma_0)^2 e^{2a\lambda_0}$

Introducing $\sin \lambda / \cos \lambda$ for $\tan \lambda$ gives

$$\Delta S_f = \frac{2K_s}{b^5 (n - 1)^5} \int_{\lambda_0}^{0} \left[(n + \tfrac{1}{2}) + (n^2 + 1) \cos 2\lambda \right.$$

$$\left. + \frac{n}{2} \cos 4\lambda \right] e^{-2a\lambda} d\lambda \qquad (40)$$

The final solution (from the reference handbook) with limits substituted becomes

$$\Delta S_f = \frac{V_0^2}{2g} \frac{(n - \cos \gamma_0)^2}{(n^2 - 1)^{5/2}} e^{2a\lambda_0} \left\{ - \frac{2n + 1}{a} - \frac{2a(n^2 + 1)}{a^2 + 1} - \frac{an}{a^2 + 4} \right.$$

$$+ e^{-2a\lambda} \left[\frac{2n + 1}{a} + \frac{2(n^2 + 1)}{a^2 + 1} (a \cos 2\lambda_0 - \sin 2\lambda_0) \right.$$

$$\left. \left. + \frac{n}{a^2 + 4} (a \cos 4\lambda_0 - 2 \sin 4\lambda_0) \right] \right\} \qquad (41)$$

The above expressions for Δt_f, Δh_f, and ΔS_f (eqs. (32), (37), and (41)) are troublesome for straight hand computations, and were therefore programmed on a desk calculator. It should be noted that the upper limit of the integrals can be retained in generalized form to allow the calculation of flare trajectory profiles.

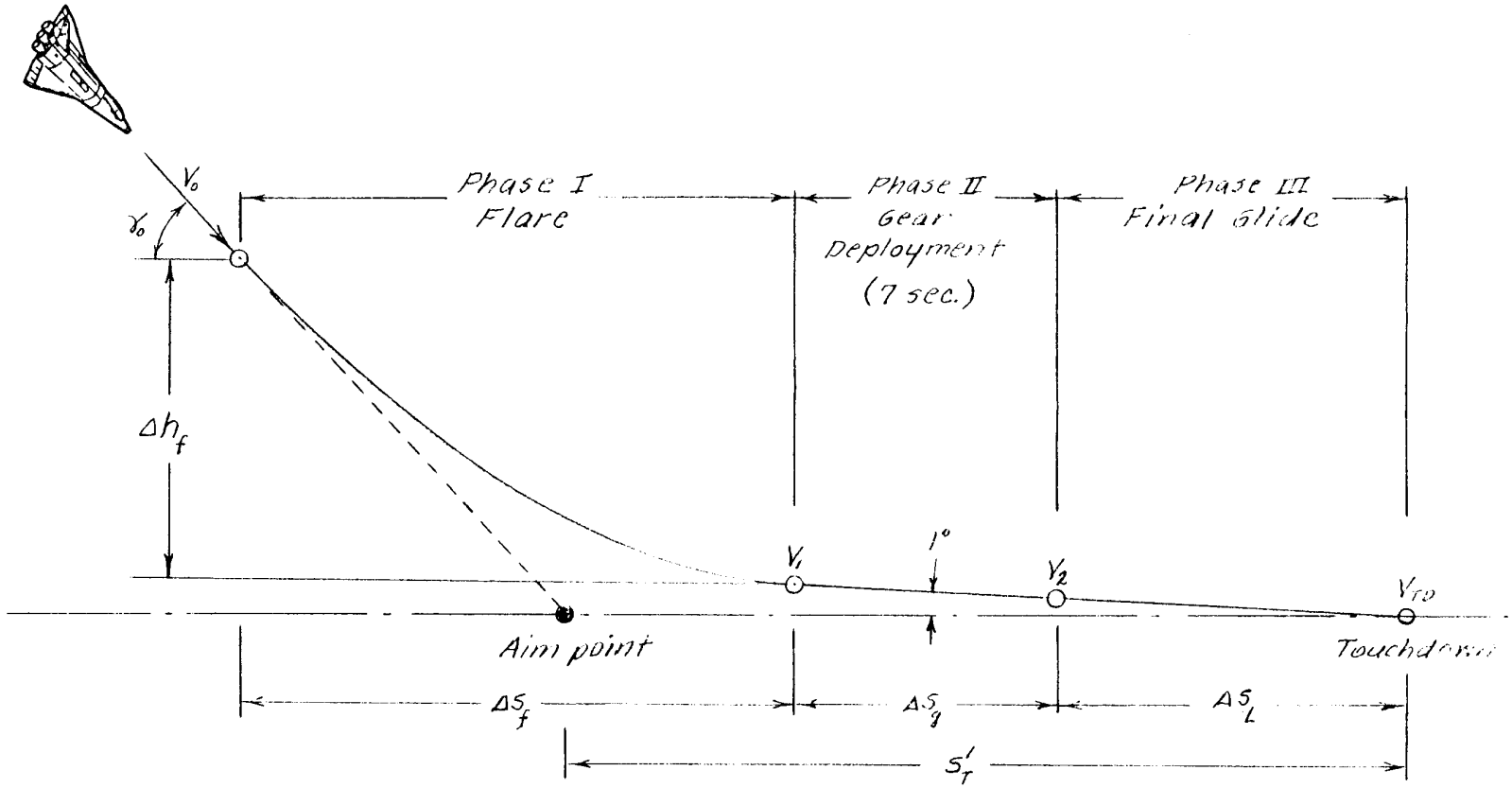

Figure 1. Schematic of three phase landing maneuver.

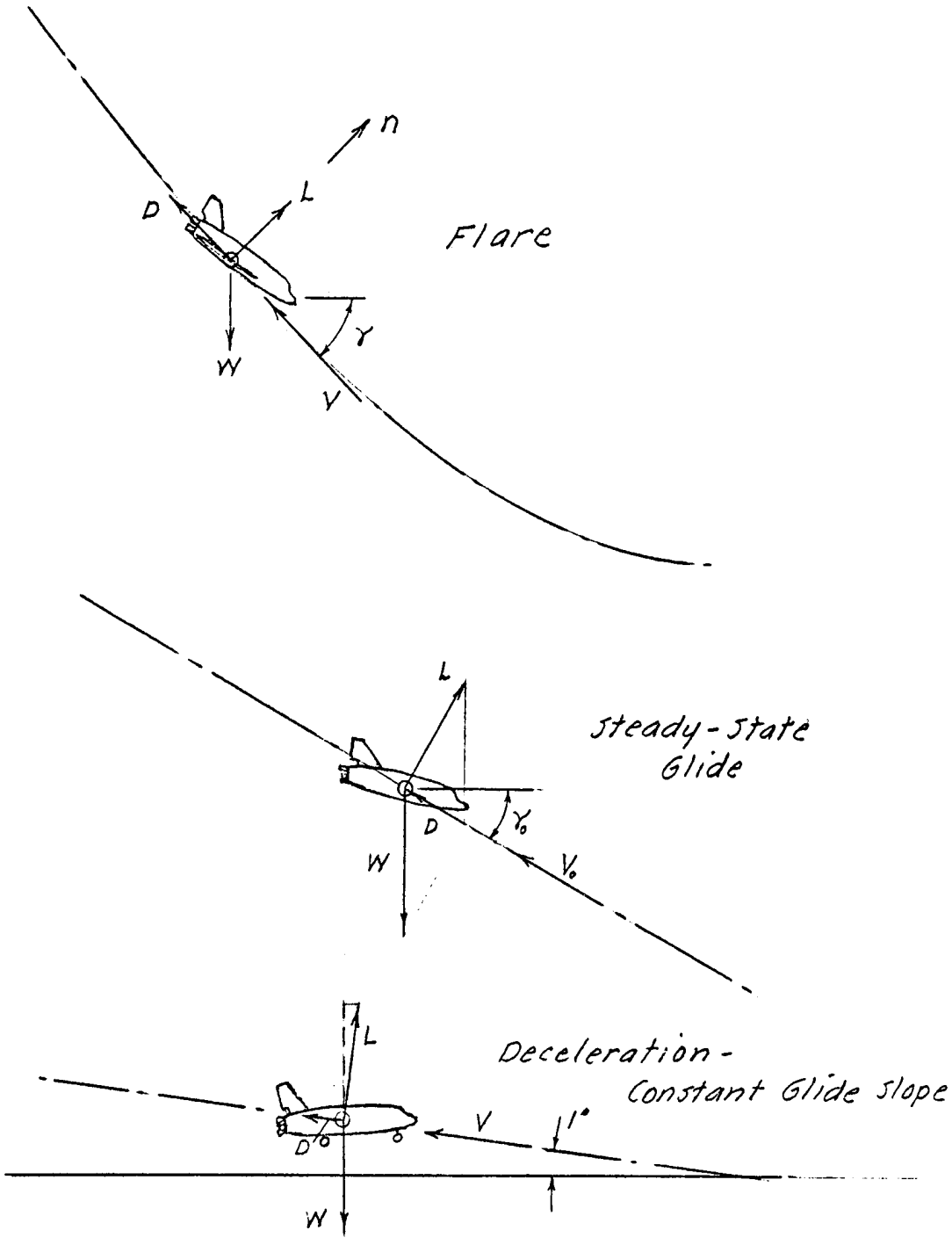

Figure 2. Force diagrams for analysis of landing maneuver.

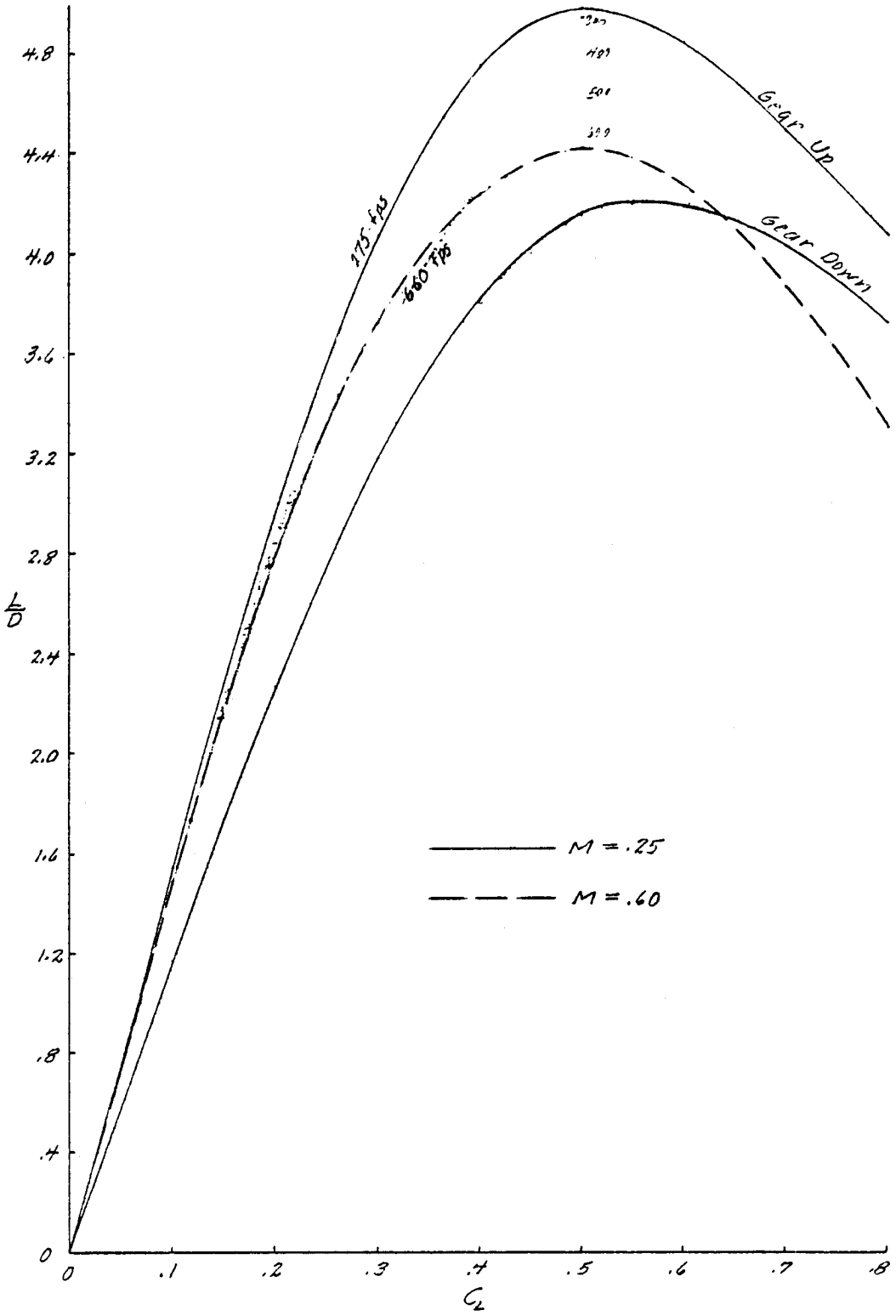

(a) $\delta_{SB} = 0°$

Figure 3. Orbiter lift-drag characteristics.

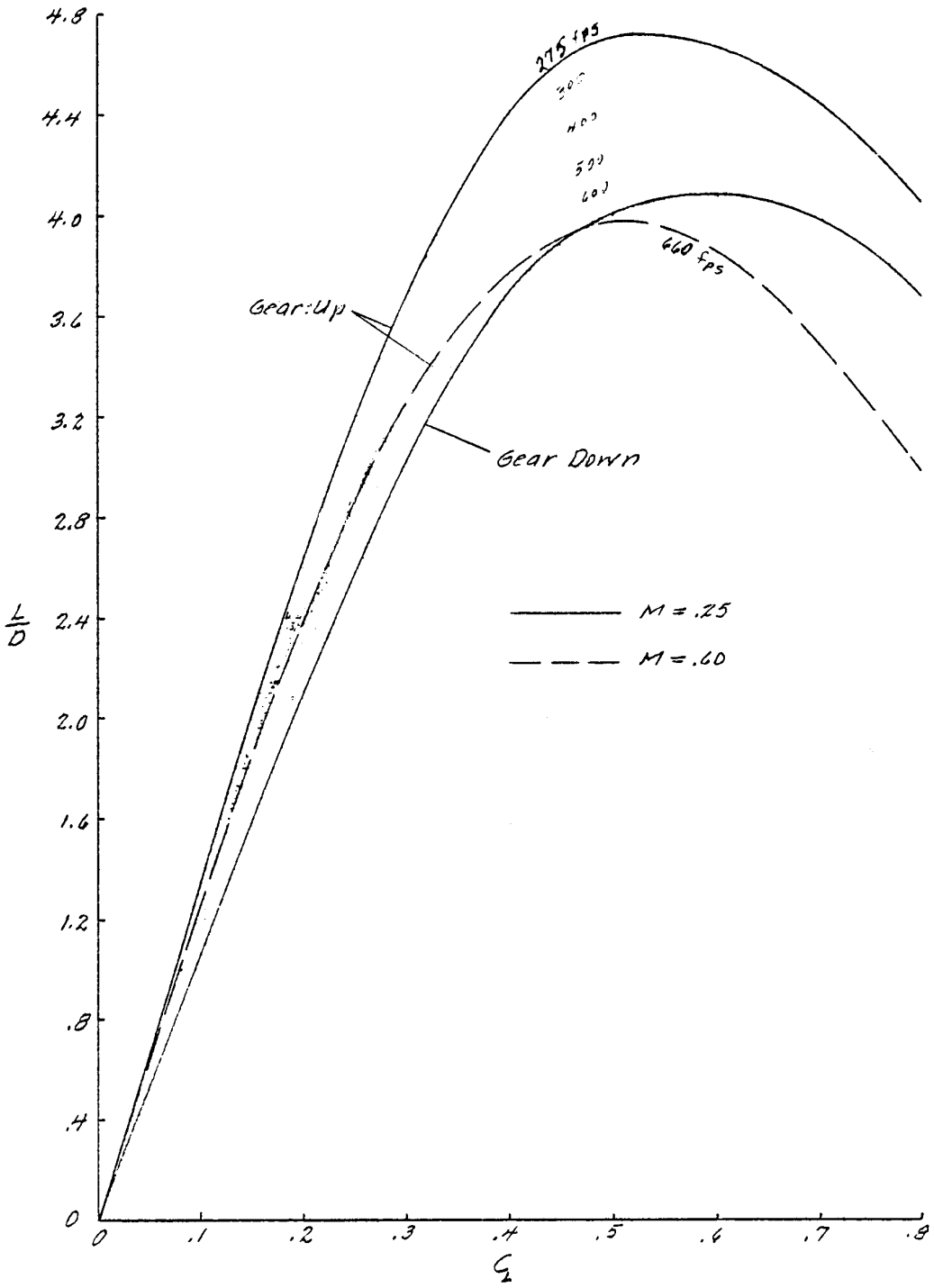

(b) $\delta_{SB} = 25°$

Figure 3. Continued.

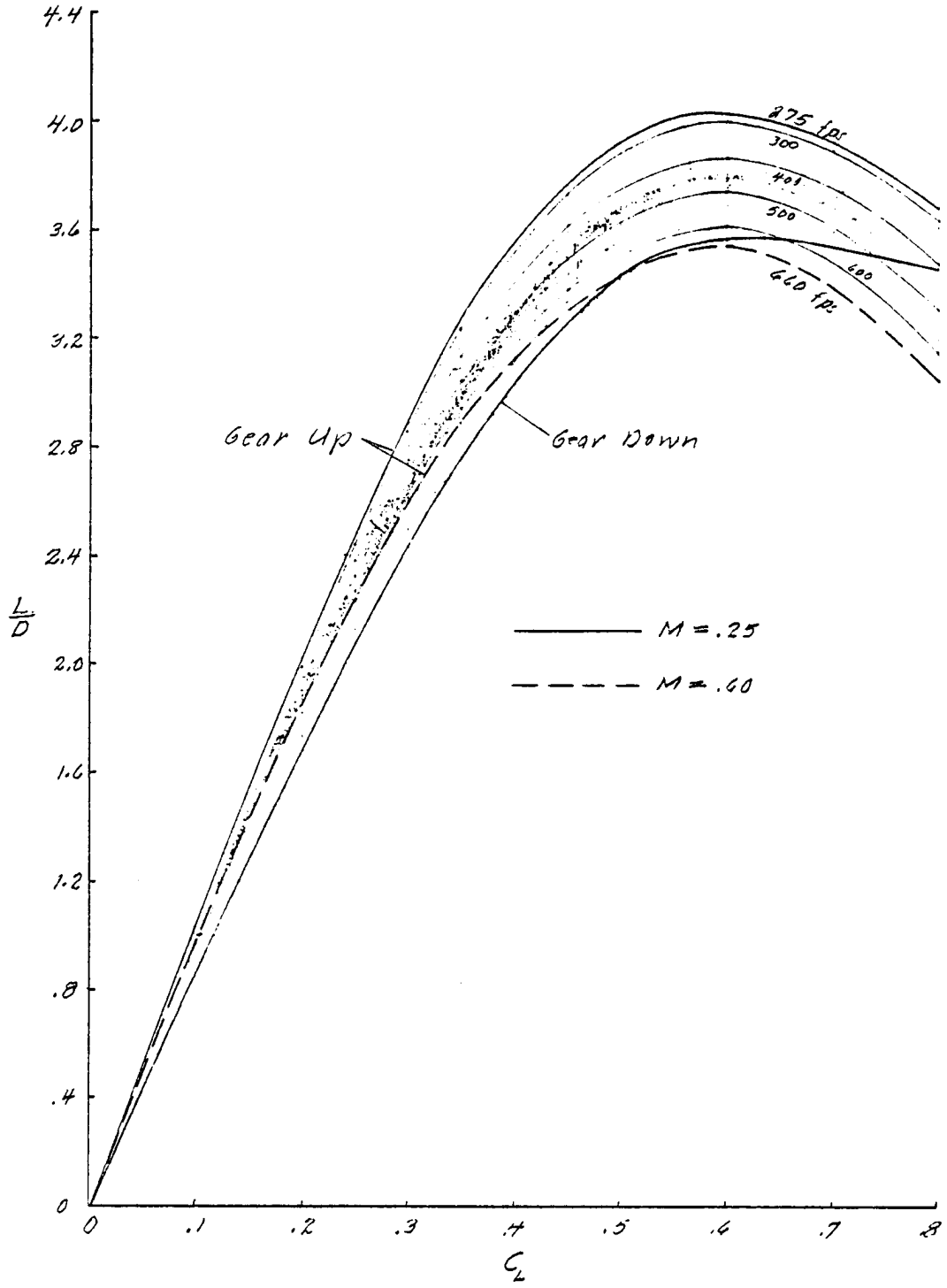

(c) $\delta_{SB} = 55°$

Figure 3. Continued.

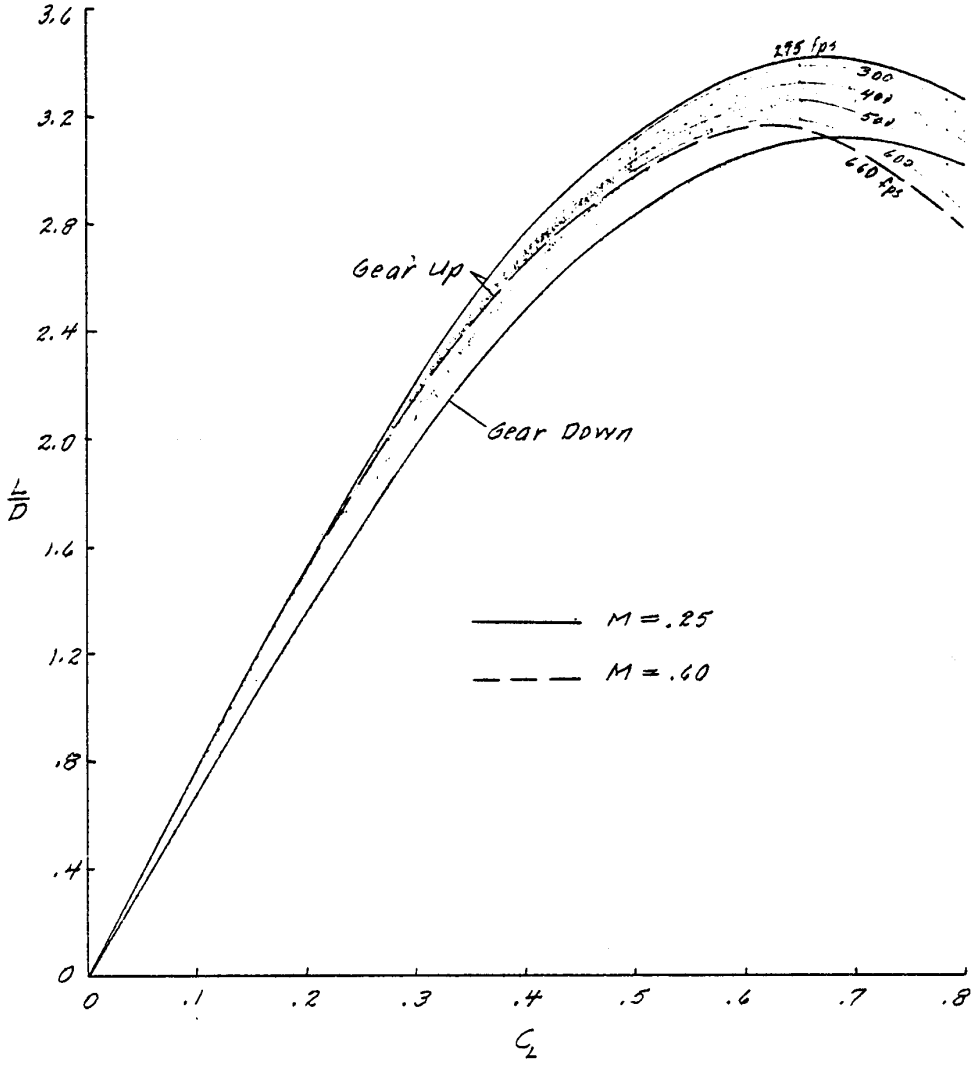

(d) $\delta_{SB} = 87°$

Figure 3 Concluded.

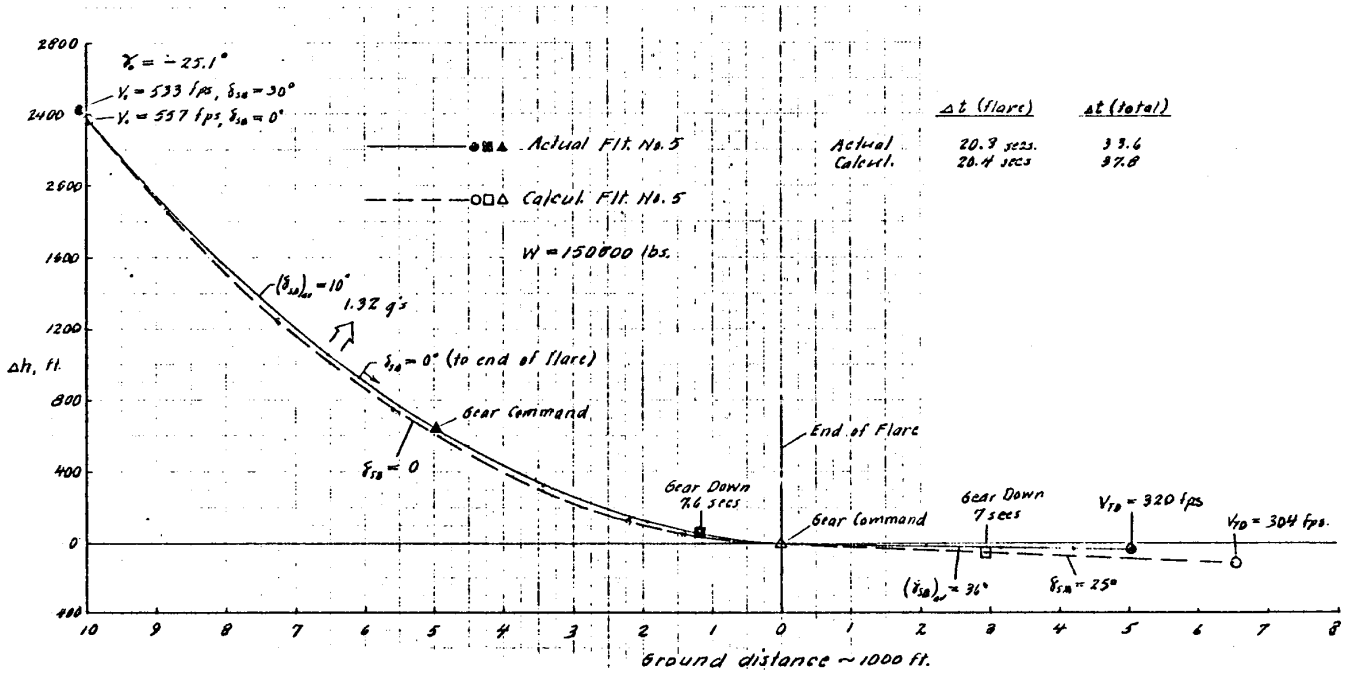

Figure 4. Comparison of the actual and calculated landing trajectories of orbiter flight number 5.

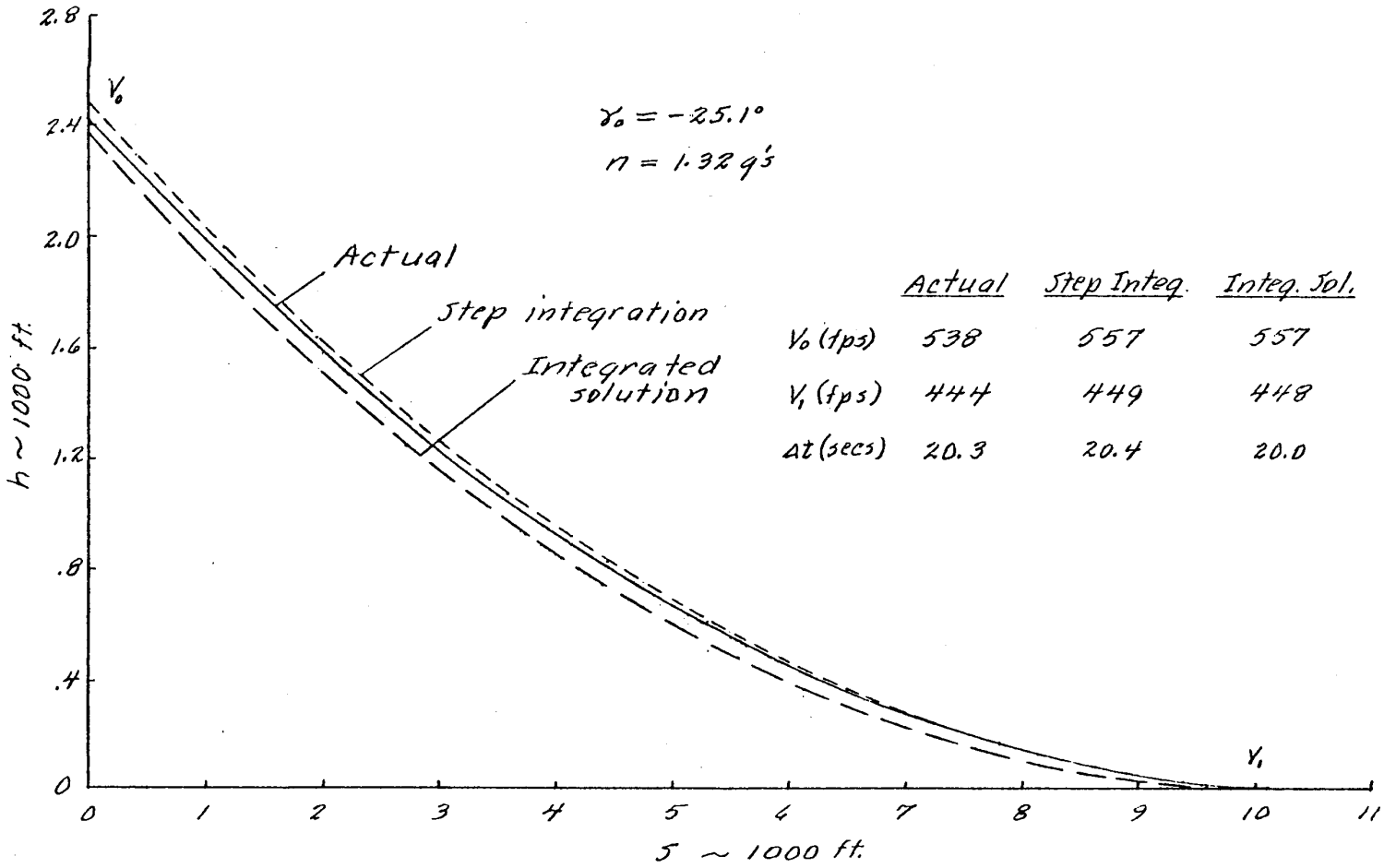

	Actual	Step Integ.	Integ. Sol.
V_0 (fps)	538	557	557
V_1 (fps)	444	449	448
Δt (secs)	20.3	20.4	20.0

Figure 5. Assessment of the method used for calculating landing trajectories by comparison of calculated and orbiter flight no. 5 flare maneuvers.

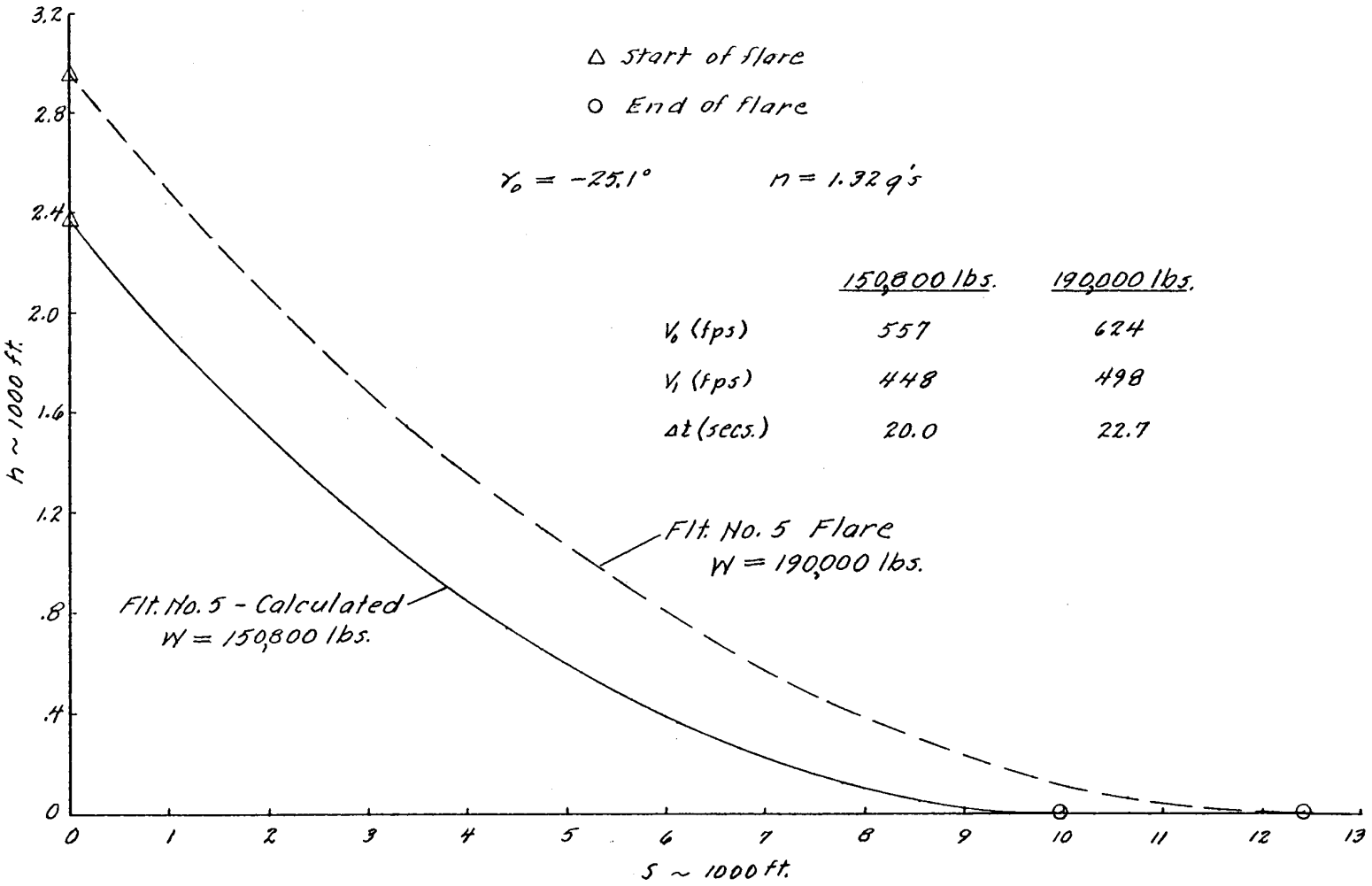

Figure 6. Effect of increased weight on the orbiter flight number 5 landing trajectory.

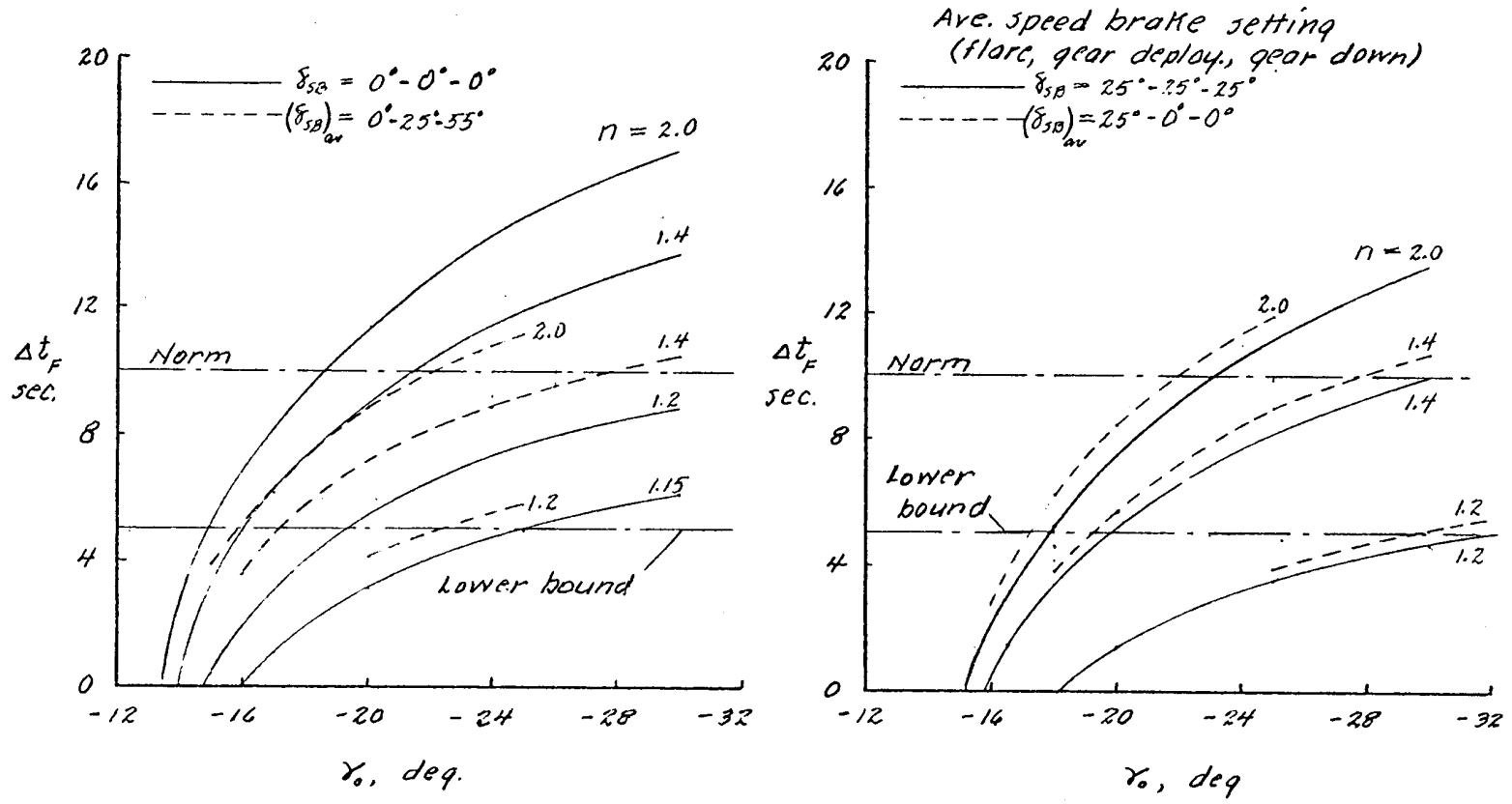

(a) 0°, 25° Speed Brake Settings

Figure 7. Variation of landing time between gear down and touch down with initial glide slope and flare load factor for various speed brake settings. W/S = 56.0 psf.

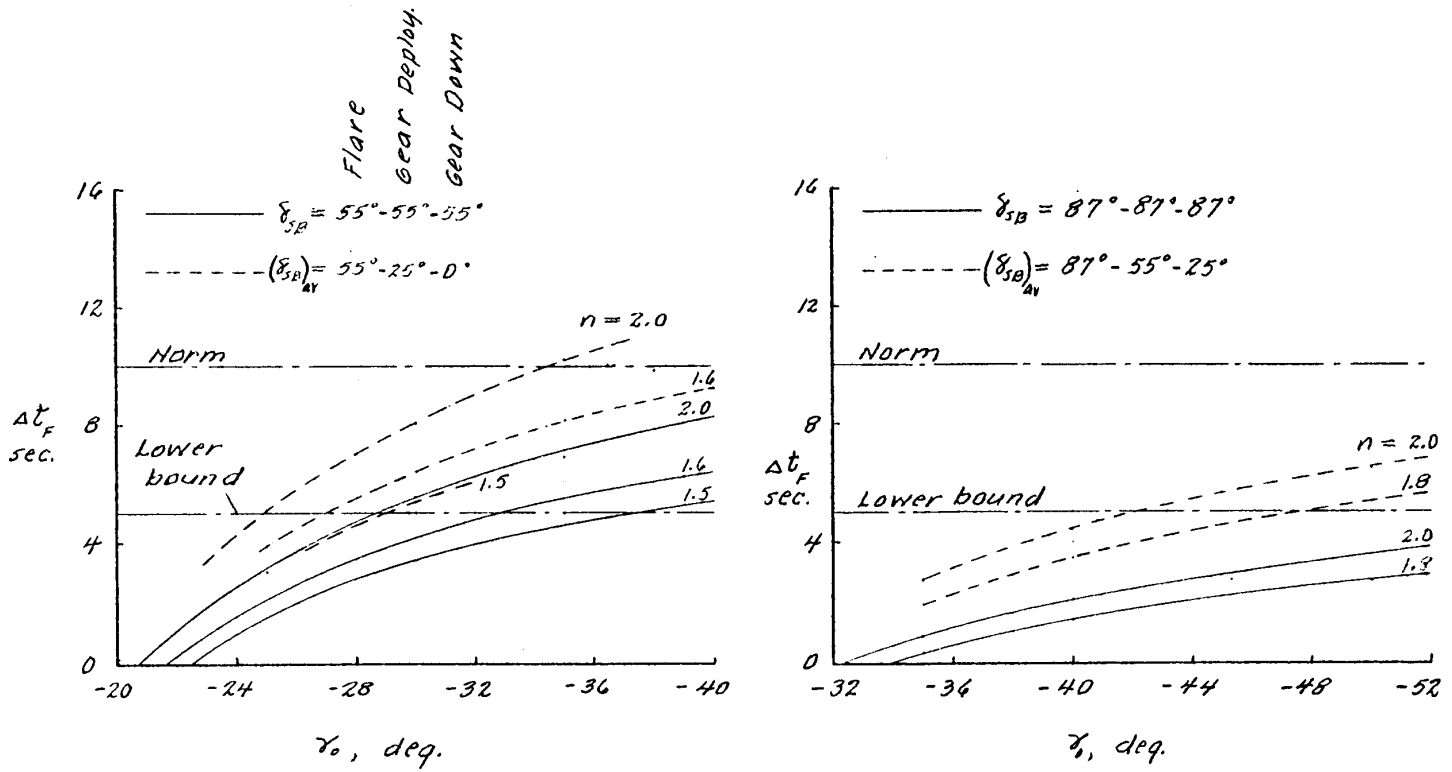

(b) 55°, 87° Speed Brake Settings

Figure 7. Completed.

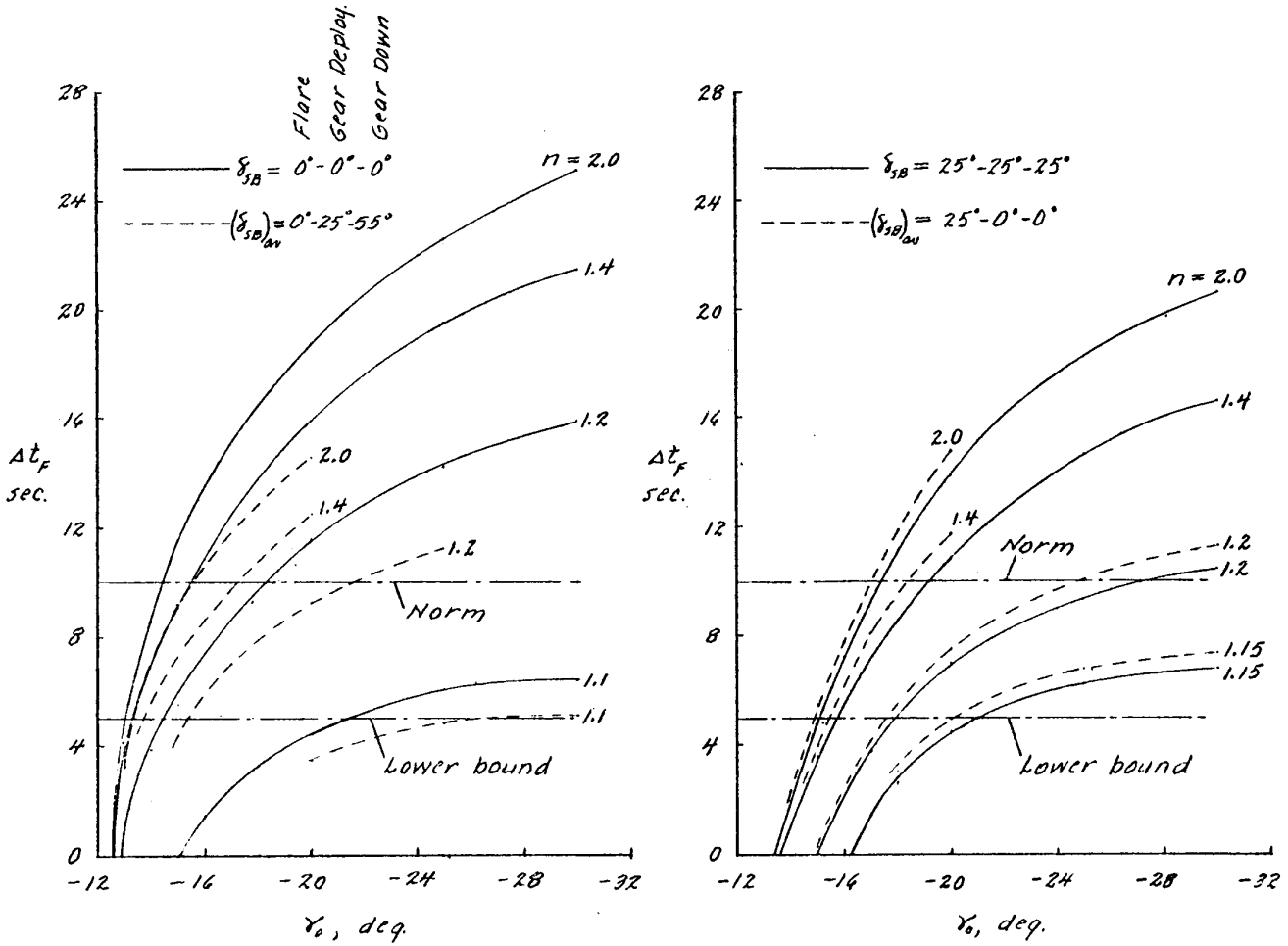

(a) 0°, 25° Speed Brake Settings

Figure 8. Variation of flight time between gear down and touch down with initial glide slope and flare load factor for various speed settings. W/S = 70.6 psf

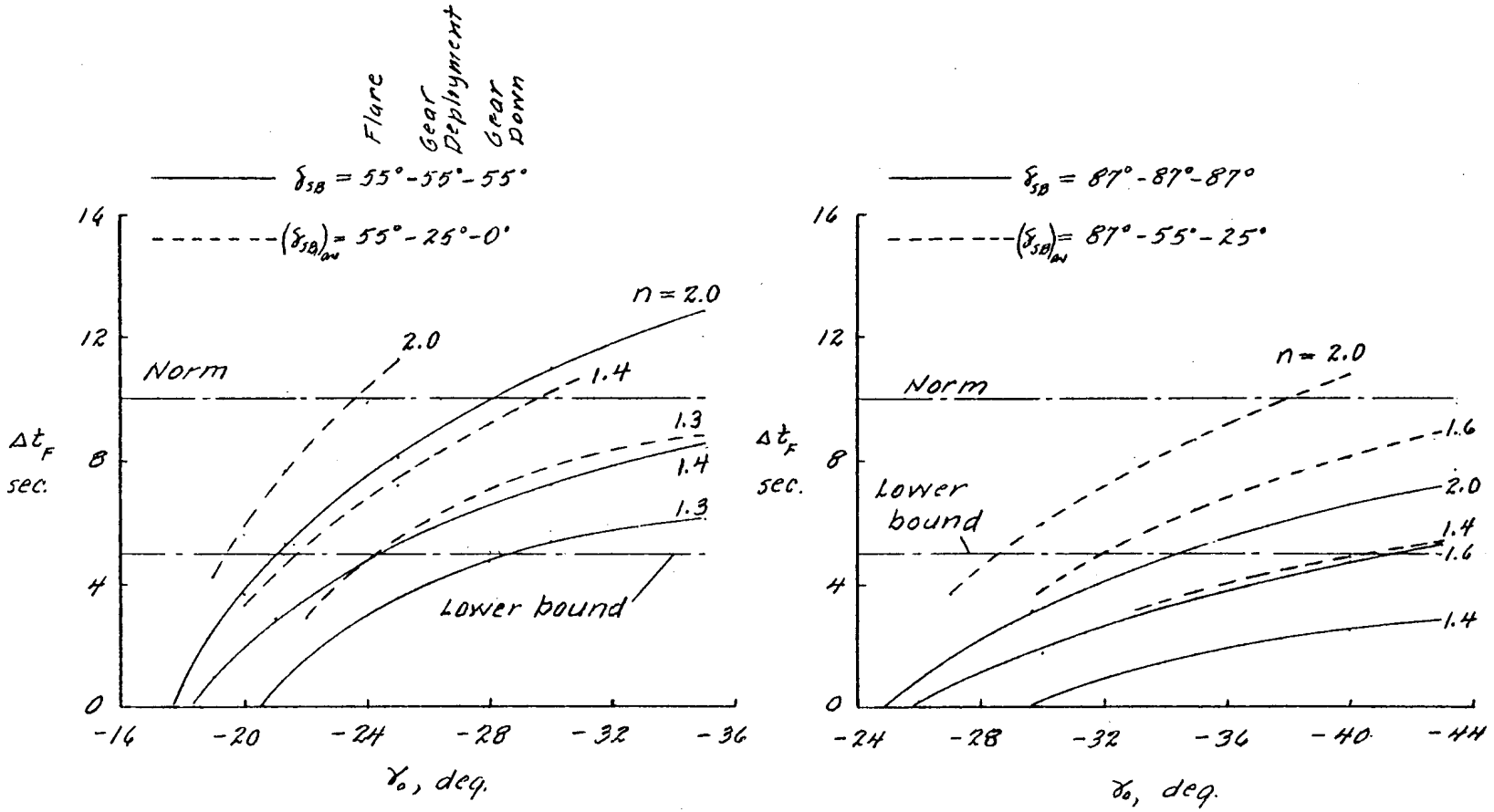

(b) 55°, 87° Speed Brake Settings

Figure 8. Completed.

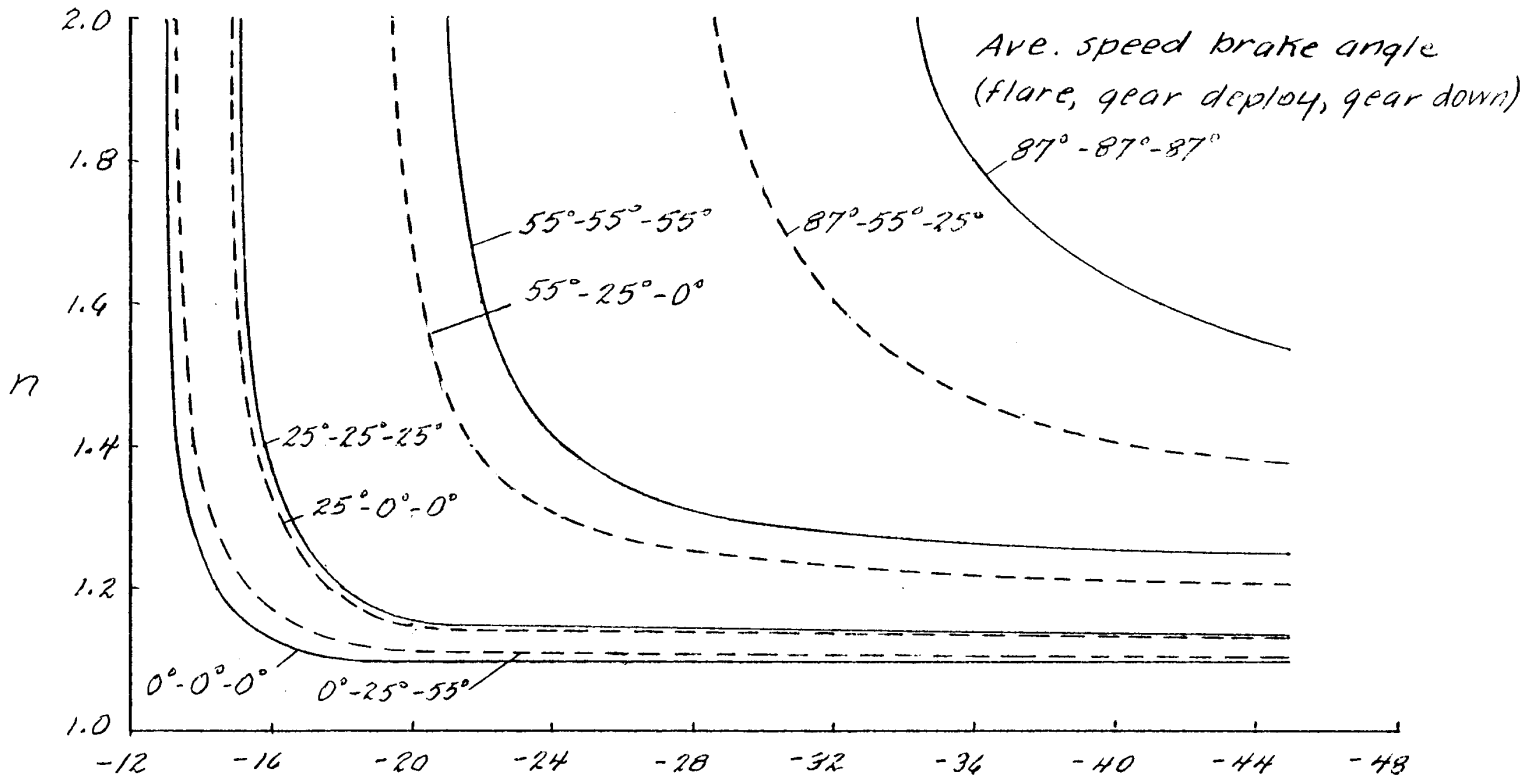

(a) $W/S = 70.6$ psf

Figure 9. Boundaries for minimal landing performance in terms of load factor, initial glide slope, and average speed brake setting. $\Delta t_1 = 5$ sec.

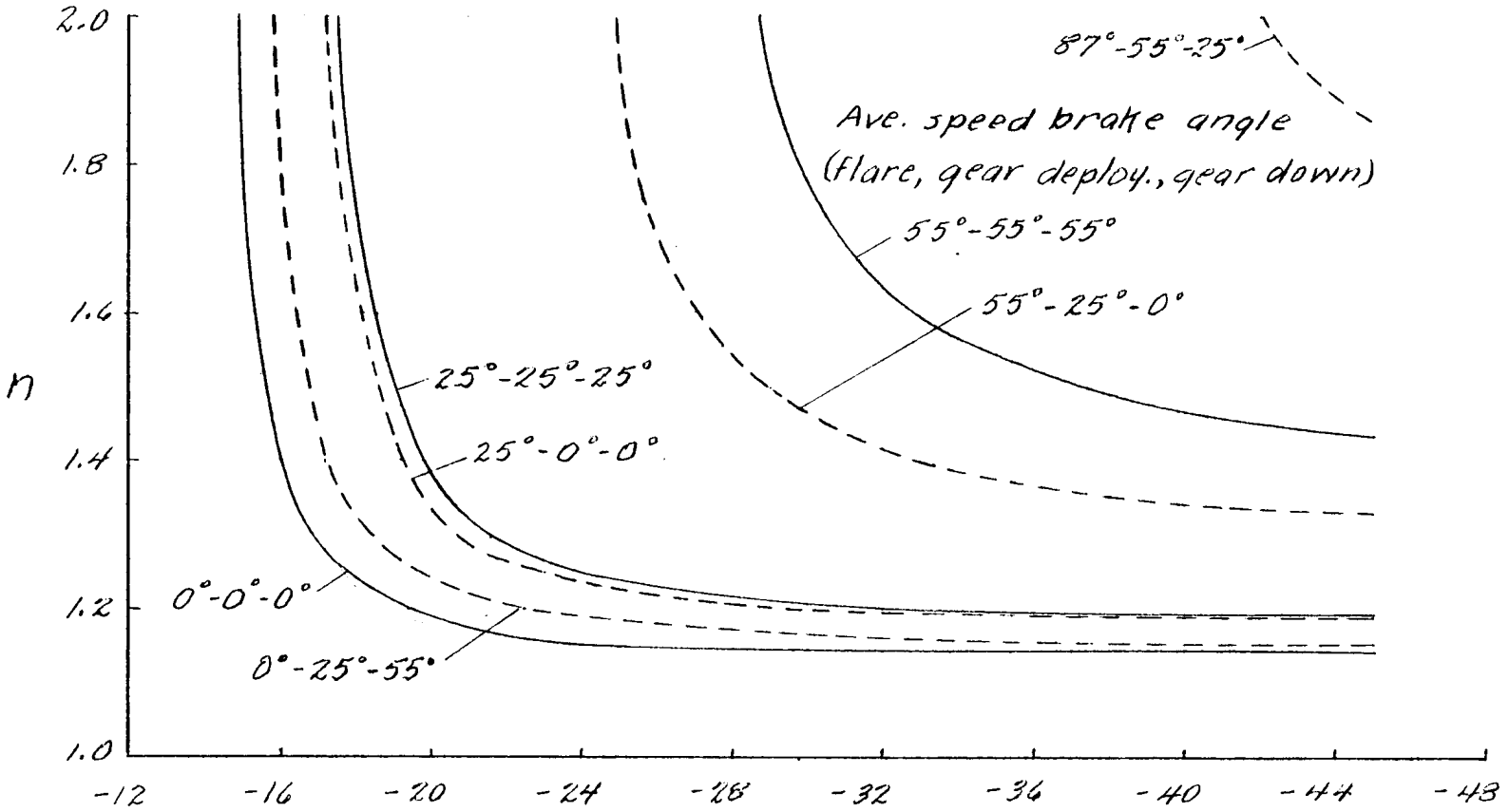

(b) $W/S = 56.0$ psf

Figure 9. Completed.

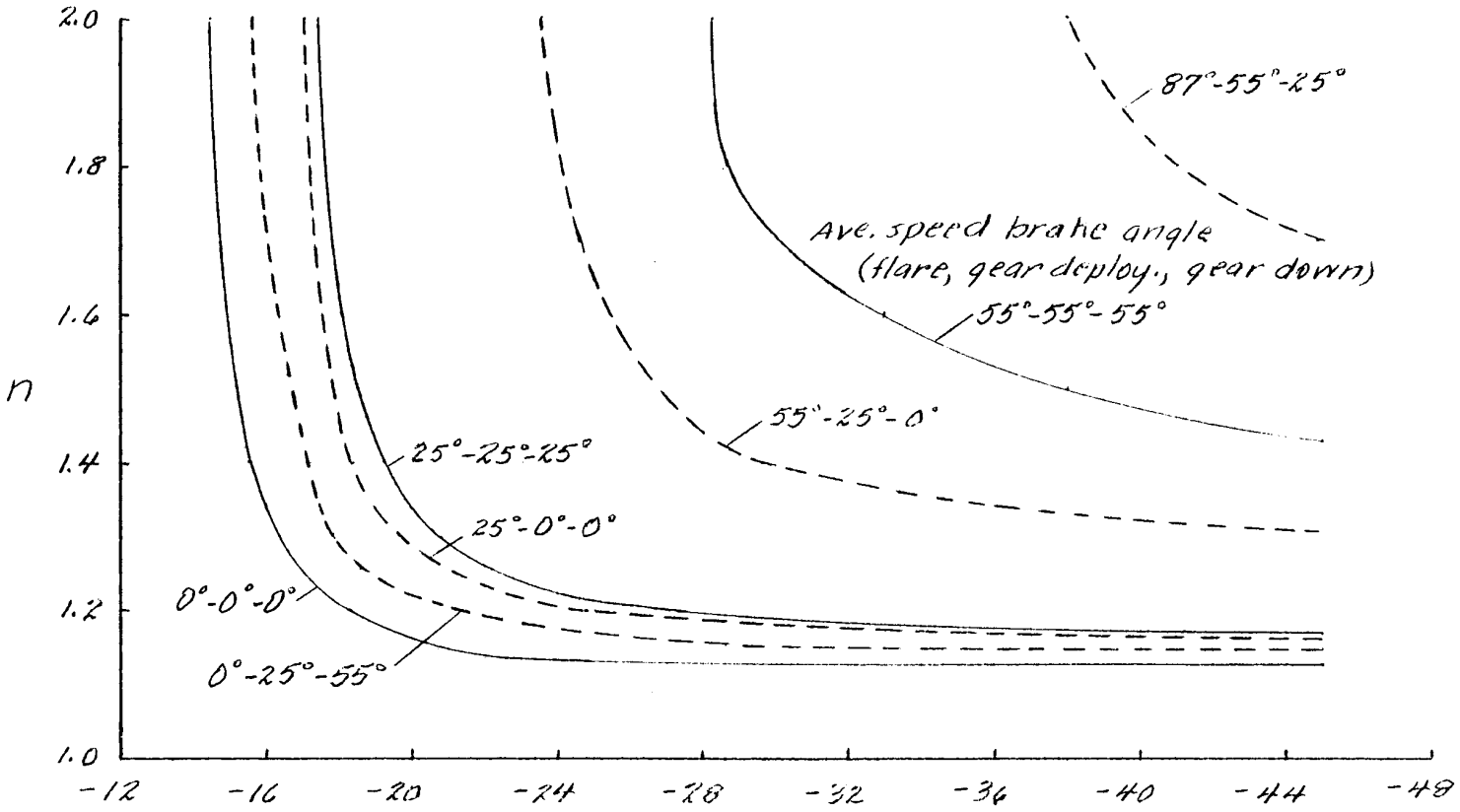

(a) $W/S = 70.4$ psf

Figure 10. Boundaries for normal landing performance in terms of load factor, initial glide slope, and average speed brake setting. $\Delta t_2 = 10$ sec.

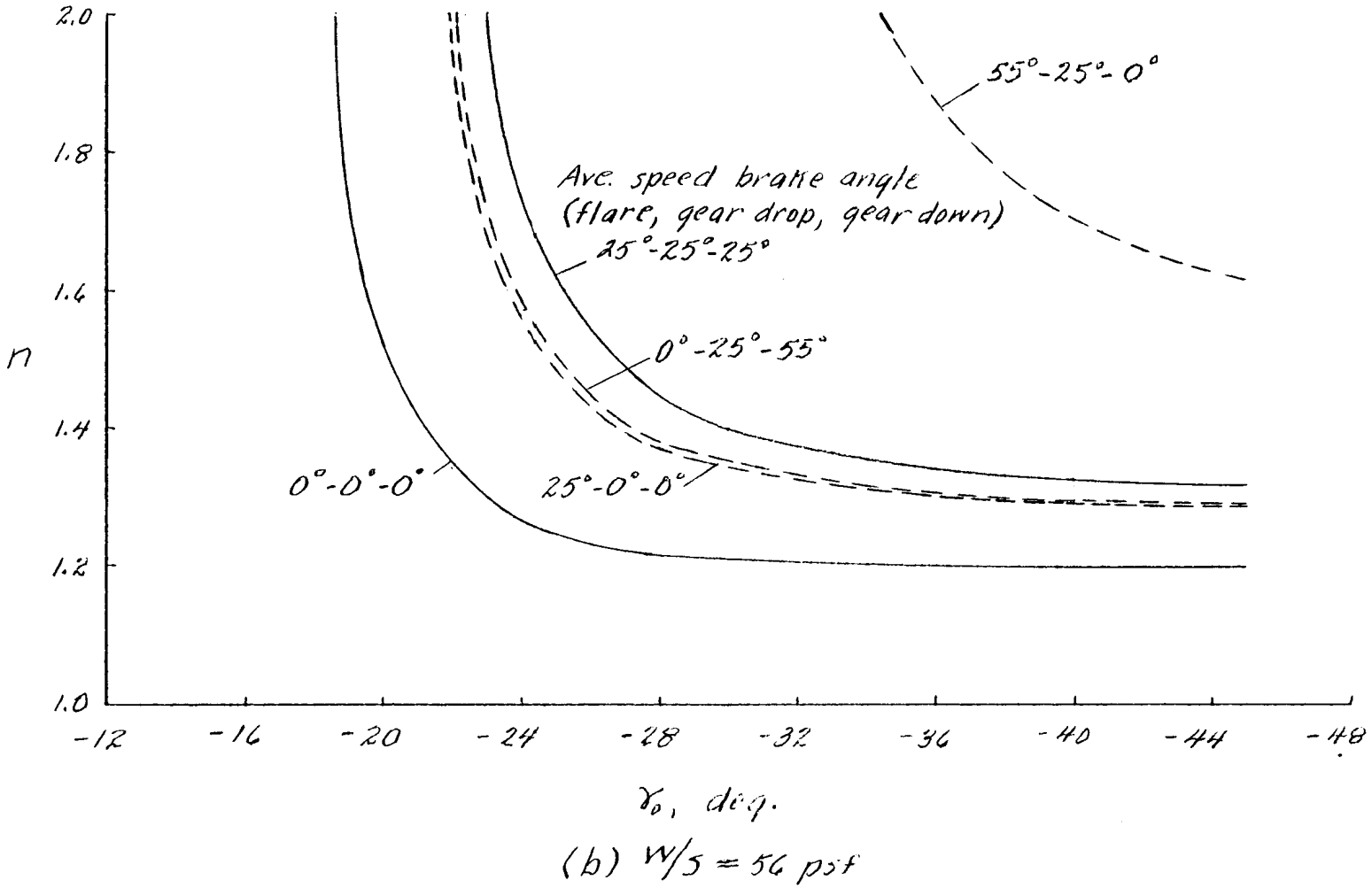

(b) $W/S = 56$ psf

Figure 10. Concluded.

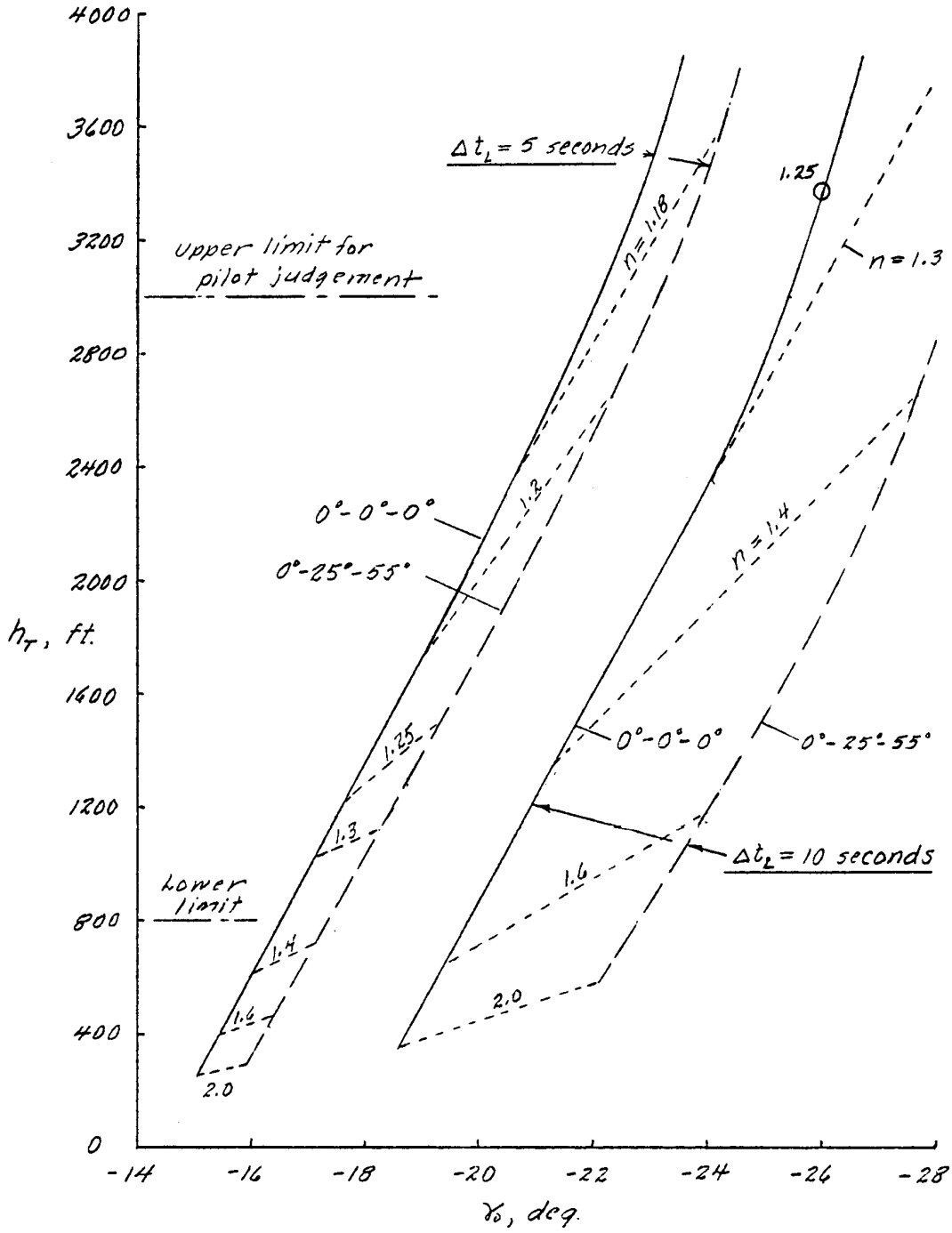

(a) Configurations 0°-0°-0°, 0°-25°-55°

Figure 11. Variation of total altitude change in the landing maneuver with initial glide angle. W/S = 56 psf.

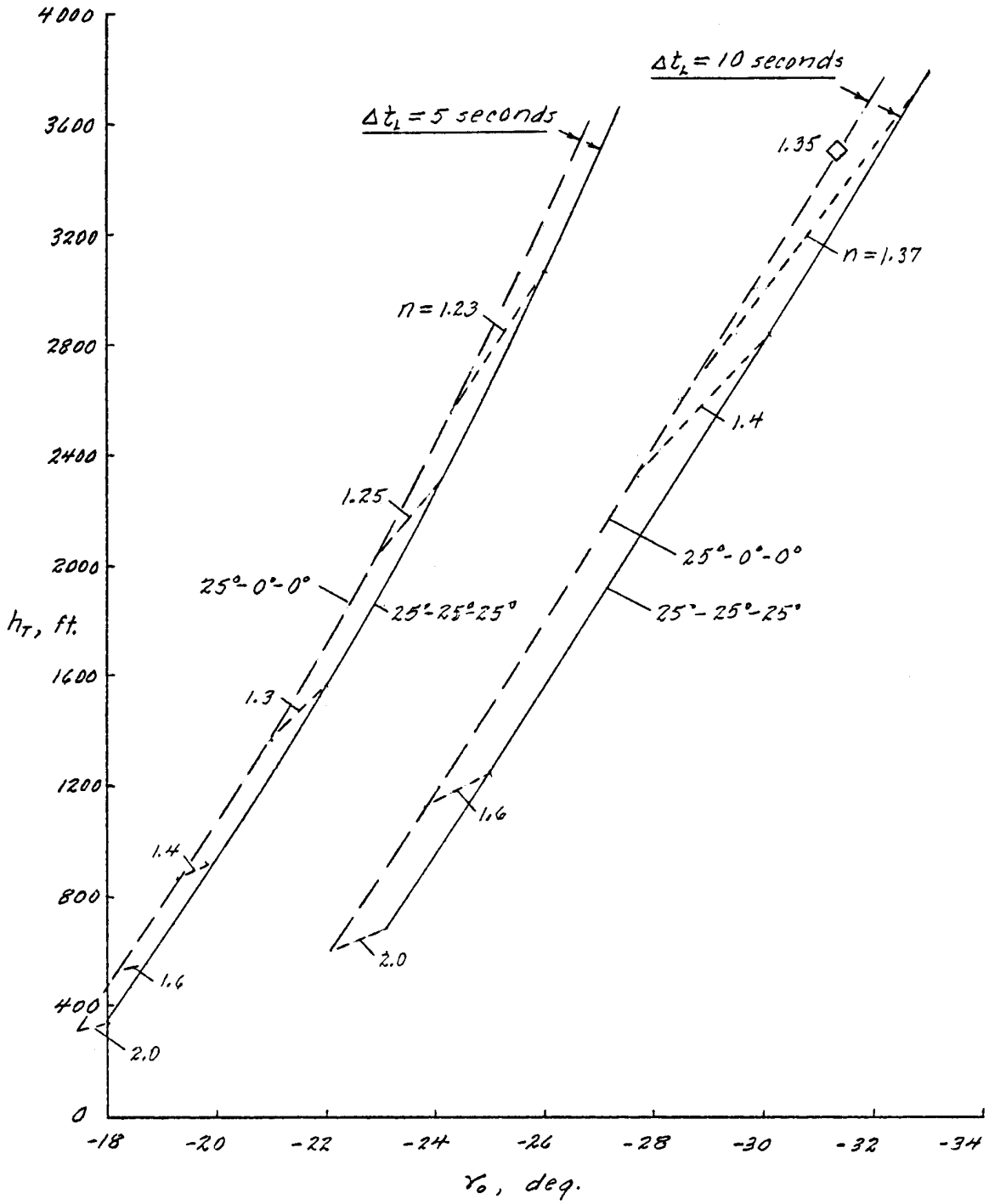

(b) Configurations 25°-25°-25°, 25°-0°-0°

Figure 11. Continued.

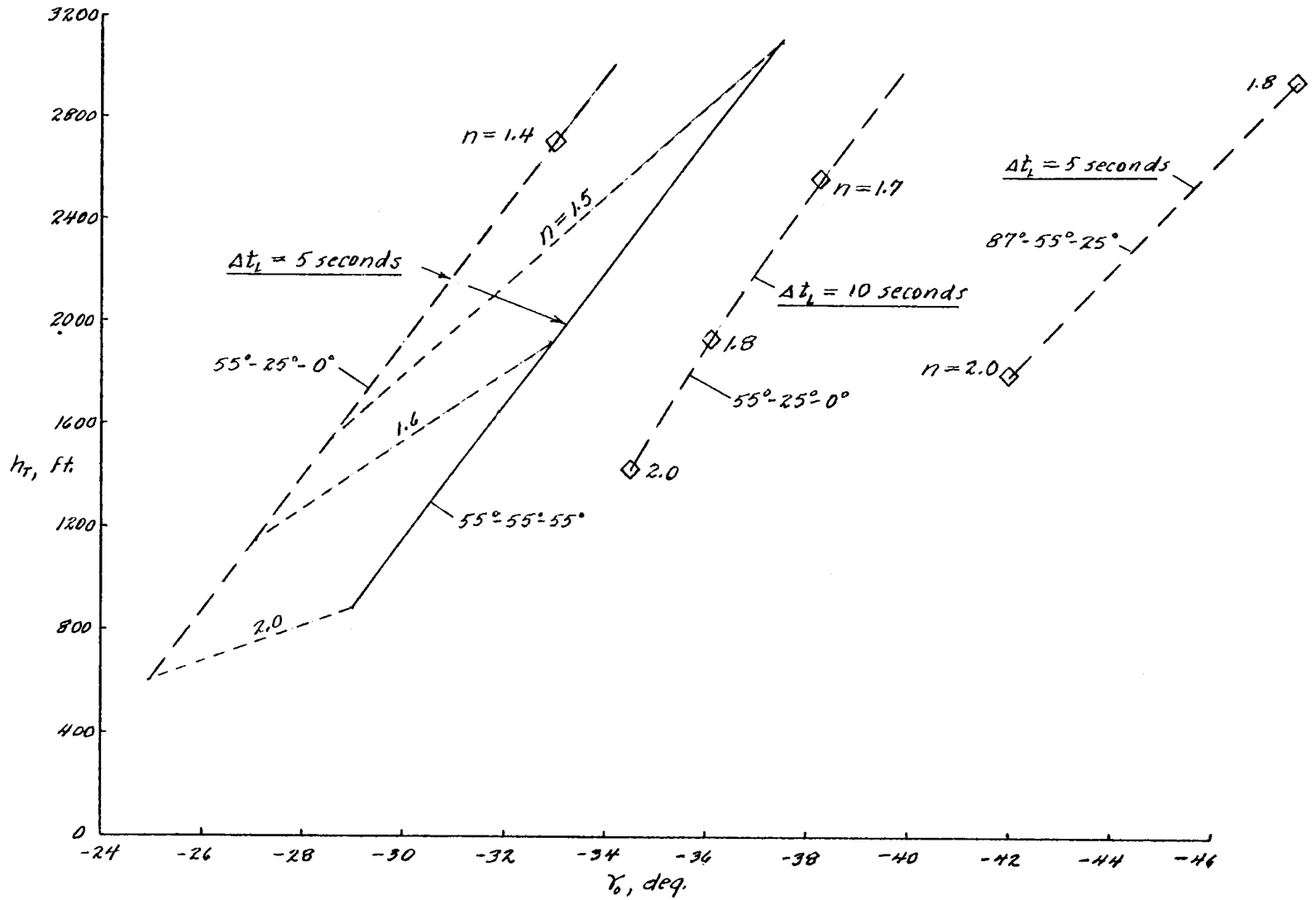

(c) Configurations 55°-55°-55°, 55°-25°-0°, 87°-55°-25°

Figure 11. Concluded.

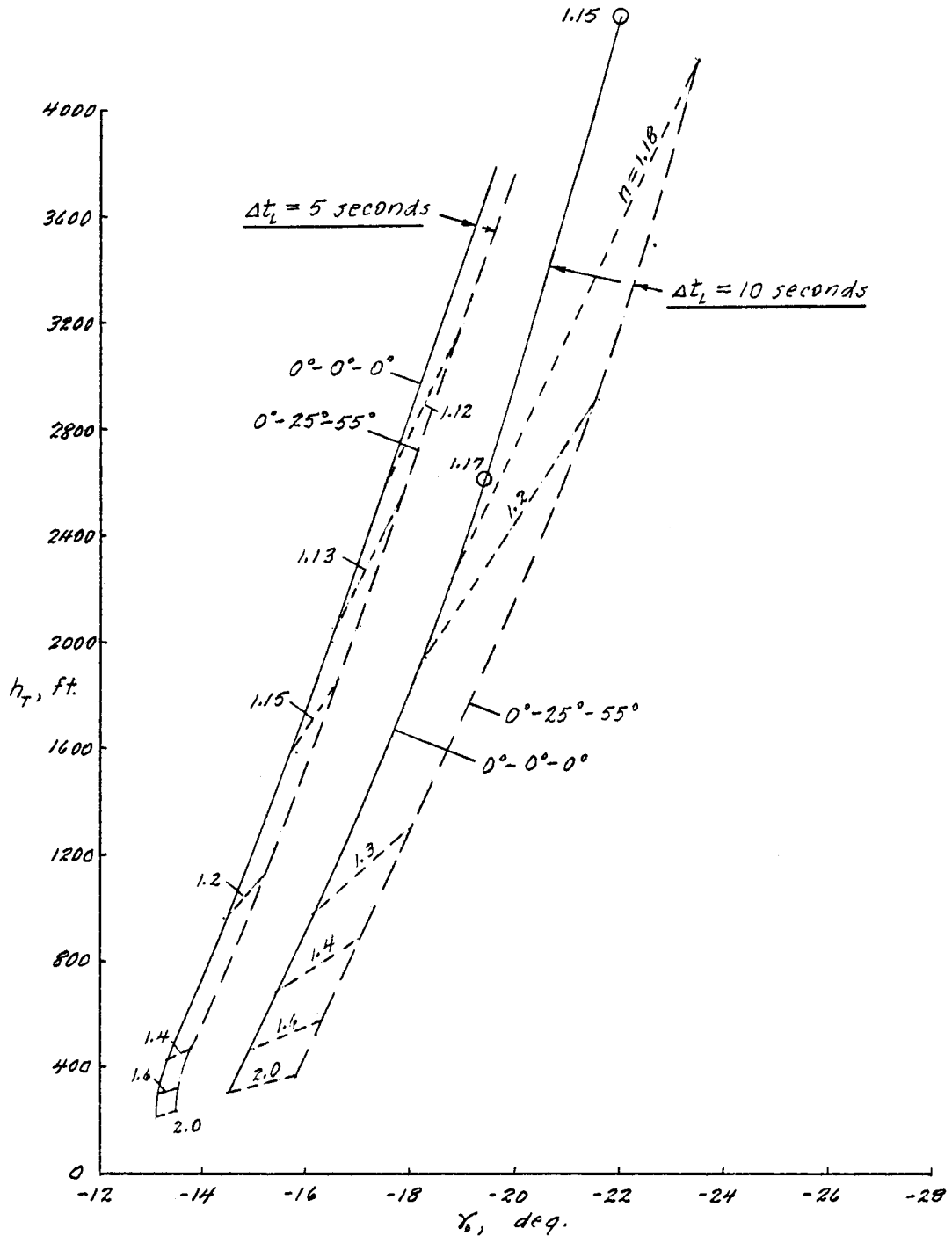

(a) Configurations 0°-0°-0°, 0°-25°-55°

Figure 12. Variation of total altitude change in the landing maneuver with initial glide slope. W/S = 70.6 psf.

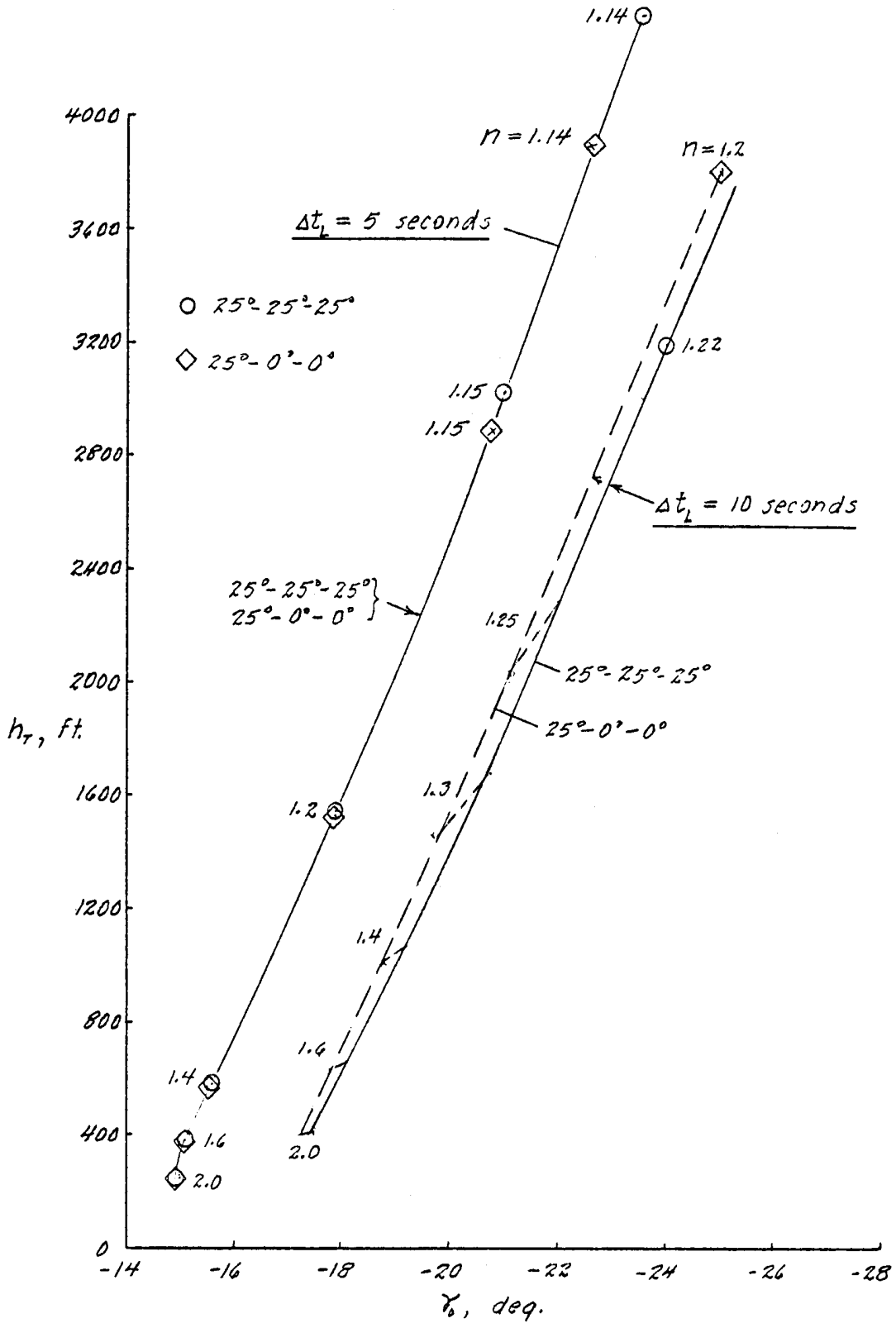

(b) Configurations 25°-25°-25°, 25°-0°-0°

Figure 12, Continued.

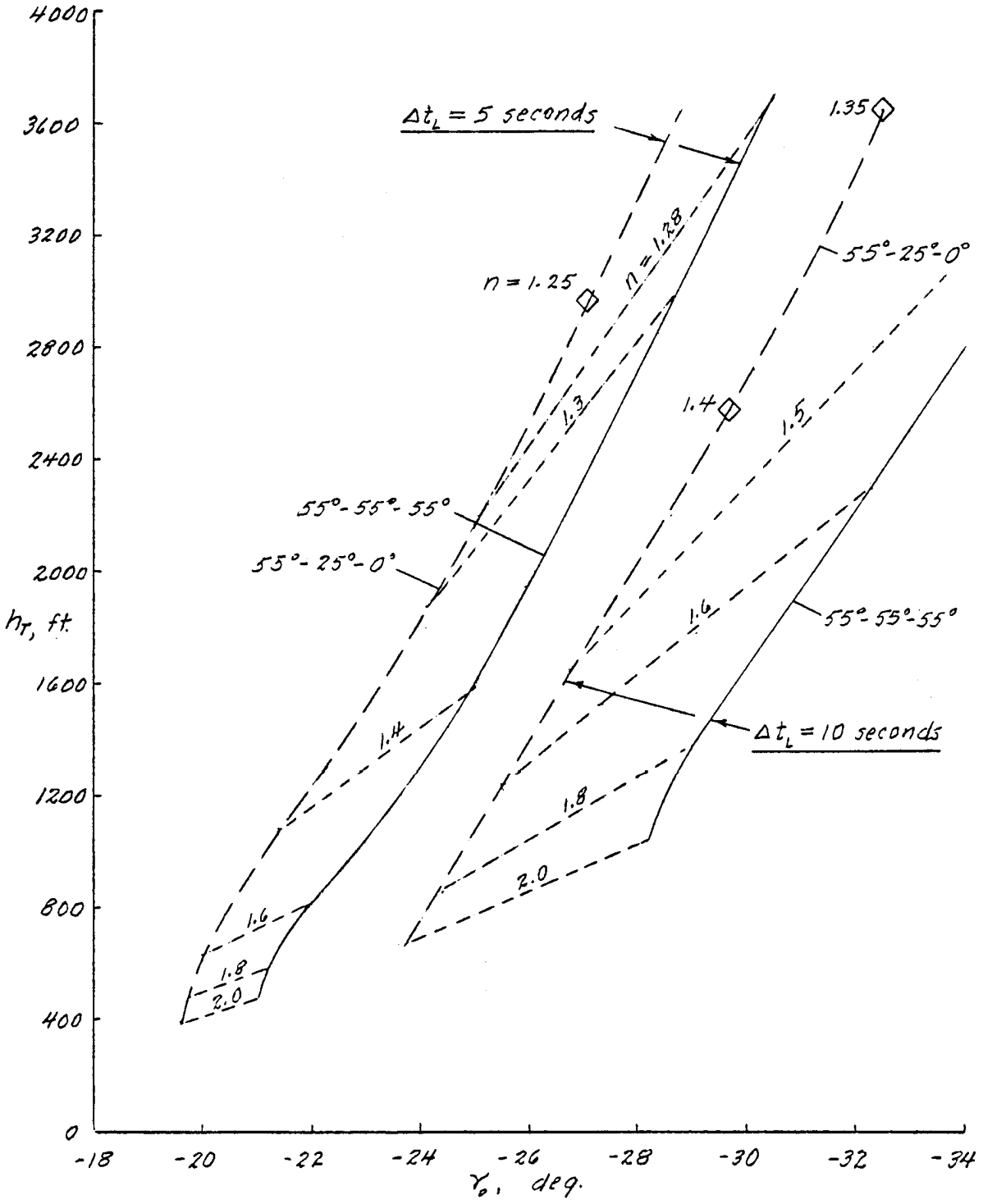

(c) Configurations 55°-55°-25°, 55°-25°-0°

Figure 12. Continued.

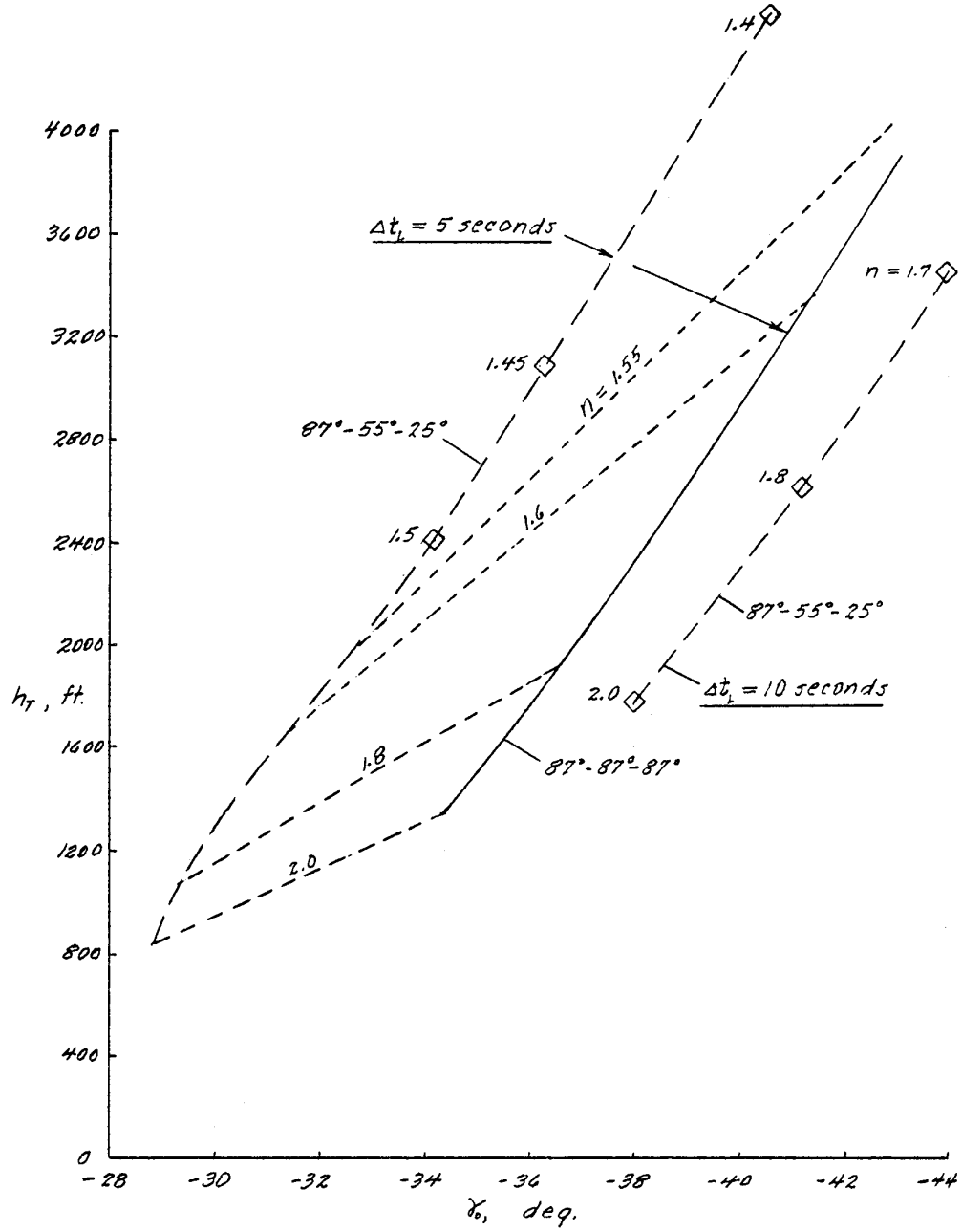

(d) Configurations 87°-87°-87°; 87°-55°-25°

Figure 12. Concluded.

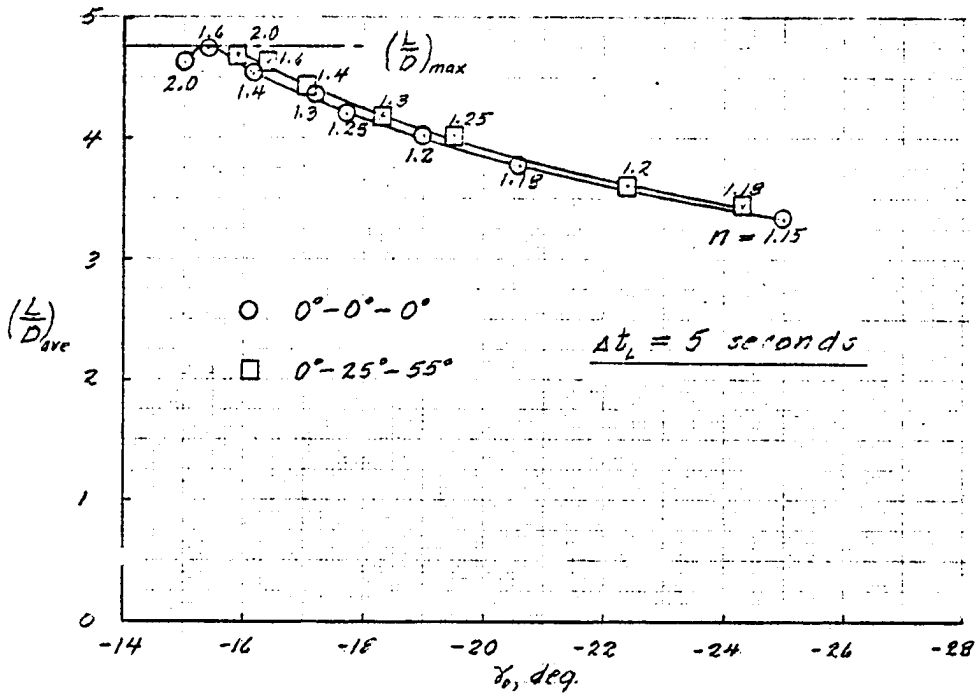

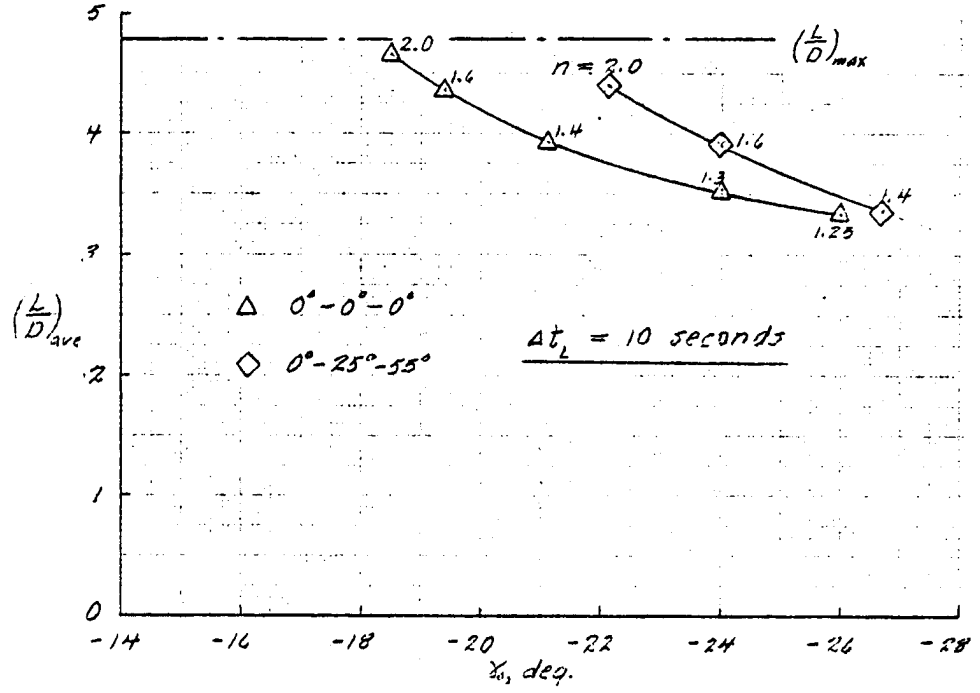

(a) Configurations 0°-0°-0°, 0°-25°-55°

Figure 13. Variation of average lift-to-drag ratio during the landing maneuver with initial glide angle. W/S = 56 psf.

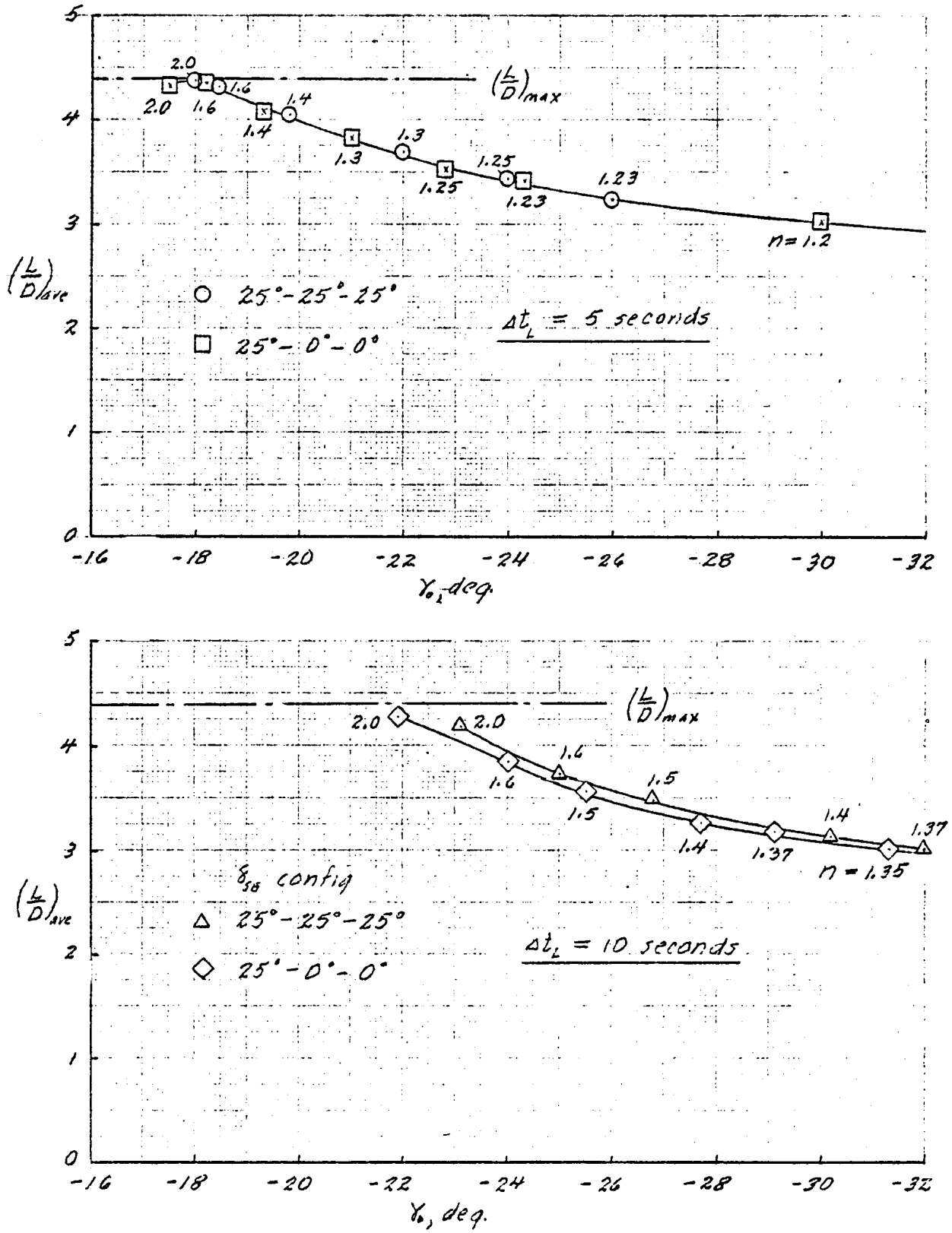

(b) Configurations 25°-25°-25°, 25°-0°-0°

Figure 13 Continued

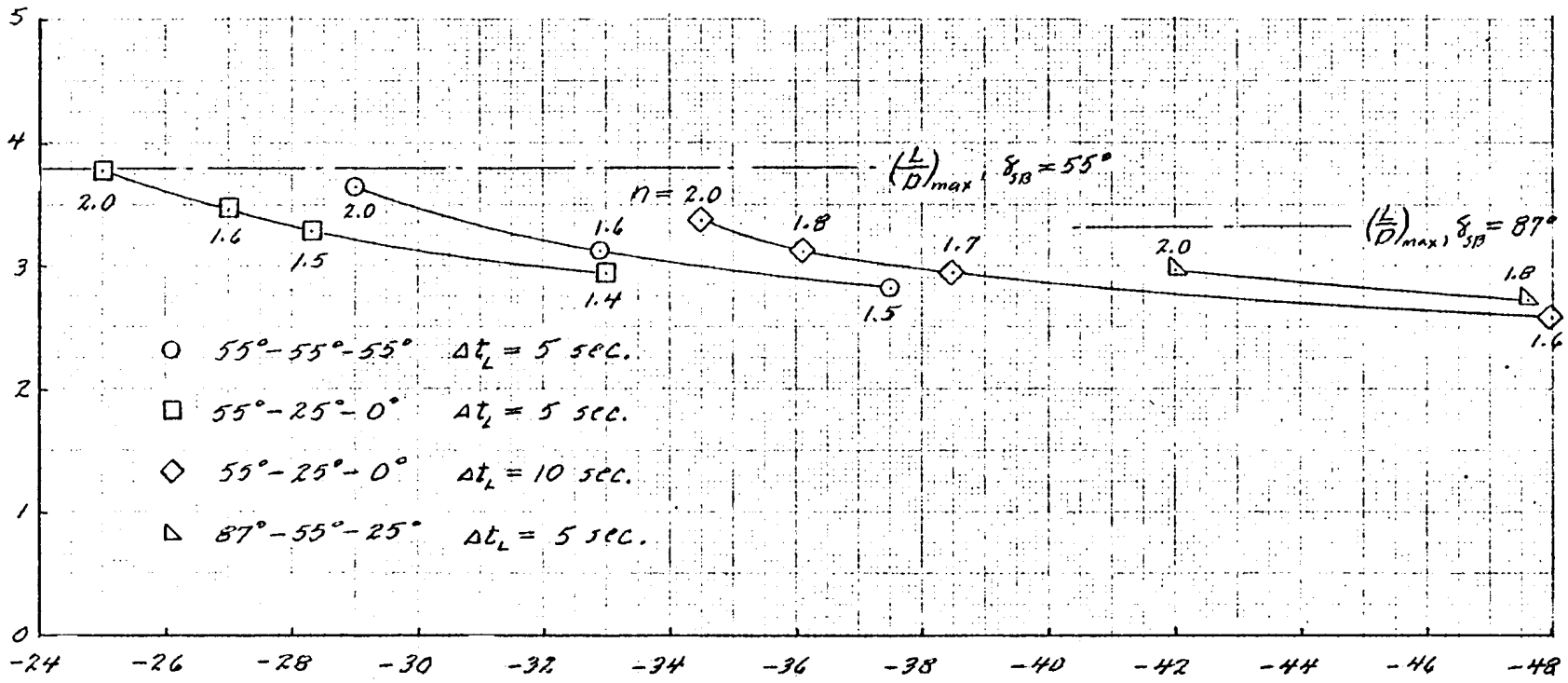

(c) Configurations 55°-55°-55°, 55°-25°-0°, 87°-55°-25°

Figure 13. Concluded.

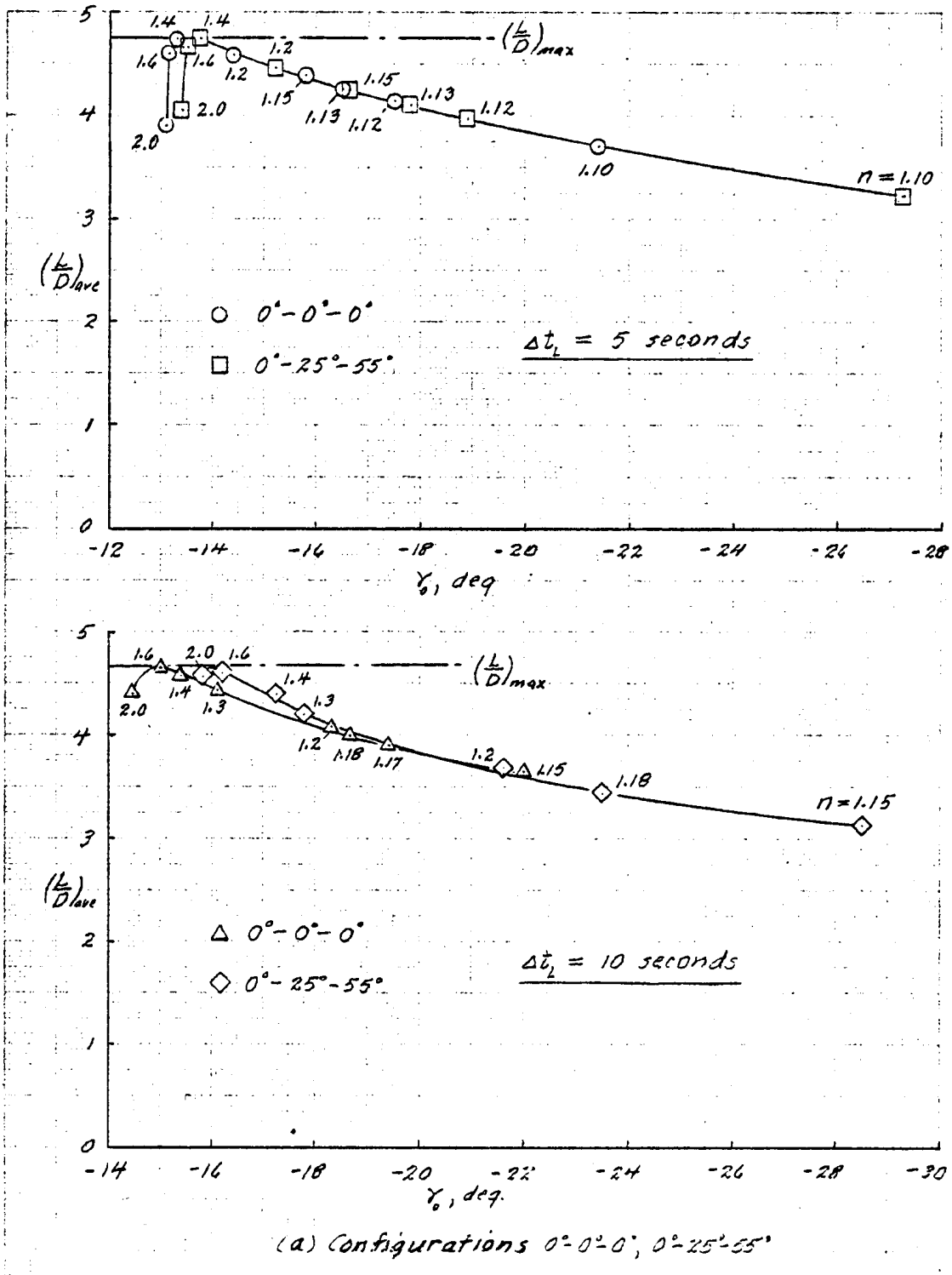

(a) Configurations 0°-0°-0°, 0°-25°-55°

Figure 14. Variation of average lift-to-drag ratio during the landing maneuver with initial glide angle. W/S = 70.6 psf

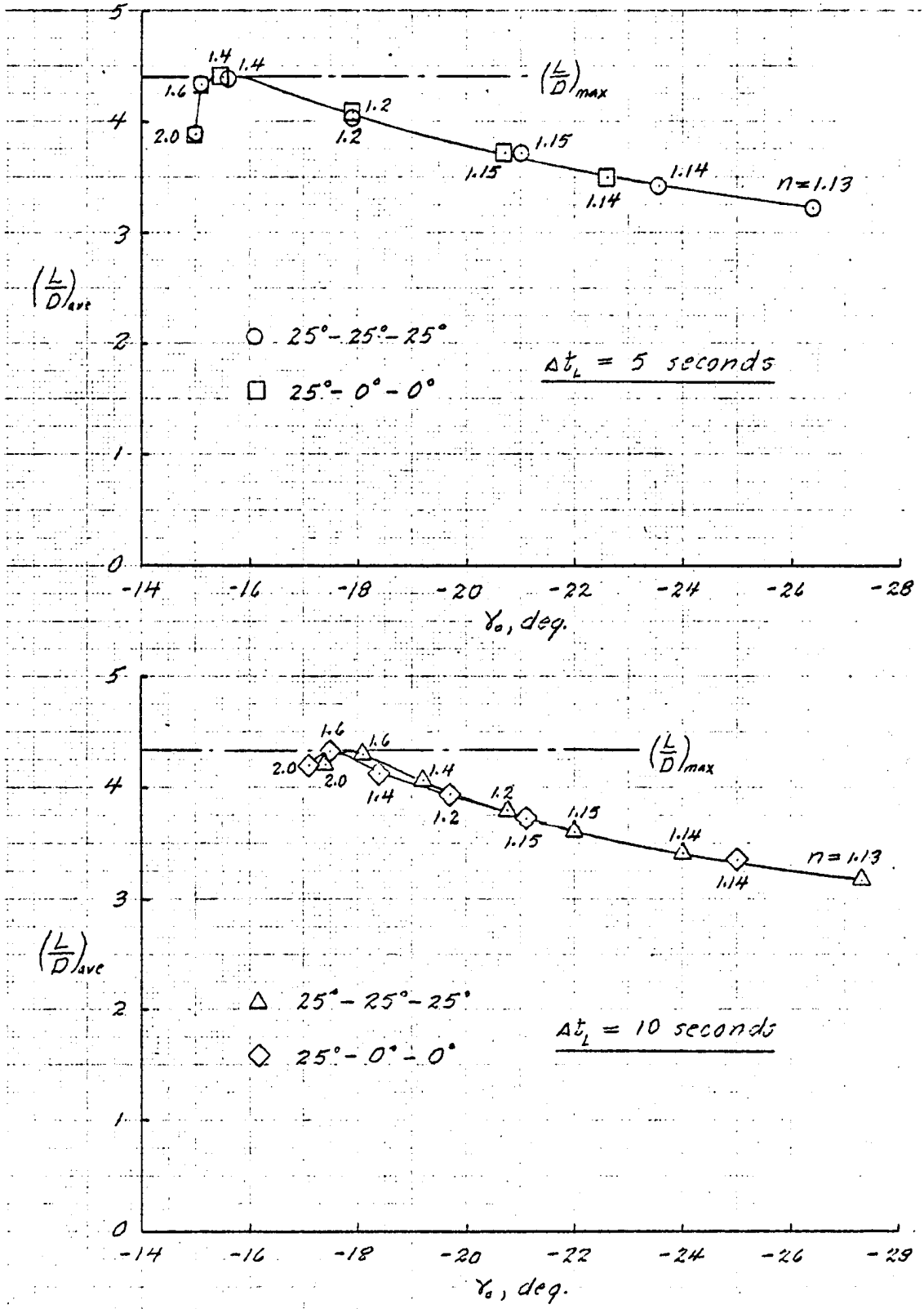

(b) Configurations 25°-25°-25°, 25°-0°-0°

Figure 14. Continued.

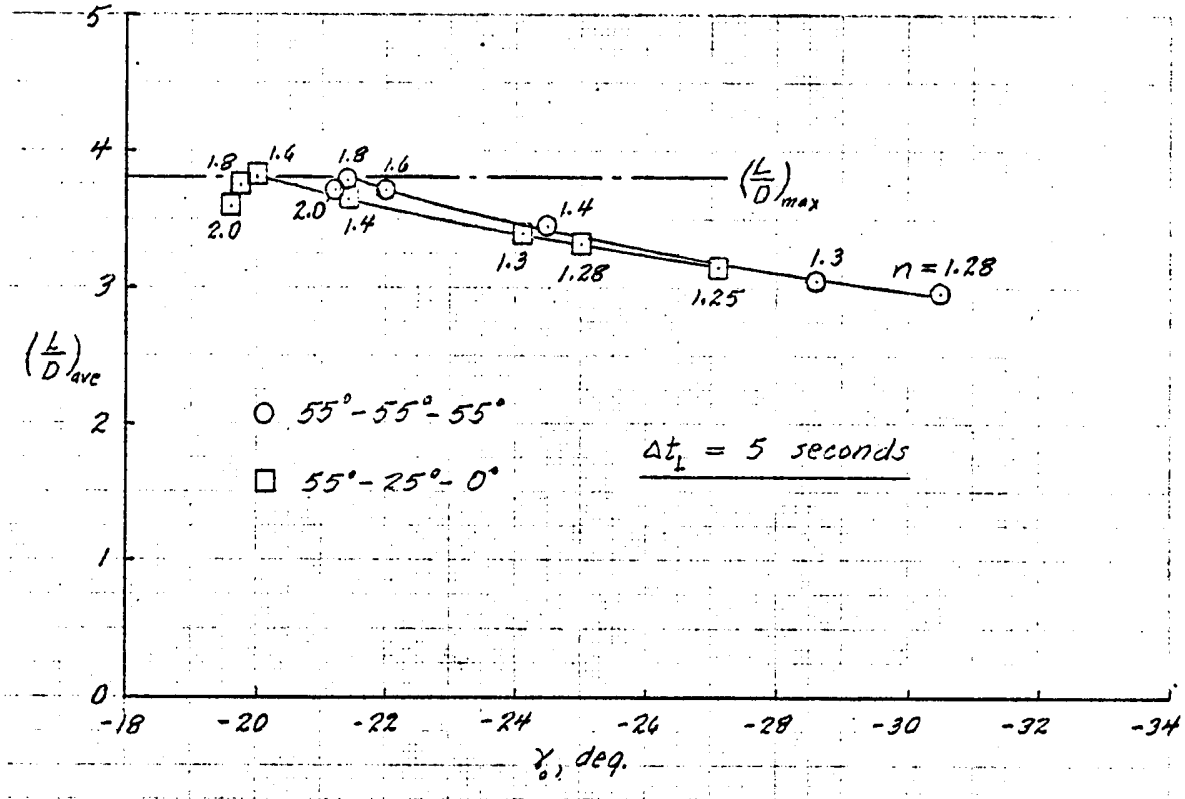

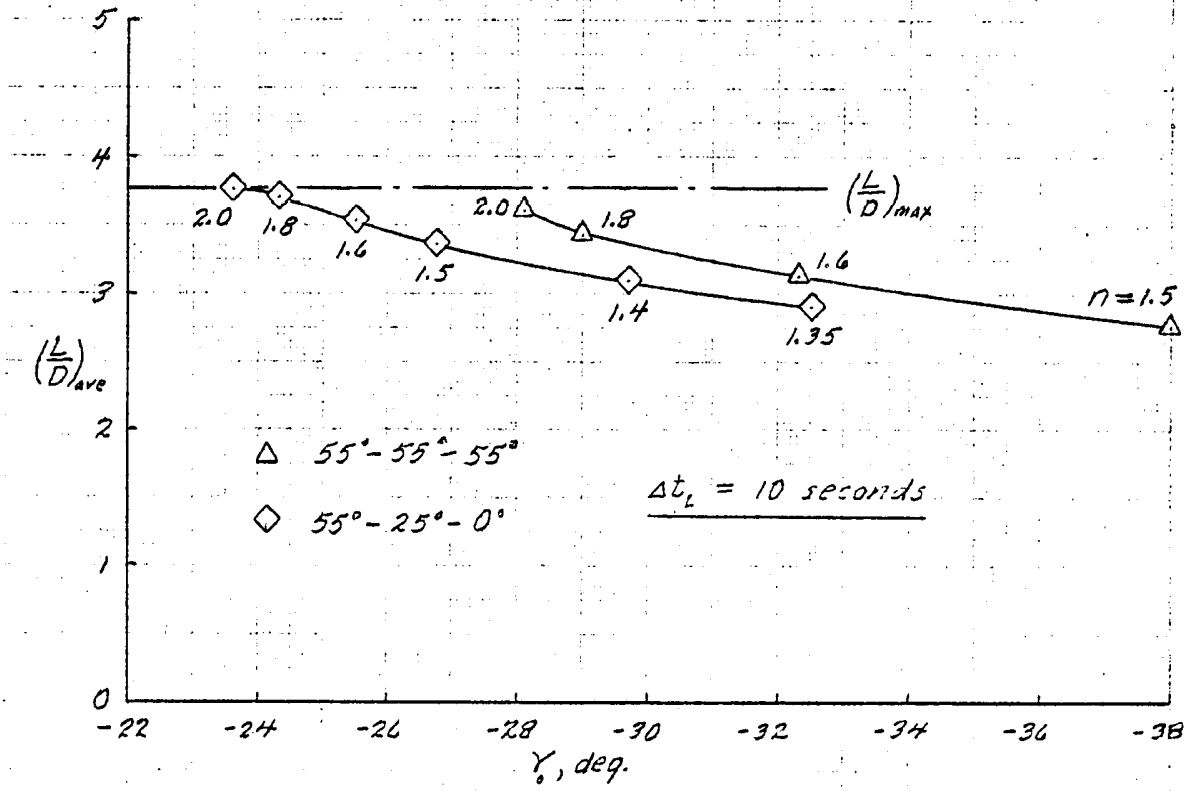

(c) Configurations 55°-55°-55°, 55°-25°-0°

Figure 14. Continued.

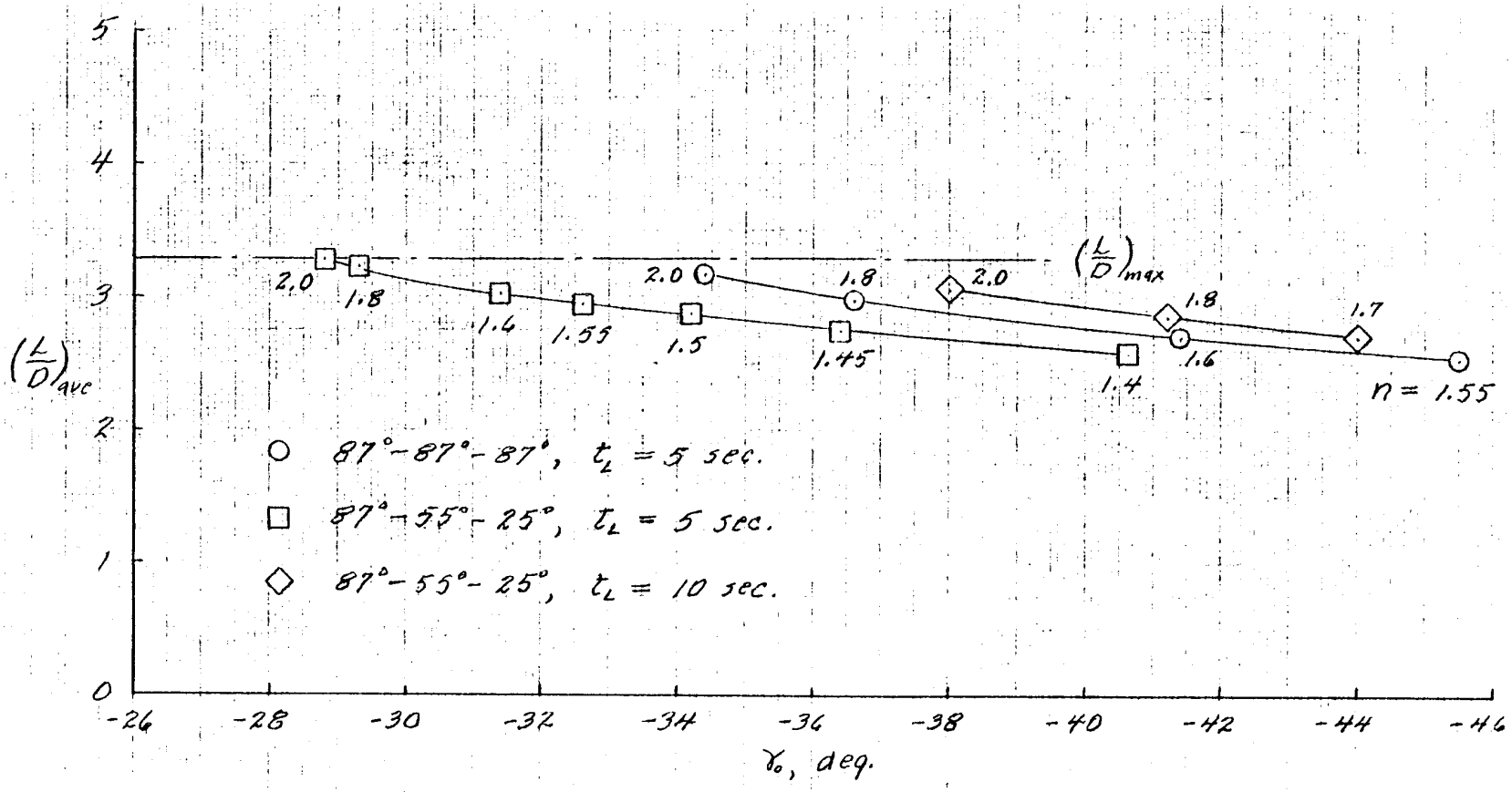

(d) Configurations 87°-87°-87°, 87°-55°-25°

Figure 14. Concluded.

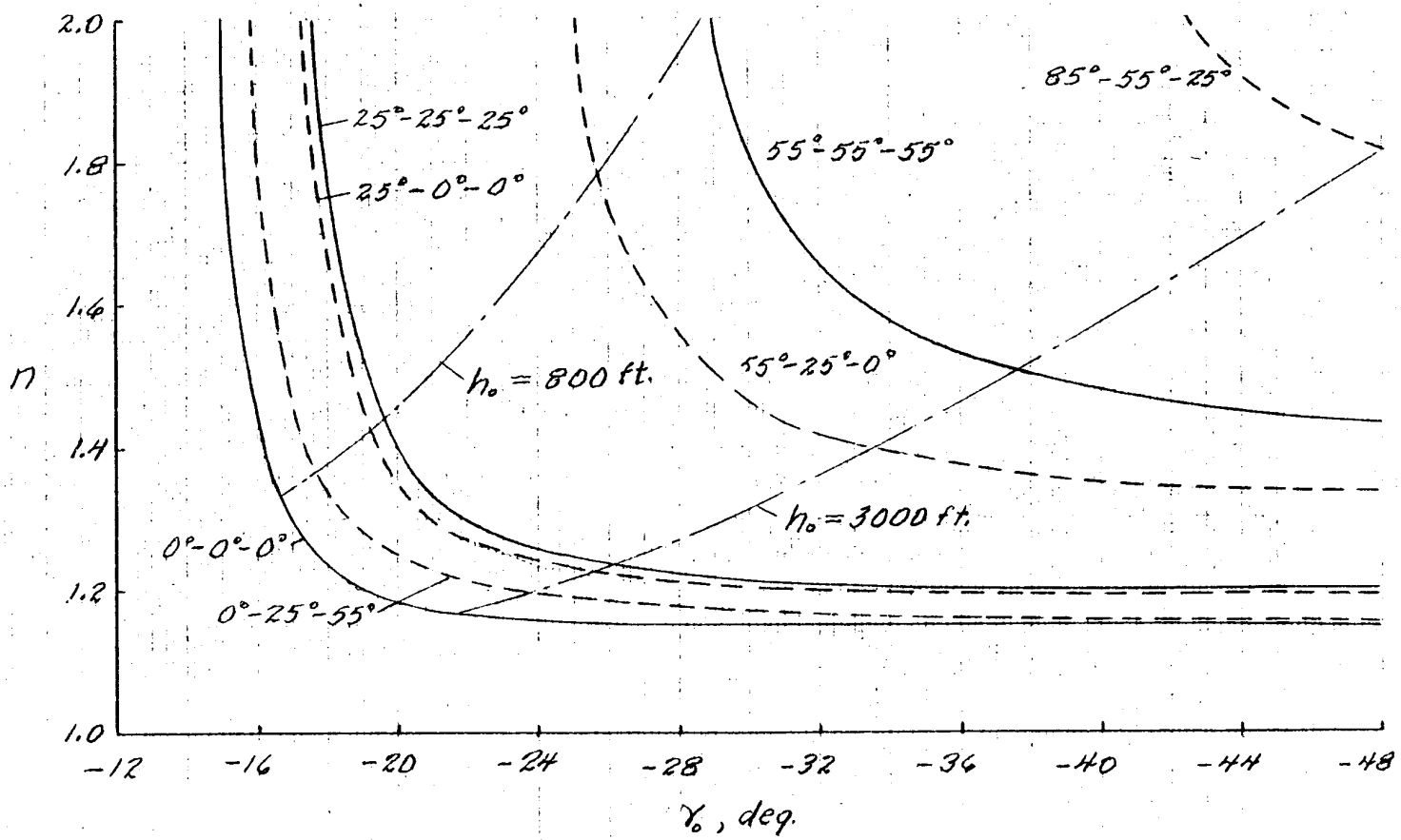

(a) Δt_L = 5 seconds

Figure 15, Modified landing boundaries for limitations of pilot altitude judgement for flare initiation. W/S = 56 psf.

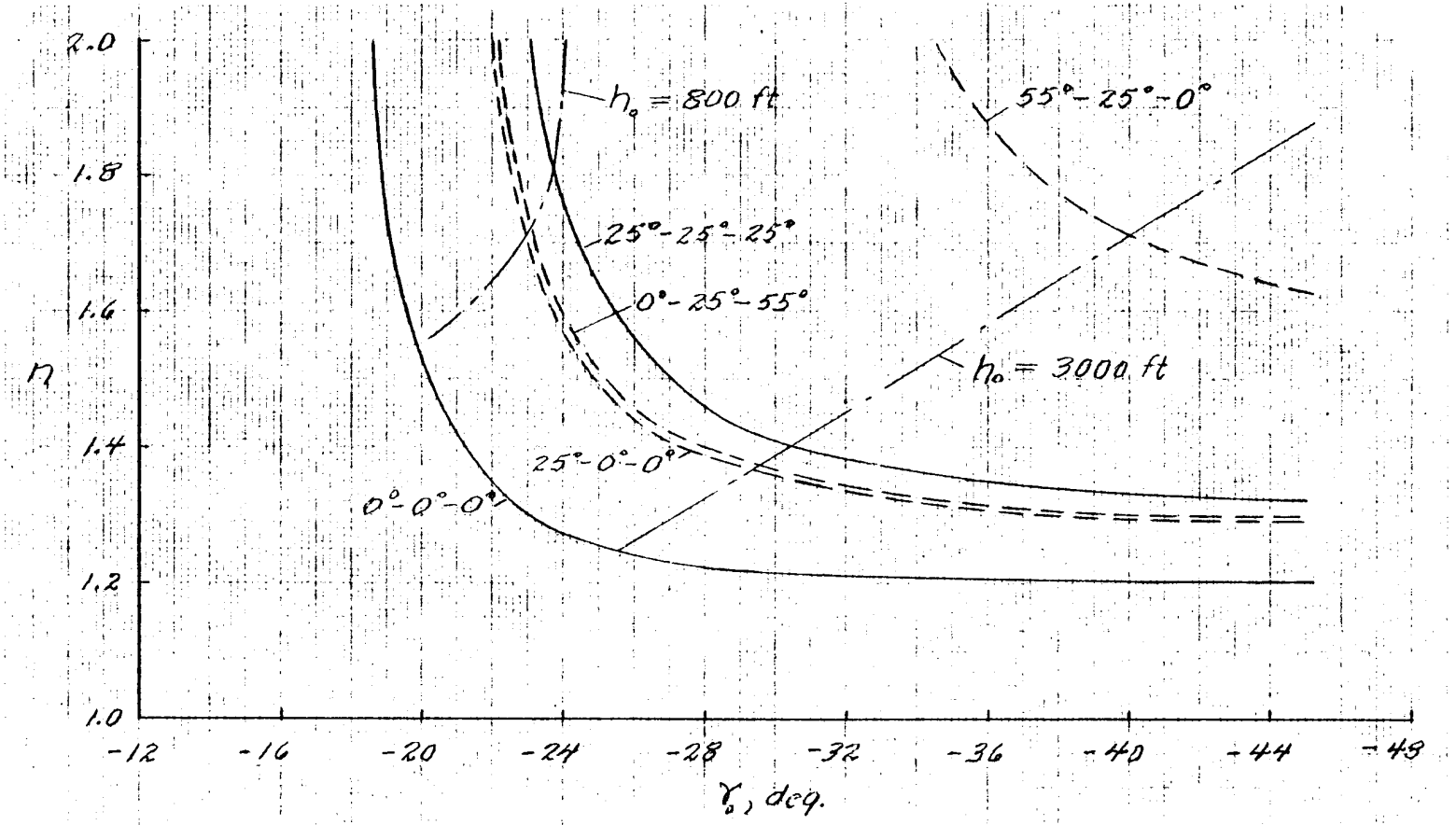

(b) $\Delta t_L = 10$ seconds

Figure 15. Concluded.

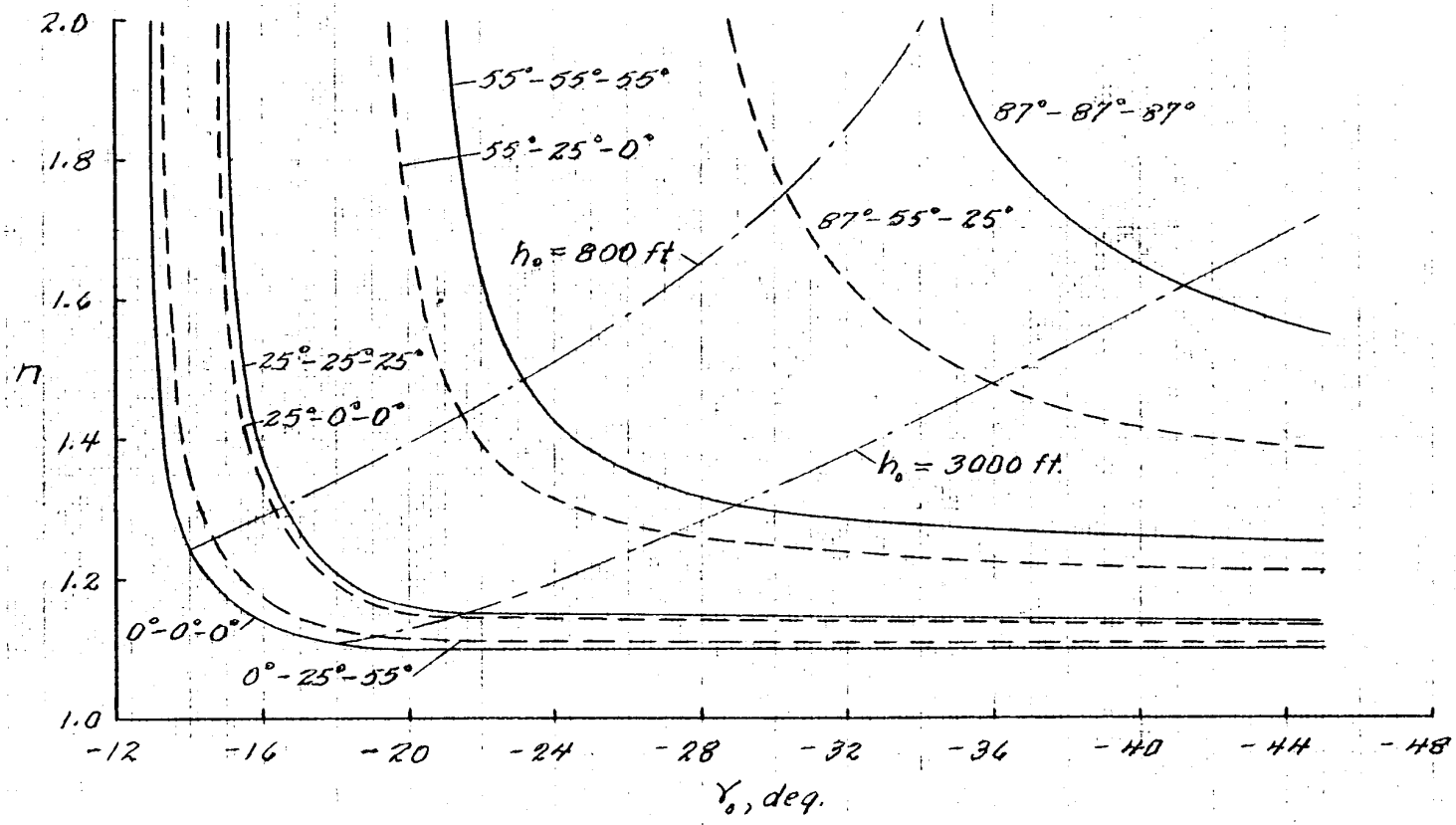

(a) Δt_L = 5 seconds

Figure 16. Modified landing boundaries for limitations of pilot altitude judgement for flare initiation. W/S = 70.6 psf.

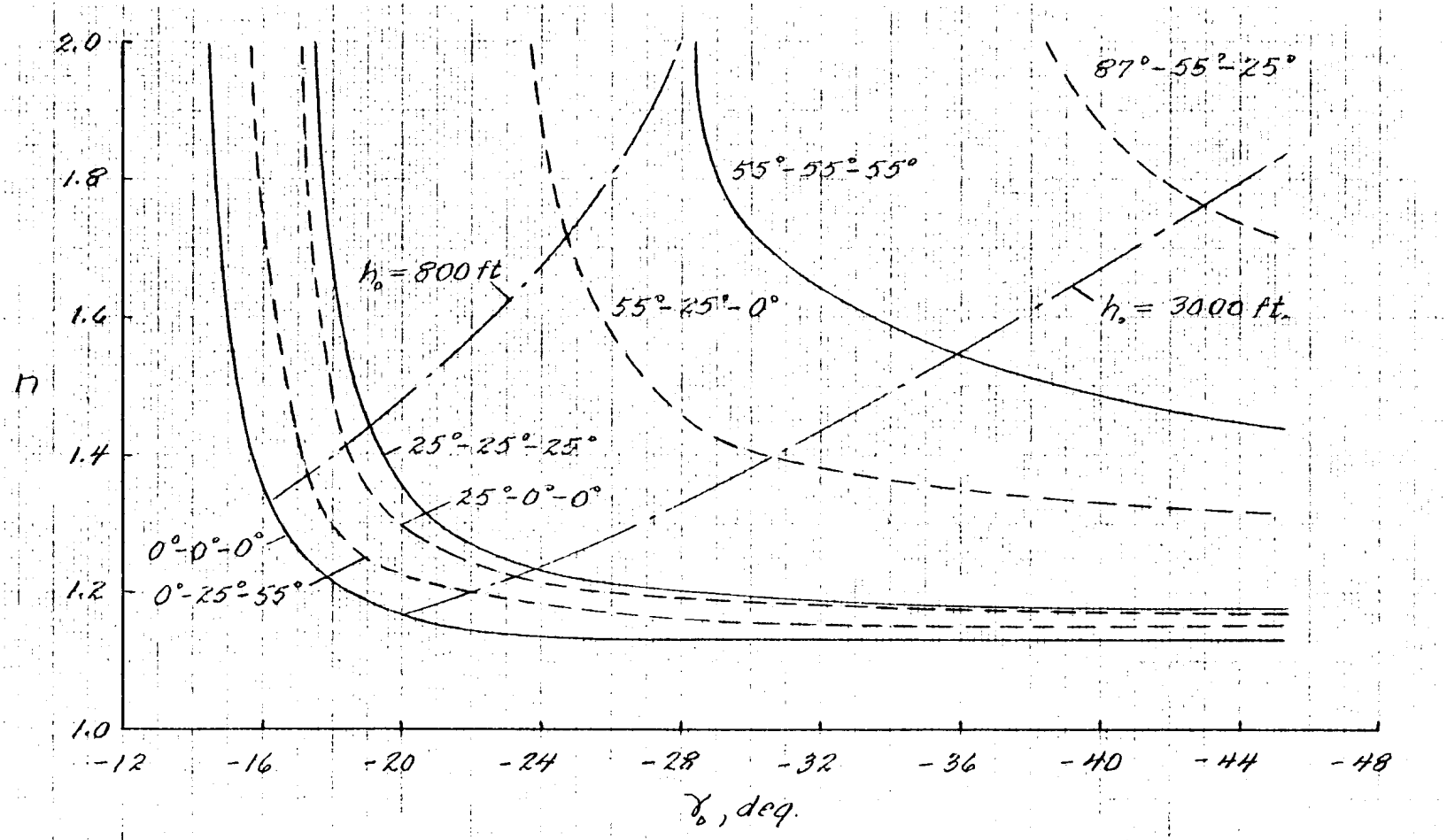

(b) Δt_L = 10 seconds

Figure 16. Concluded.

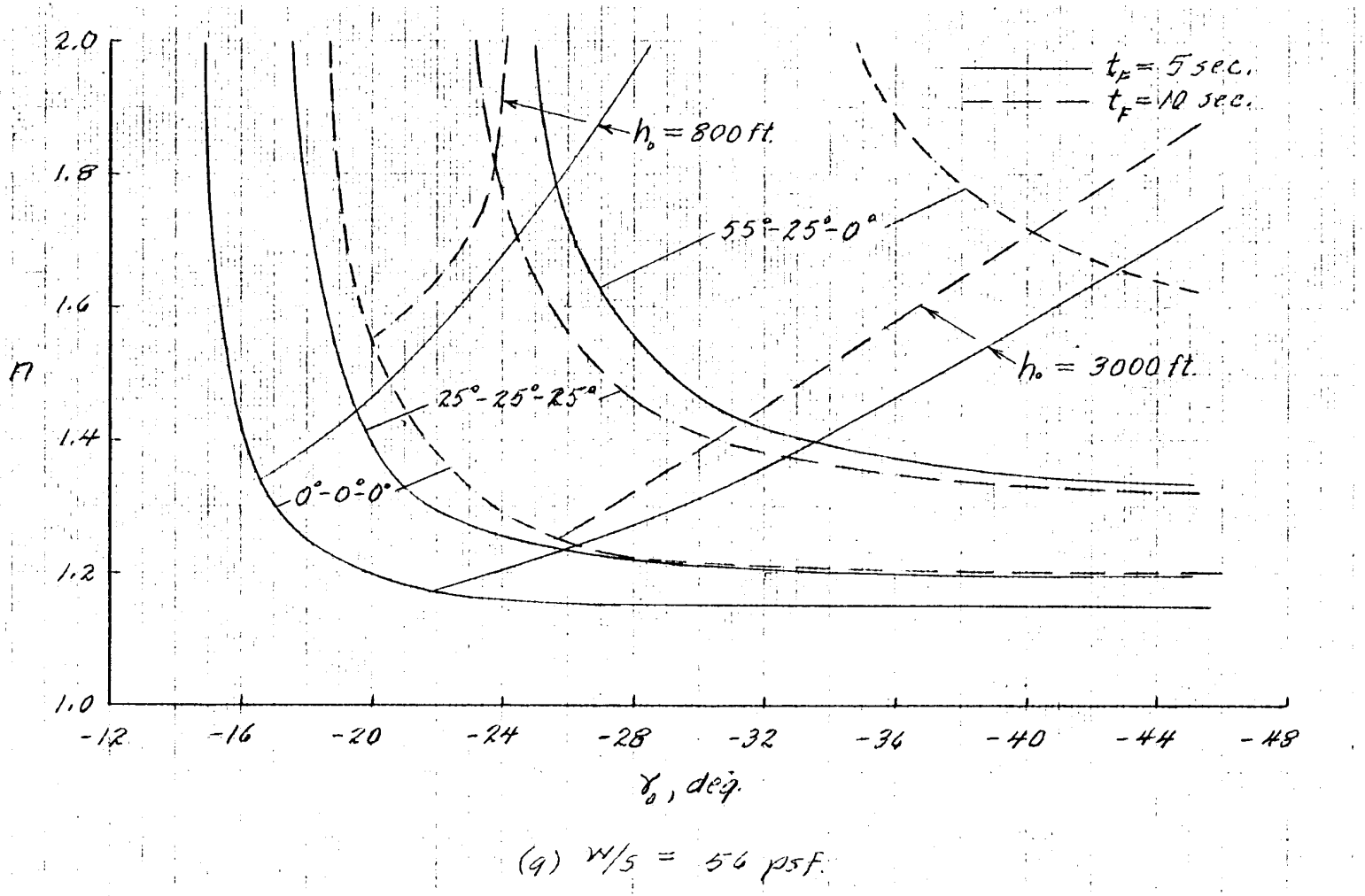

Figure 17. Effect of landing maneuver time on the landing boundaries modified for altitude limitations for flare initiation.

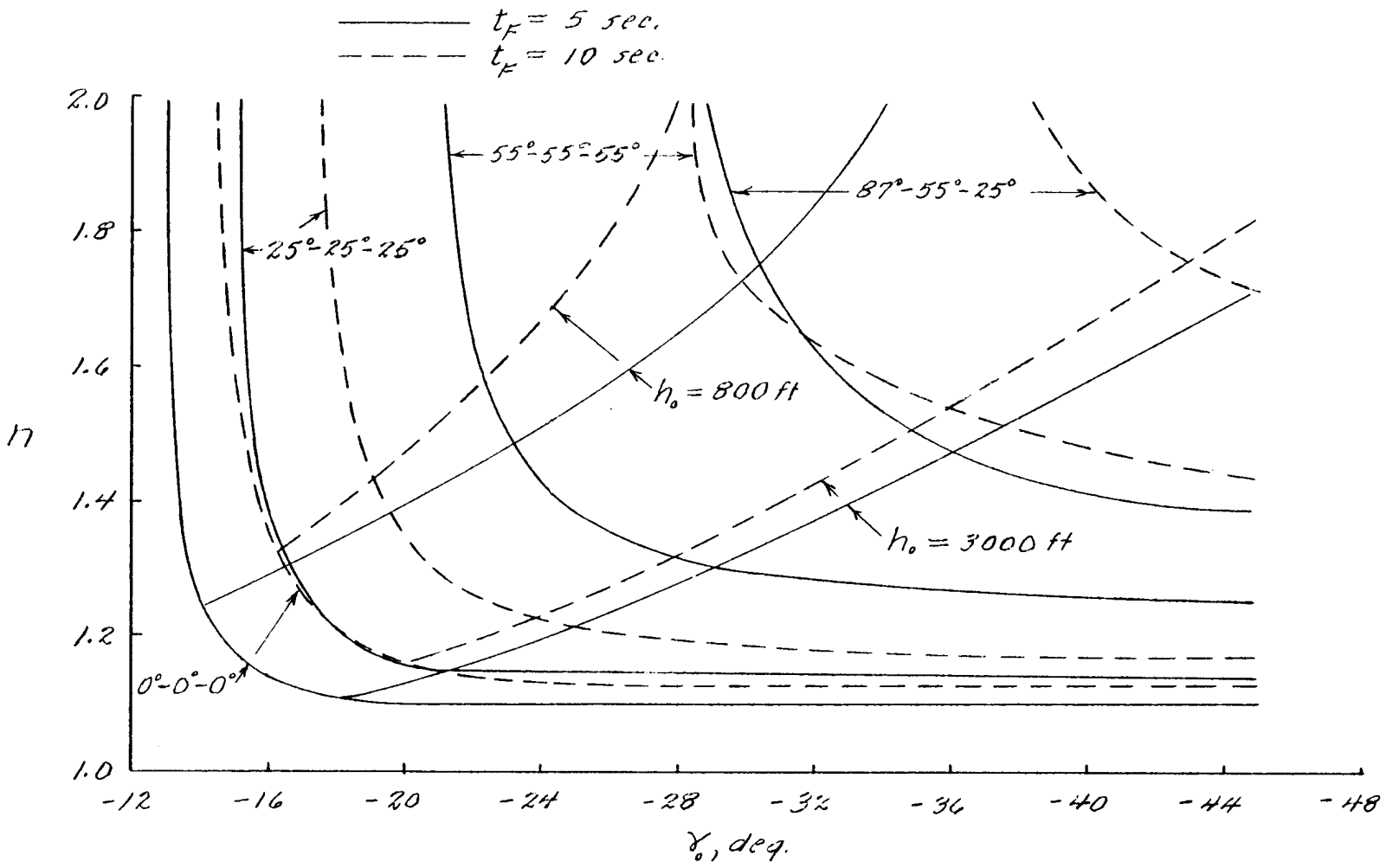

(b) W/S = 70.6 psf

Figure 17. Concluded.

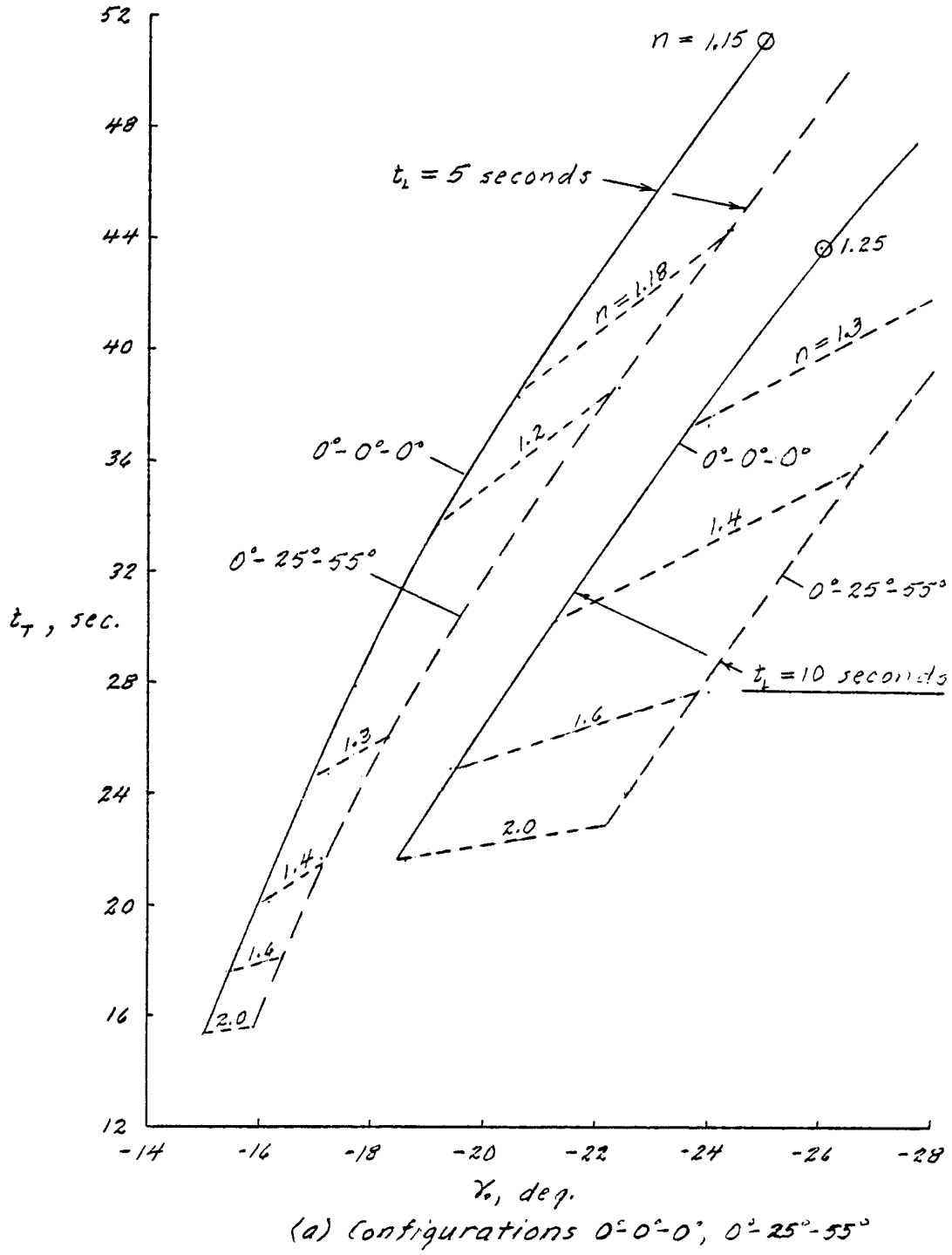

(a) Configurations 0°-0°-0°, 0°-25°-55°

Figure 18. Variation of total landing maneuver time with initial glide angle. W/S = 56 psf.

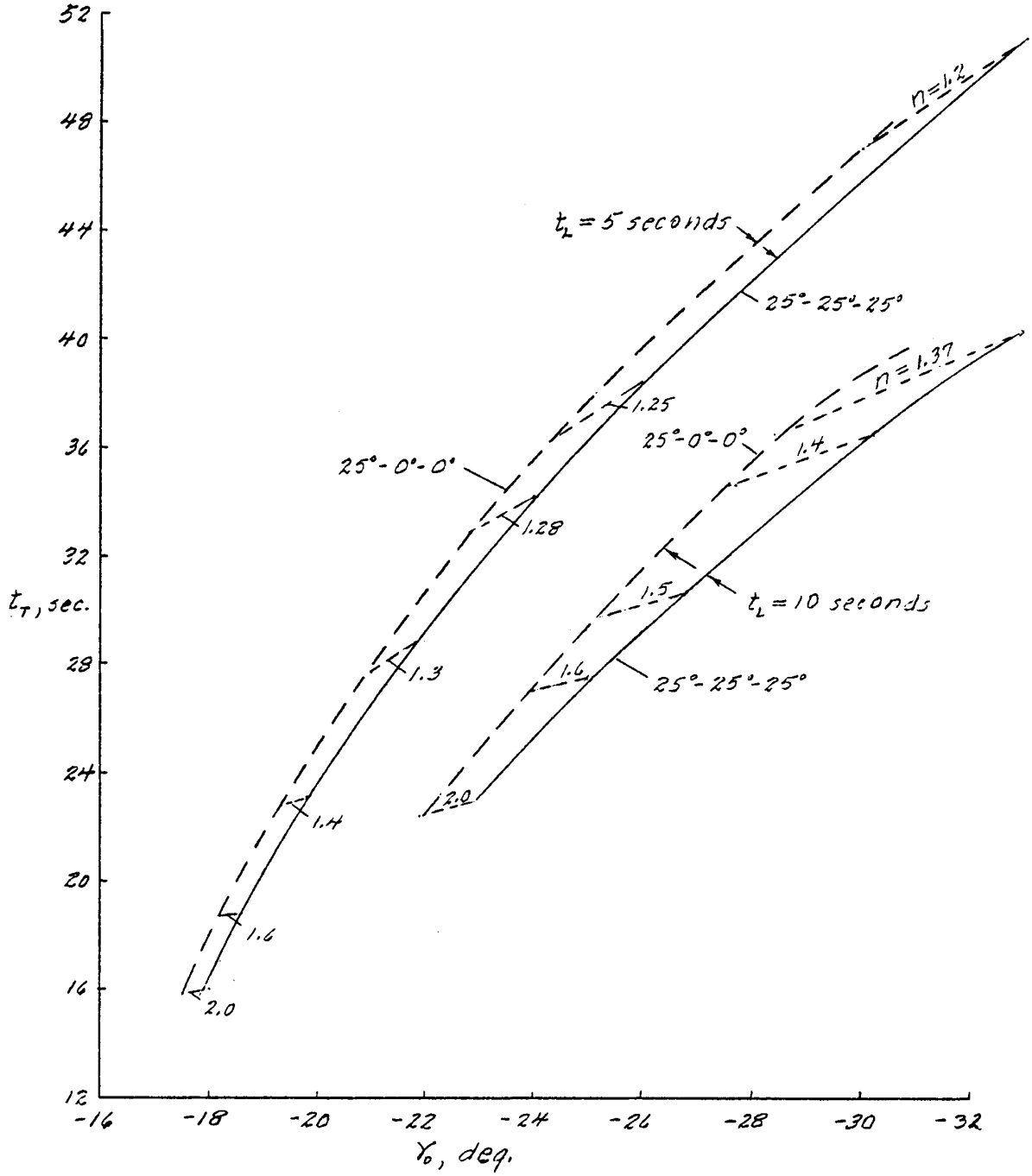

(b) Configurations 25°-25°-25°, 25°-0°-0°

Figure 18. Continued.

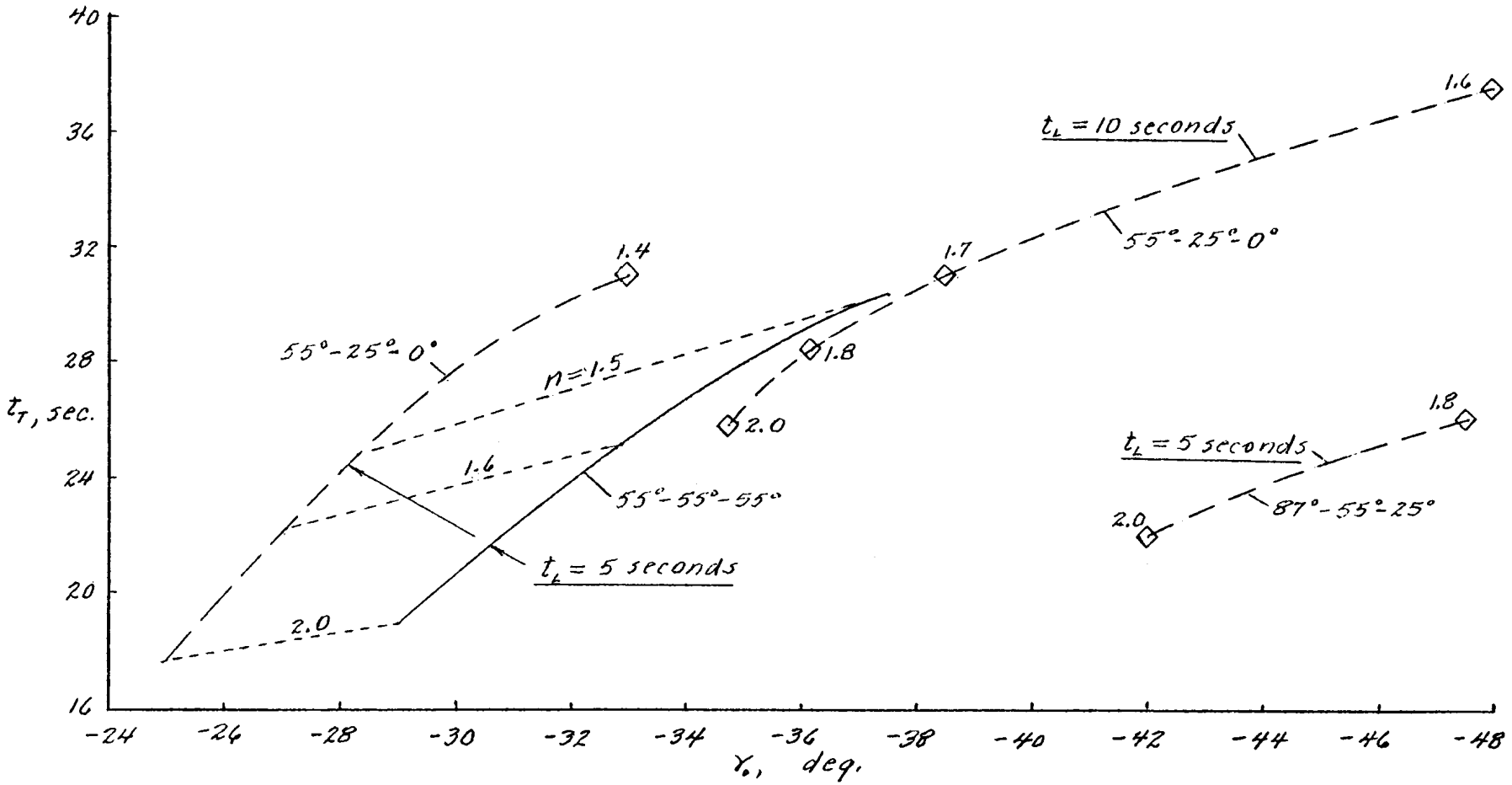

(c) Configurations 55°-55°-55°; 55°-25°-0°, 87°-55°-25°

Figure 18. Concluded.

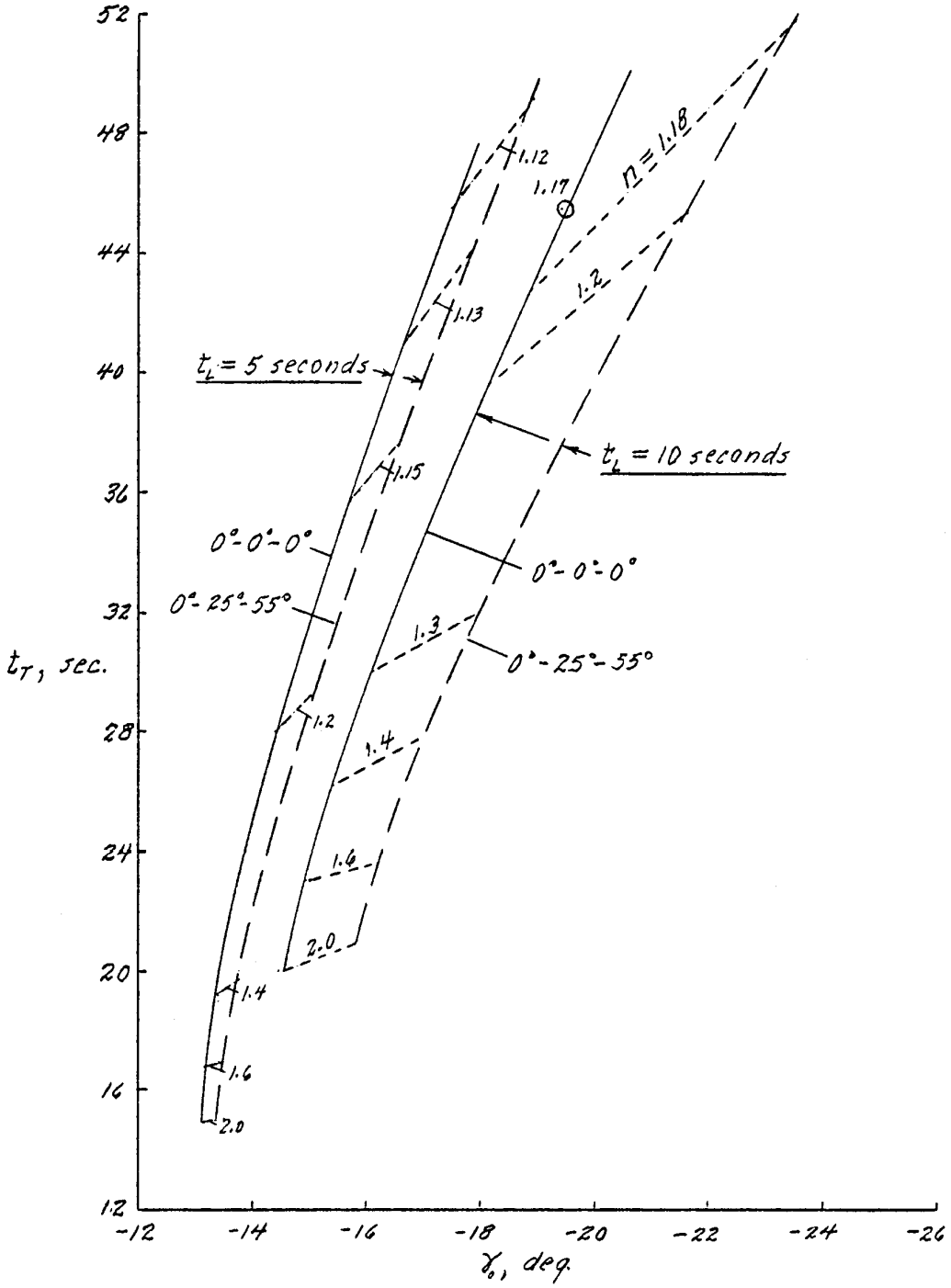

(a) Configurations 0°-0°-0°; 0°-25°-55°

Figure 19. Variation of total landing maneuver time with initial glide angle. W/S = 70.6 psf.

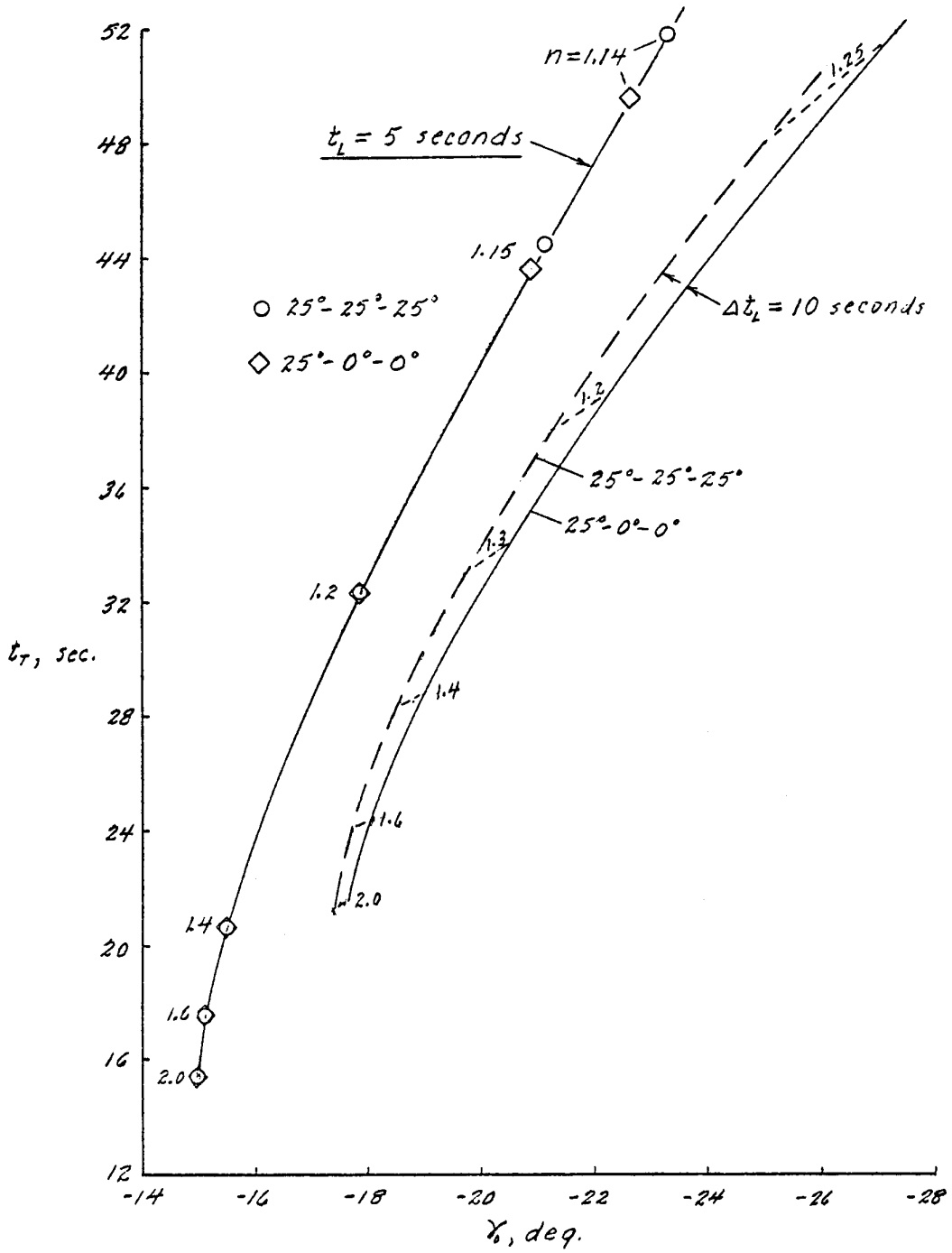

(b) Configurations 25°-25°-25°, 25°-0°-0°

Figure 19. Continued.

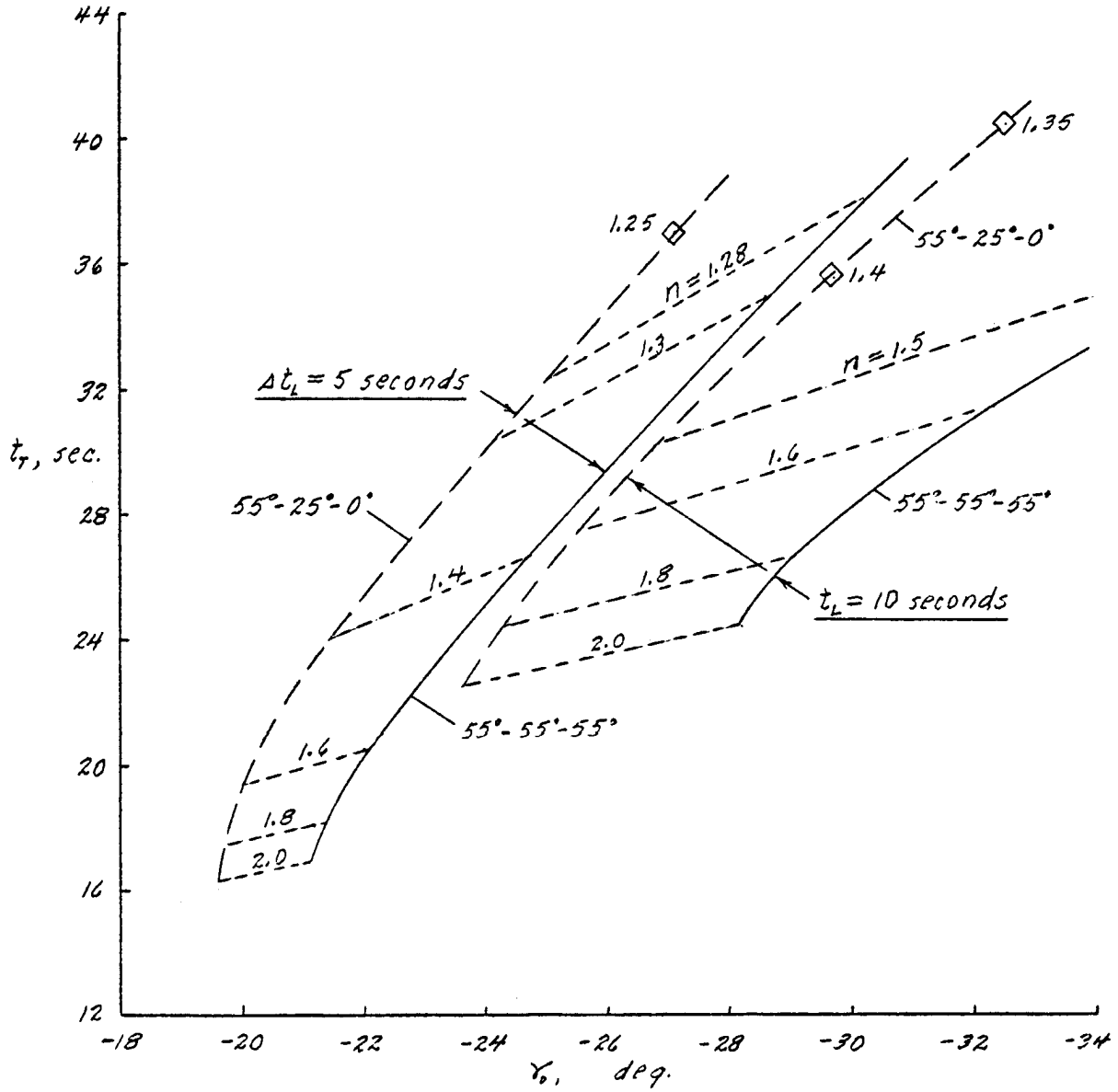

(c) Configurations 55°-55°-55°; 55°-25°-0°

Figure 19. Continued.

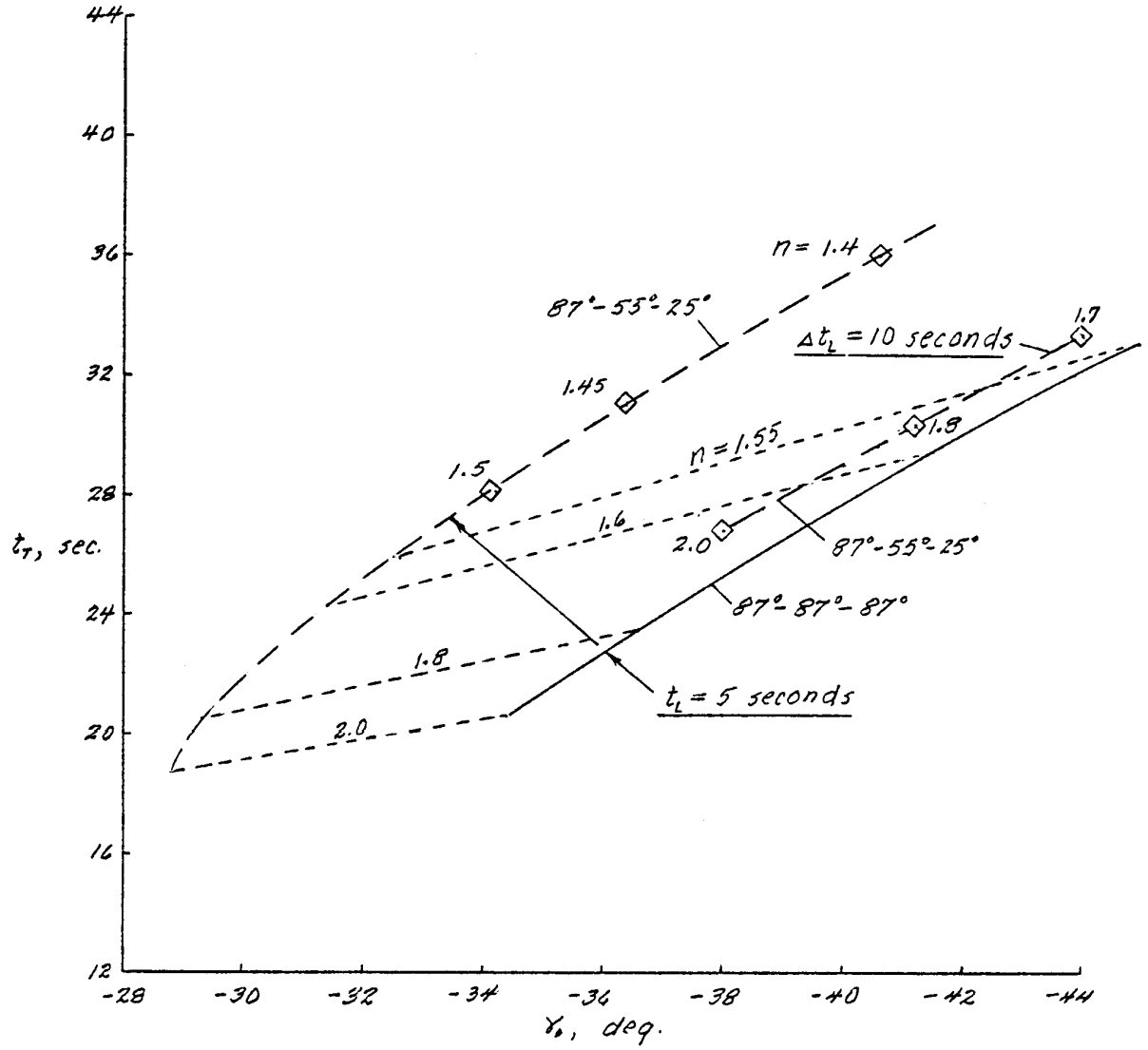

(d) Configurations 87°-87°-87°, 87°-55°-25°

Figure 19. Concluded.

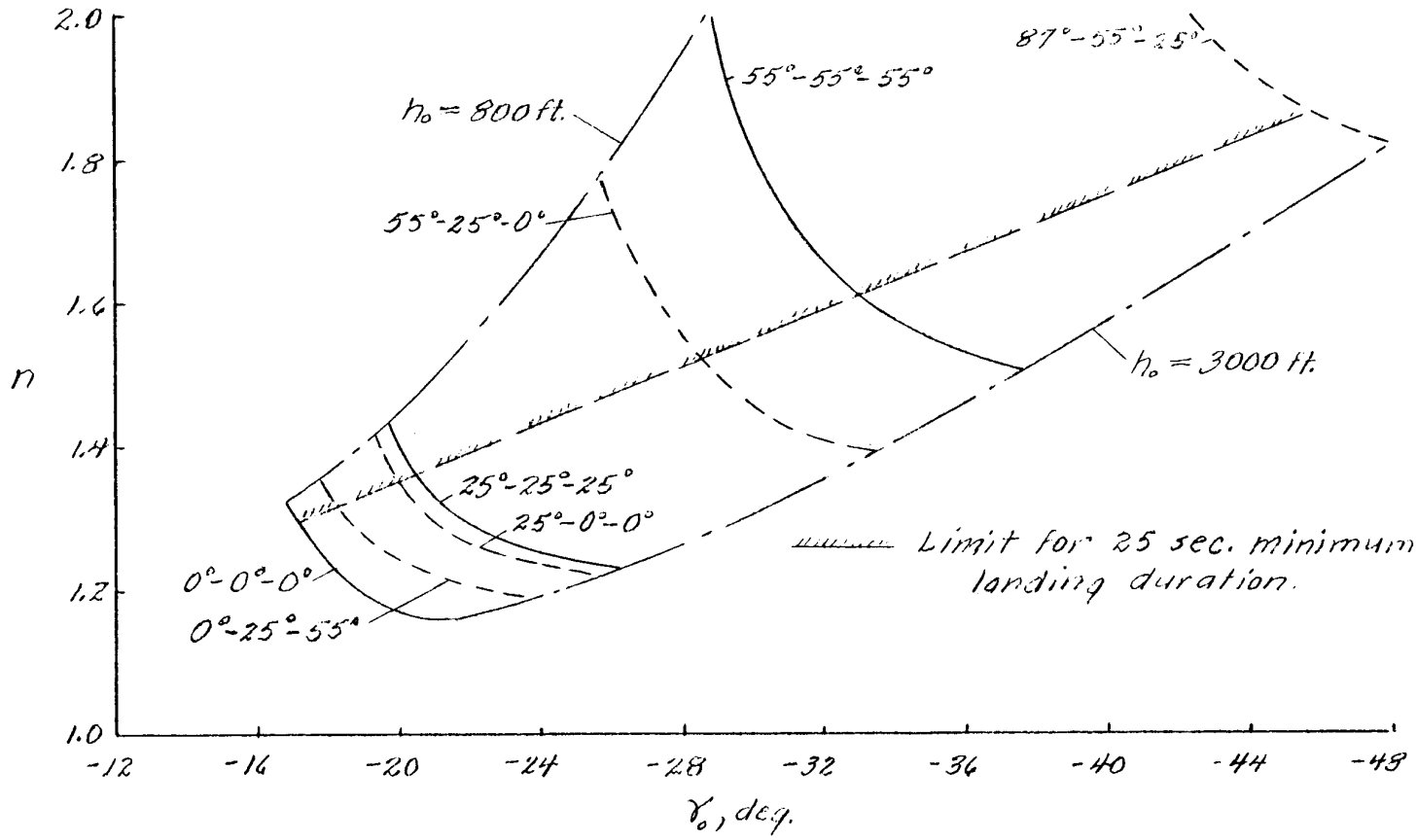

(a) Δt_L = 5 seconds

Figure 20. Effect of 25 second total landing maneuver time on landing maneuver boundaries. W/S = 56 psf.

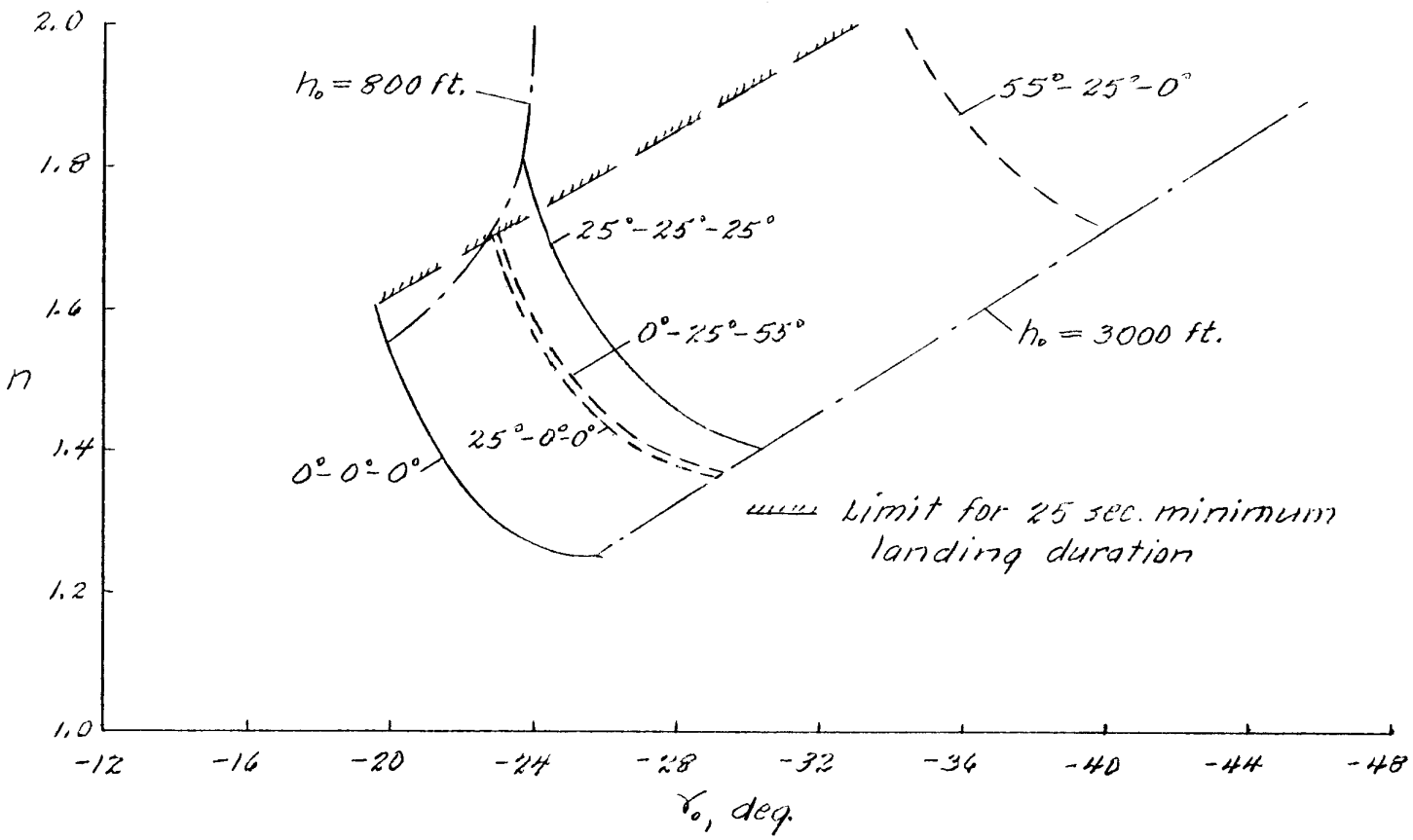

(b) Δt_L = 10 seconds

Figure 20. Concluded.

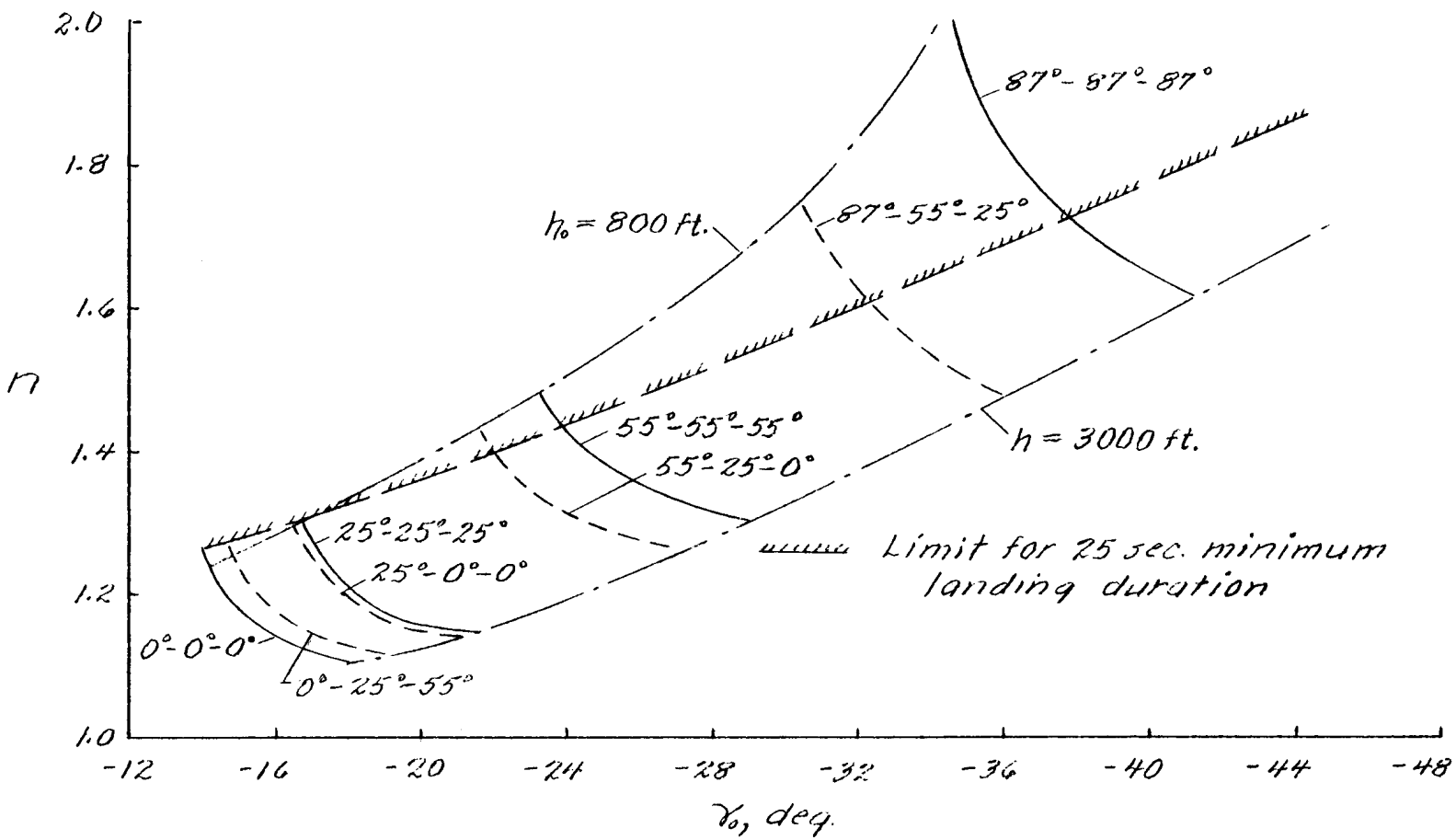

(a) Δt_L = 5 seconds

Figure 21. Effect of 25 second total landing maneuver time on the landing maneuver boundaries. W/S = 70.6 psf.

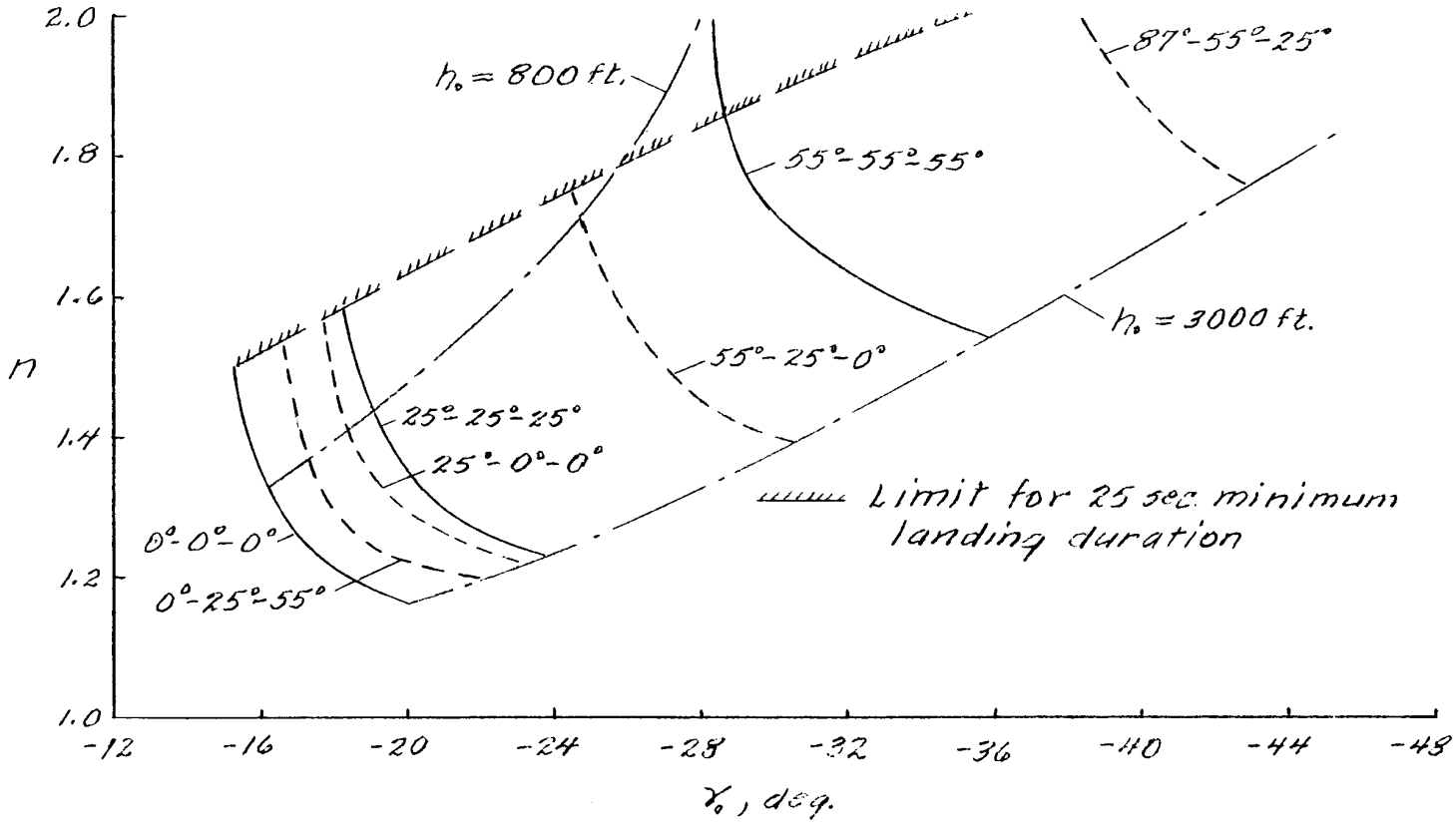

(b) Δt_L = 10 seconds

Figure 21. Concluded.

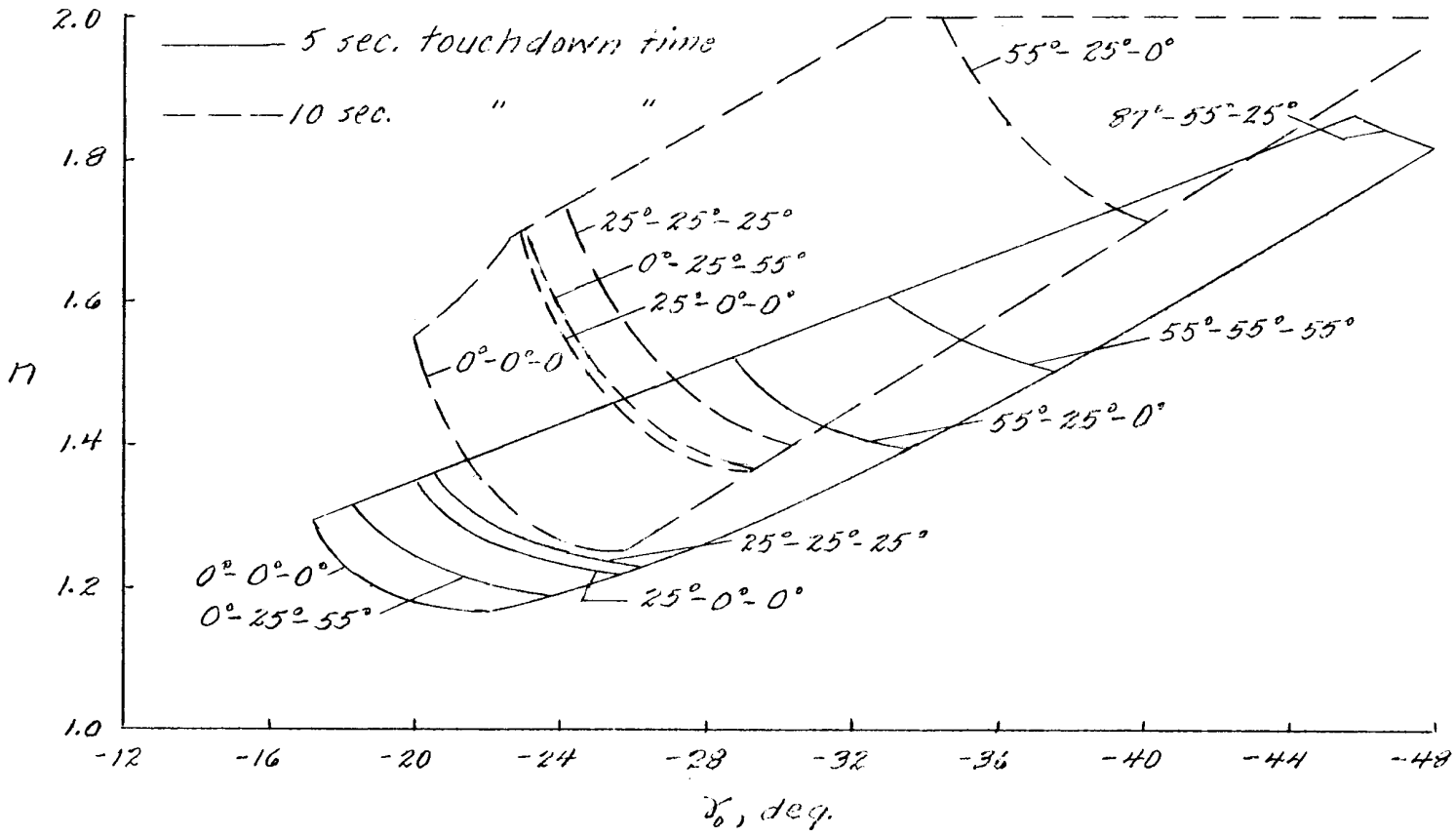

(a) $W/S = 56$ psf

Figure 22. Comparison of final landing maneuver boundaries for touchdown maneuver times of 5 and 10 seconds.

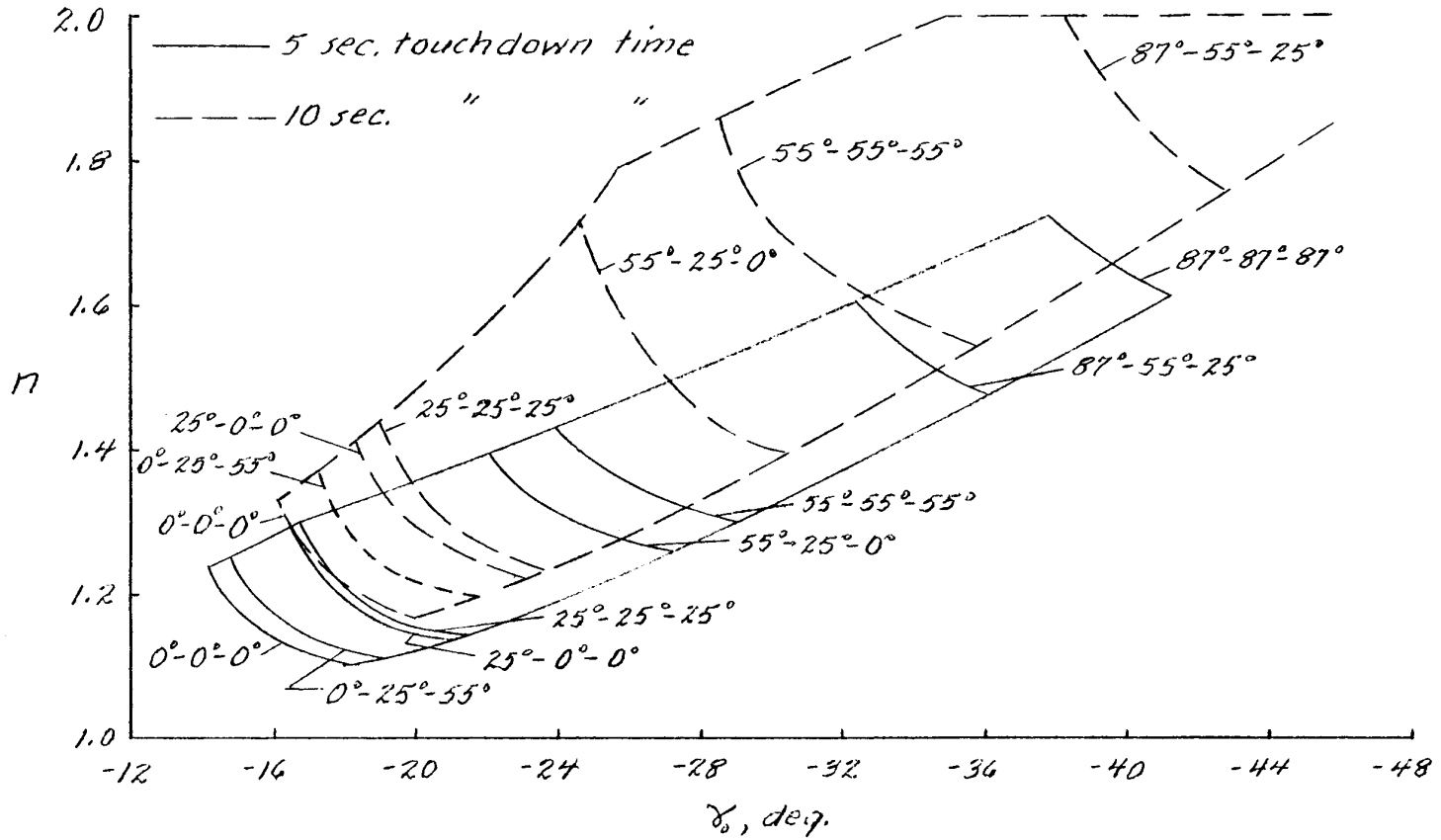

(b) W/S = 70.4 psf

Figure 22. Concluded.

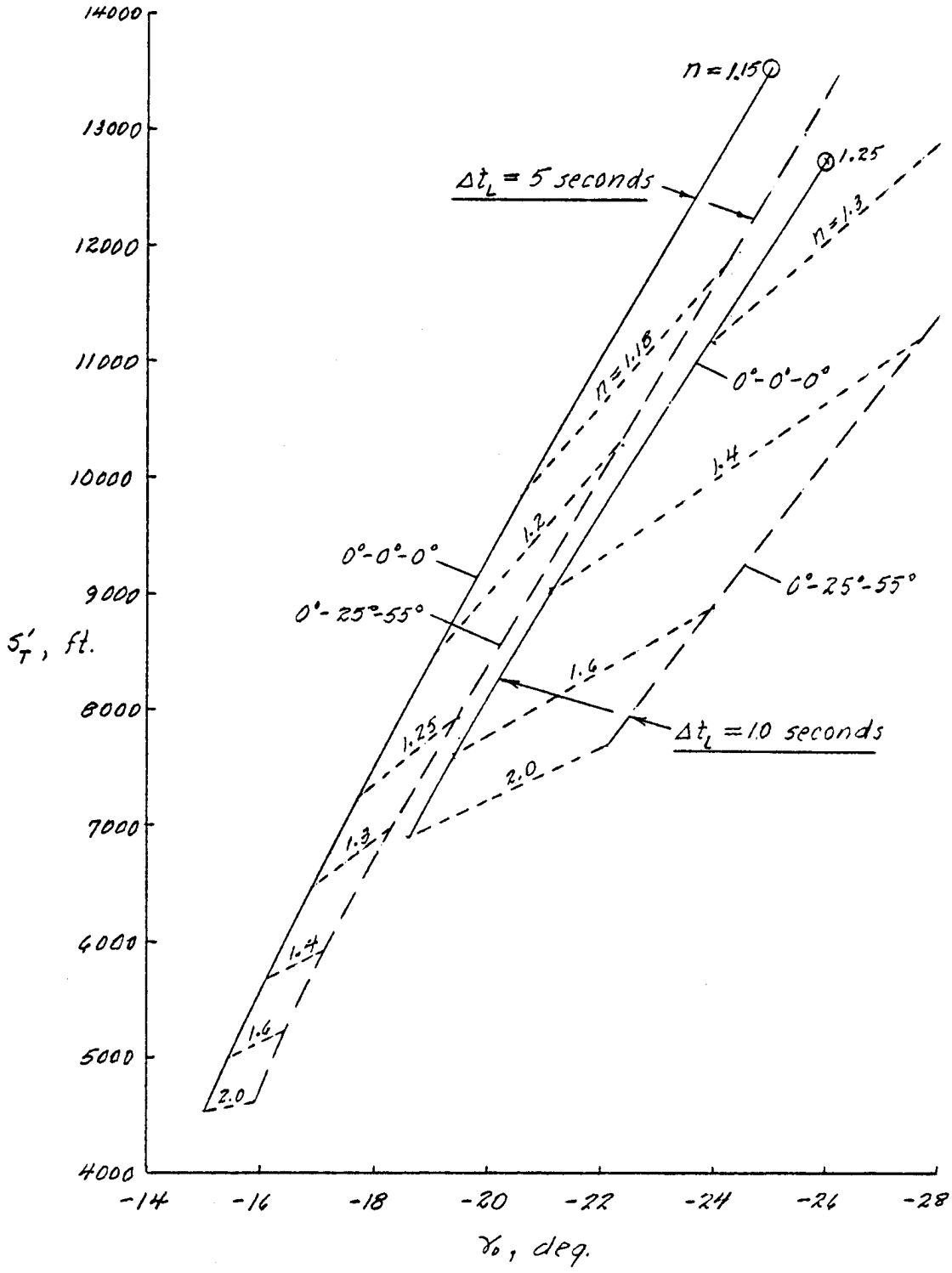

(a) Configurations 0°-0°-0°, 0°-25°-55°

Figure 23. Variation with initial glide angle of the landing distance from aimpoint to touchdown. W/S = 56 psf.

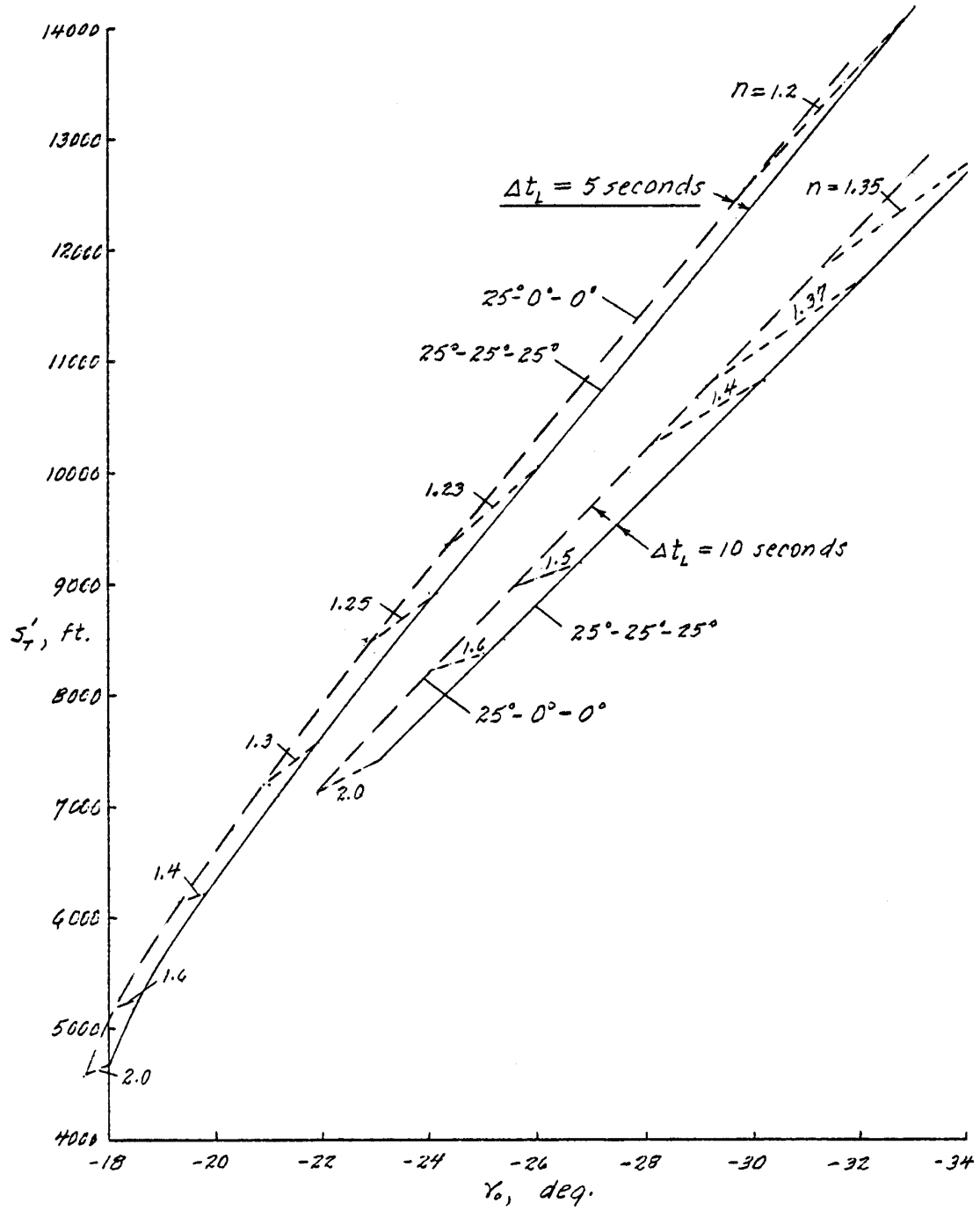

(b) Configurations 25°-25°-25°, 25°-0°-0°

Figure 23. Continued.

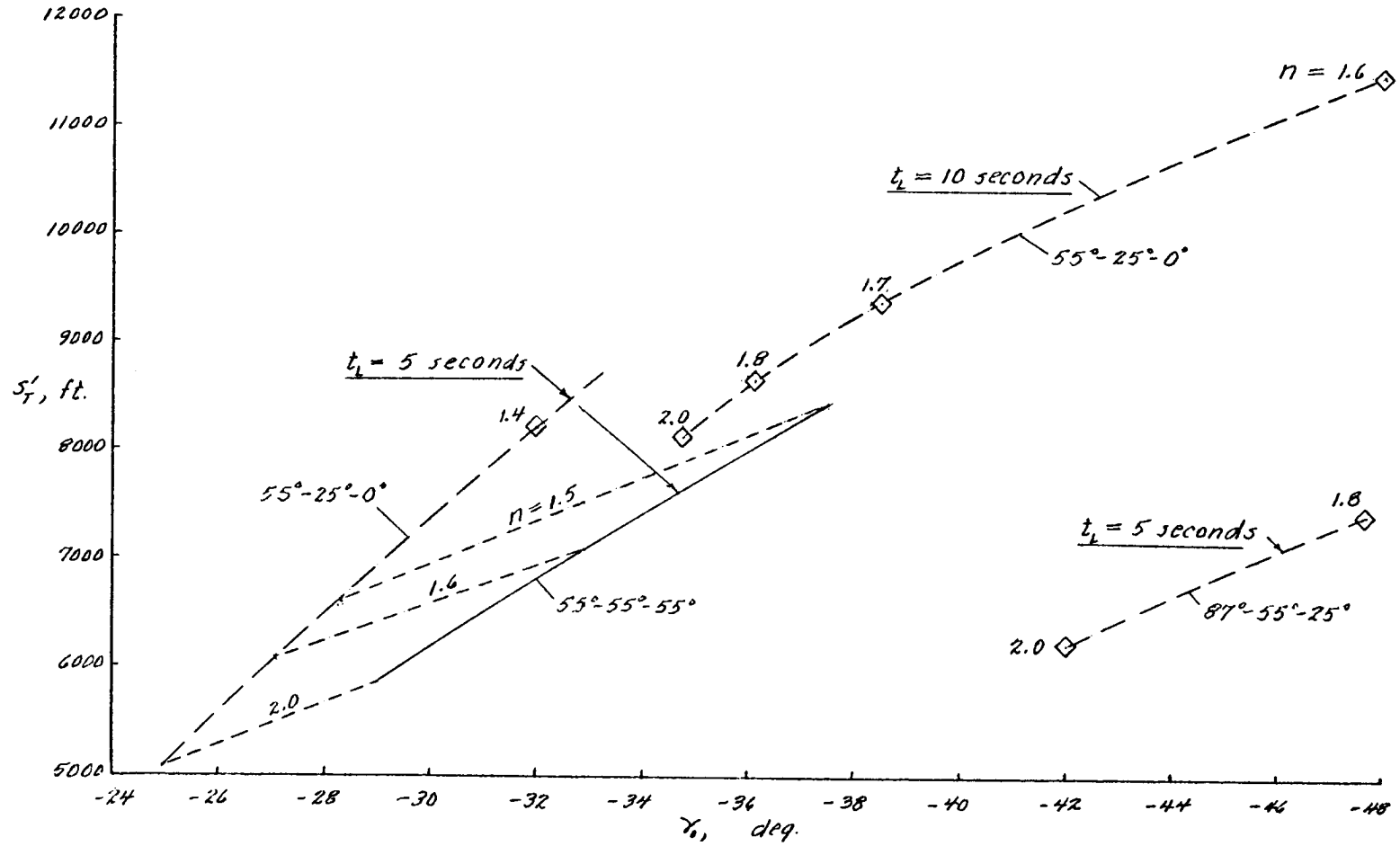

(c) Configurations 55°-55°-55°; 55°-25°-0°; 87°-55°-25°

Figure 23. Concluded.

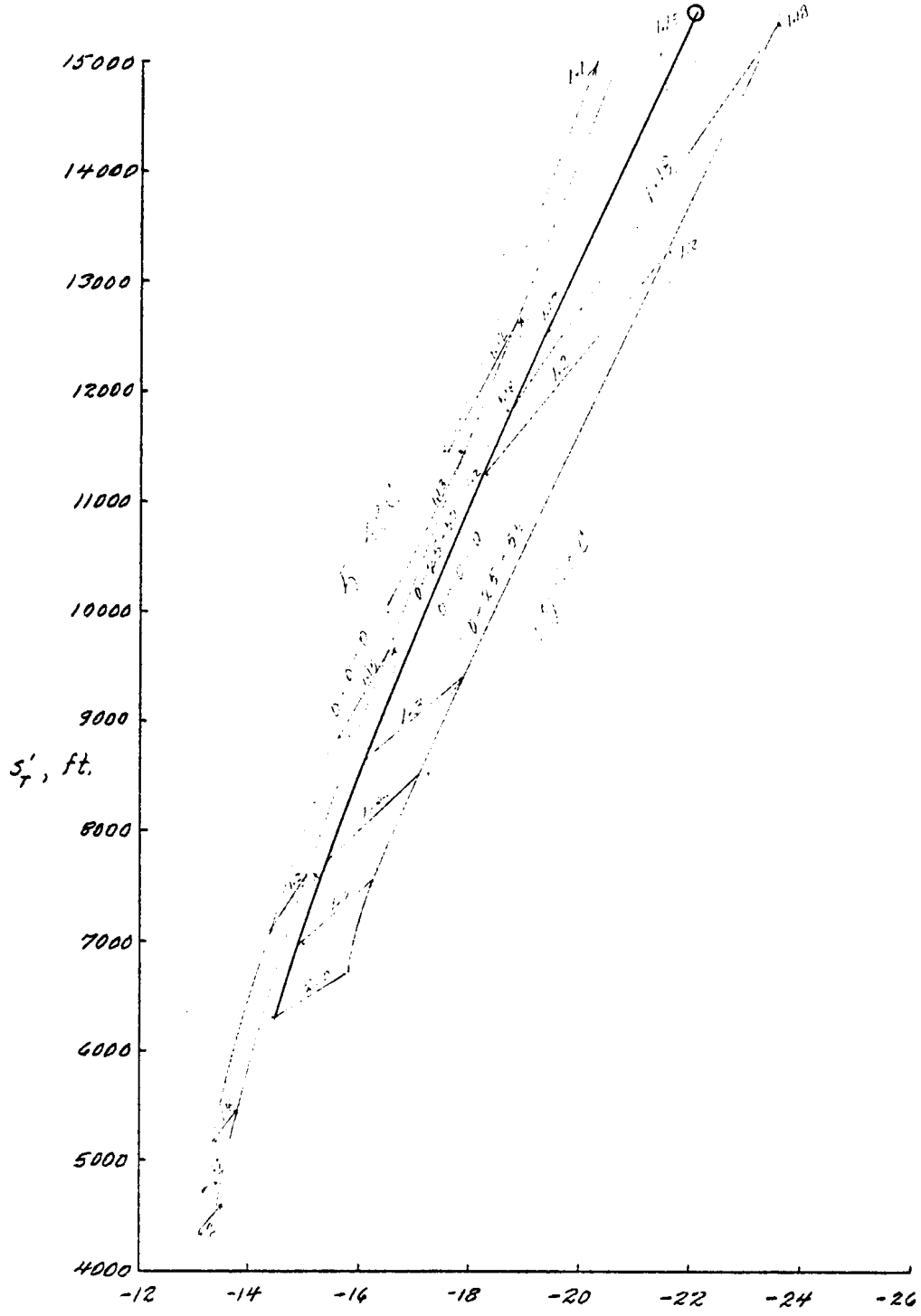

(a) Configurations 0°-0°-0°, 0°-25°-55°

Figure 24. Variation with initial glide angle of the landing distance from aimpoint to touchdown. $W/S = 70.6$ psf.

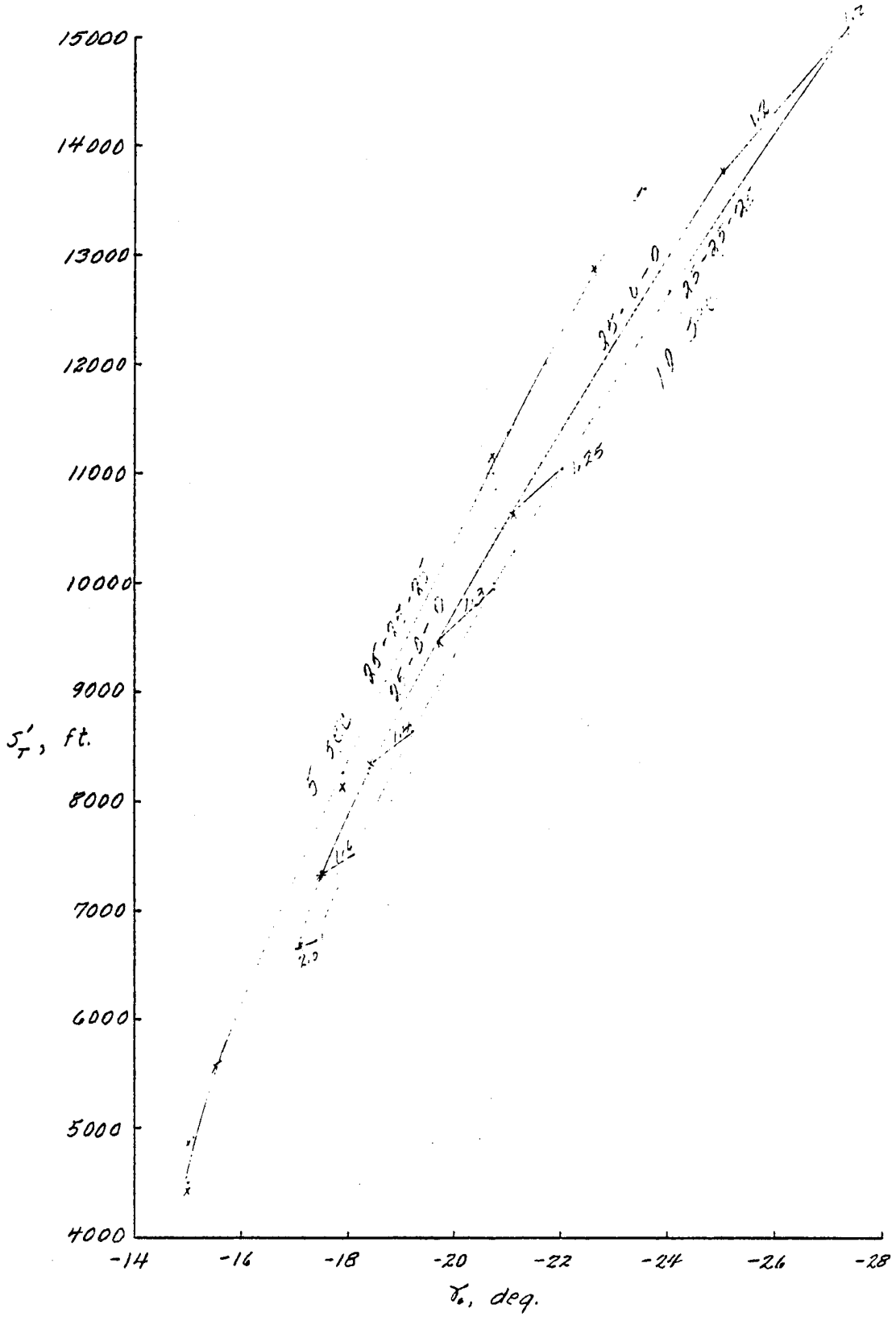

(b) Configurations 25°-25°-25°, 25°-0°-0°

Figure 24. Continued.

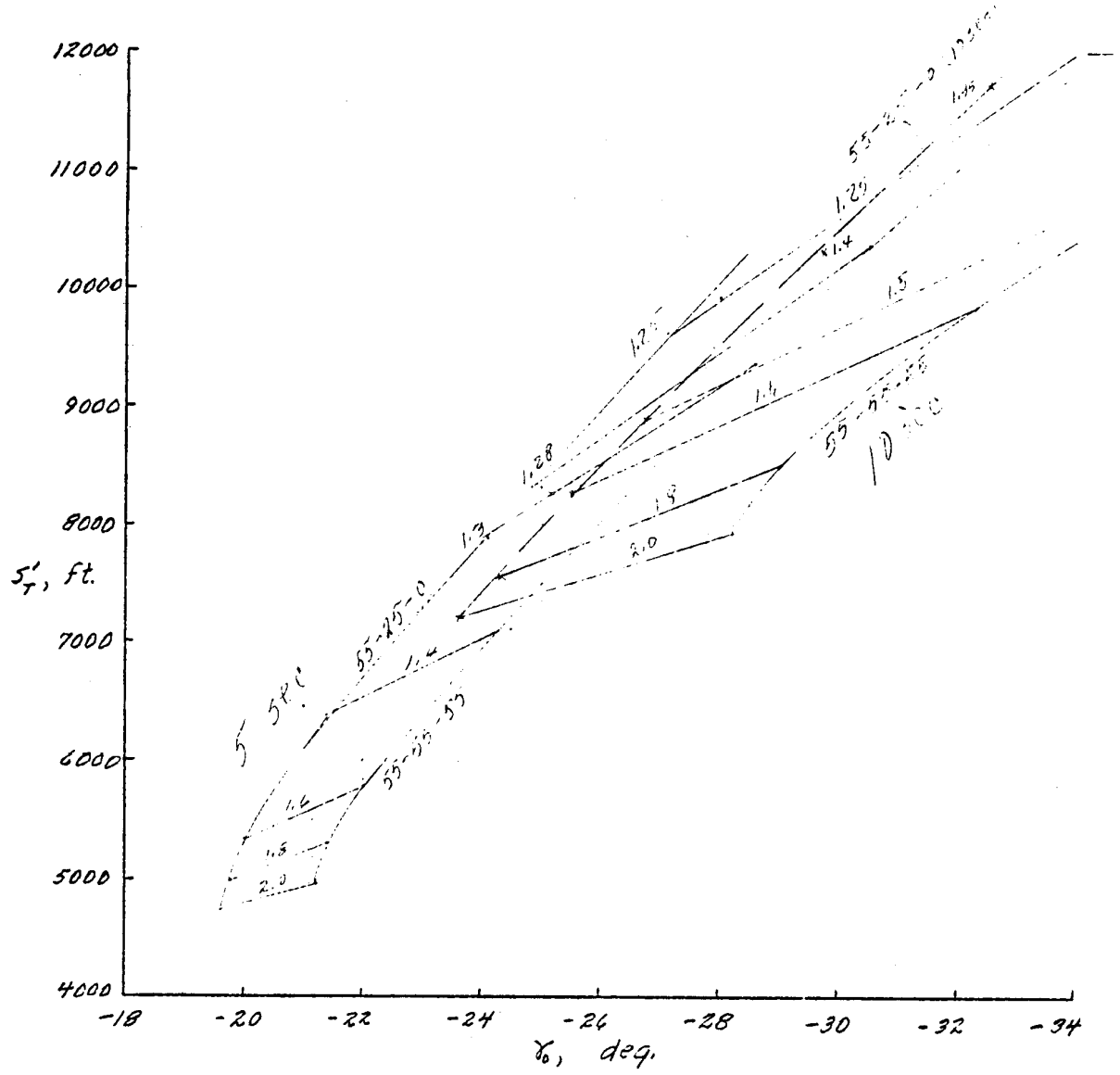

(c) Configurations 55°-55°-55°; 55°-25°-0°

Figure 24. Continued.

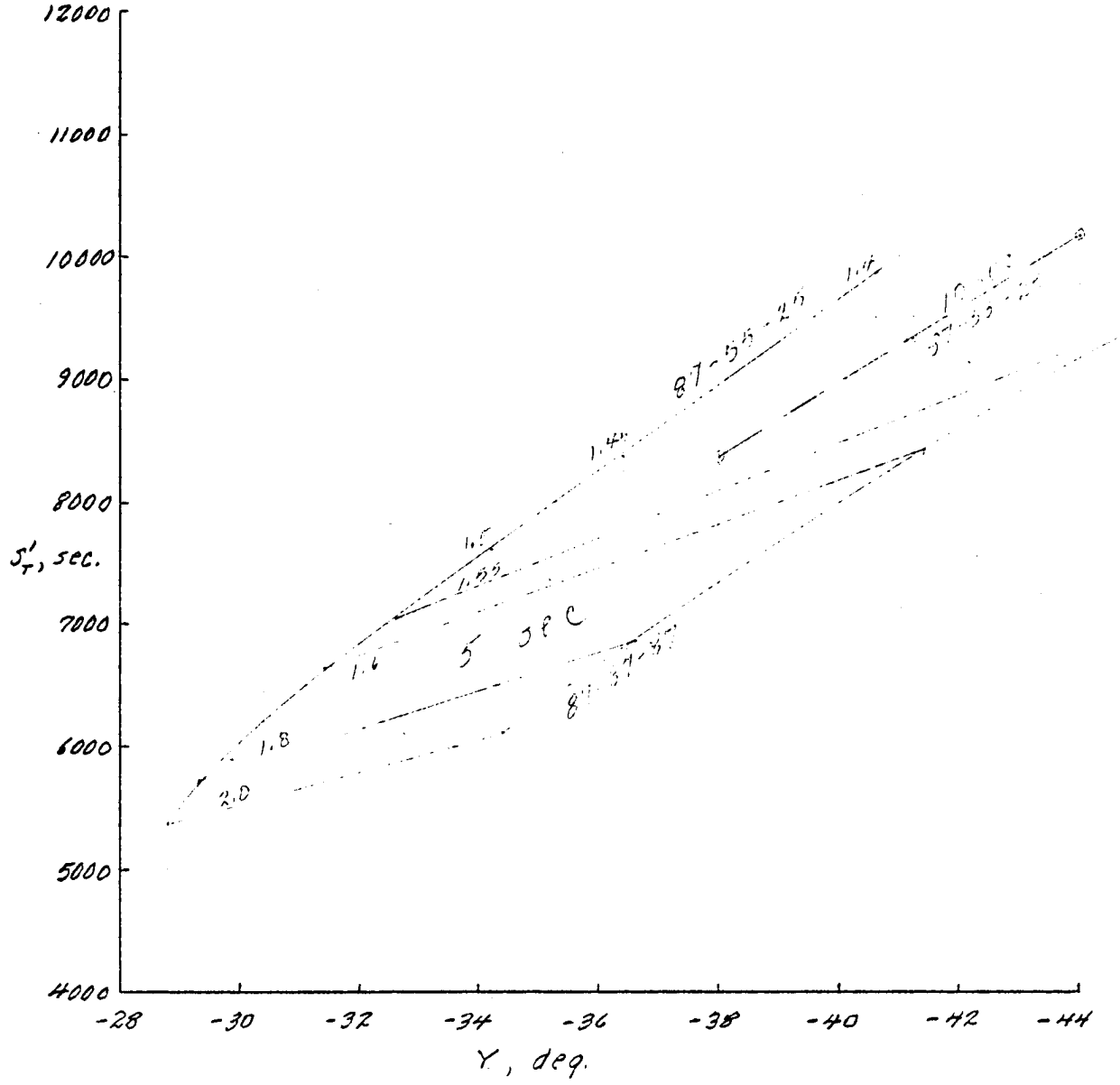

(d) Configurations 87°-87°-87°, 87°-55°-25°

Figure 24. Concluded.

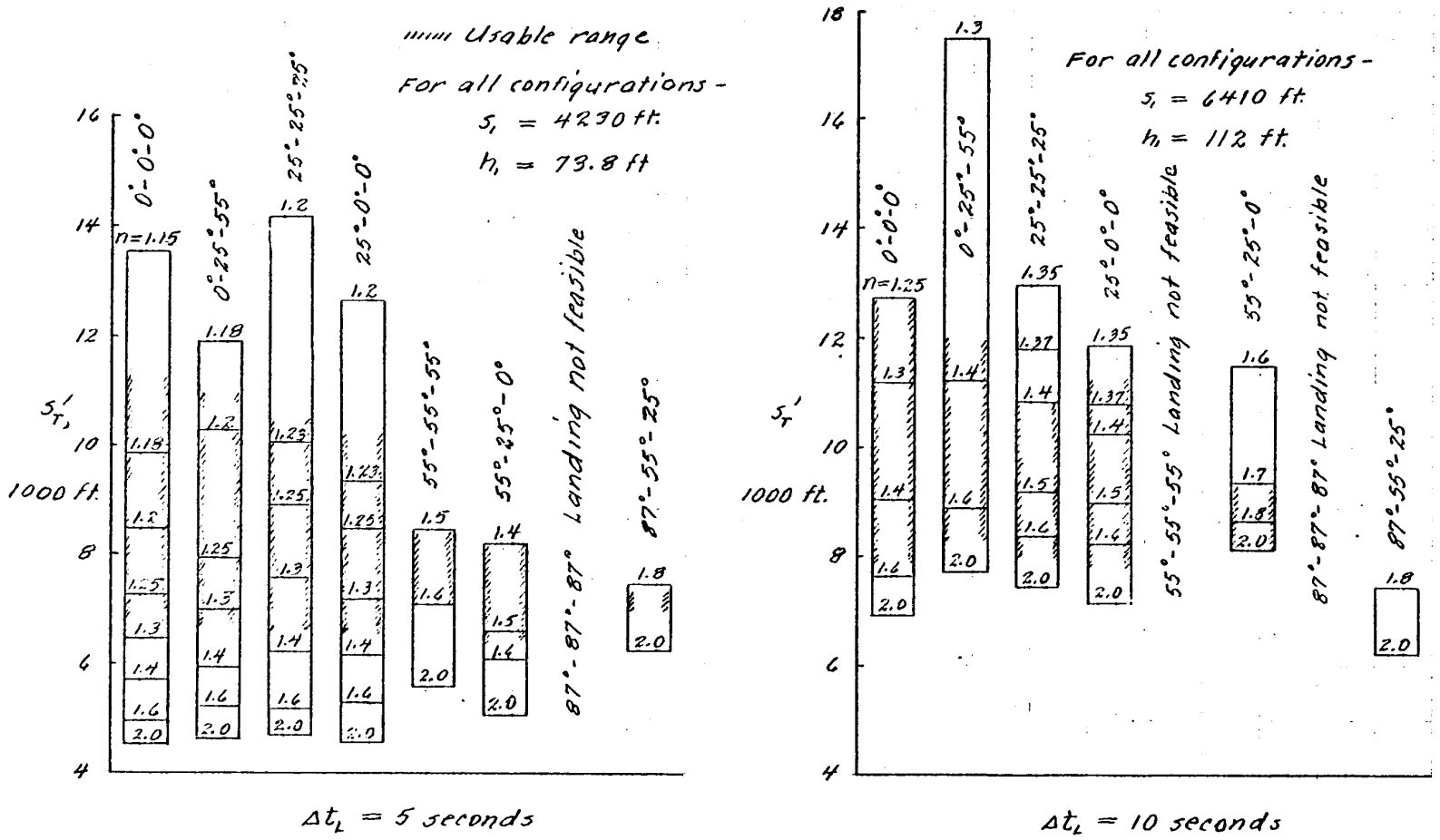

(a) W/S = 56 psf

Figure 25. Summary of landing distances from aimpoint to touchdown.

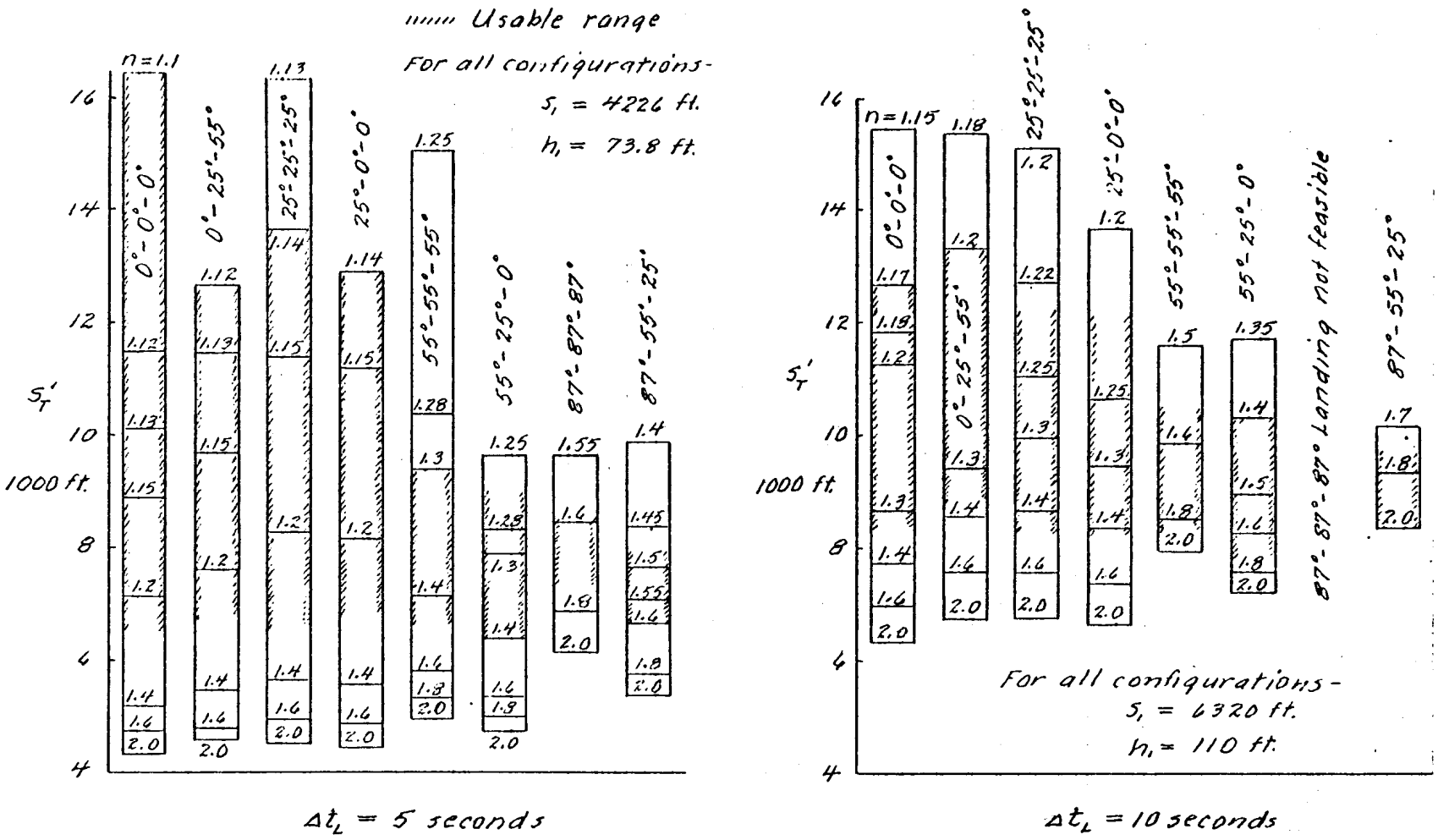

(b) W/S = 70.6 psf

Figure 25. Concluded.

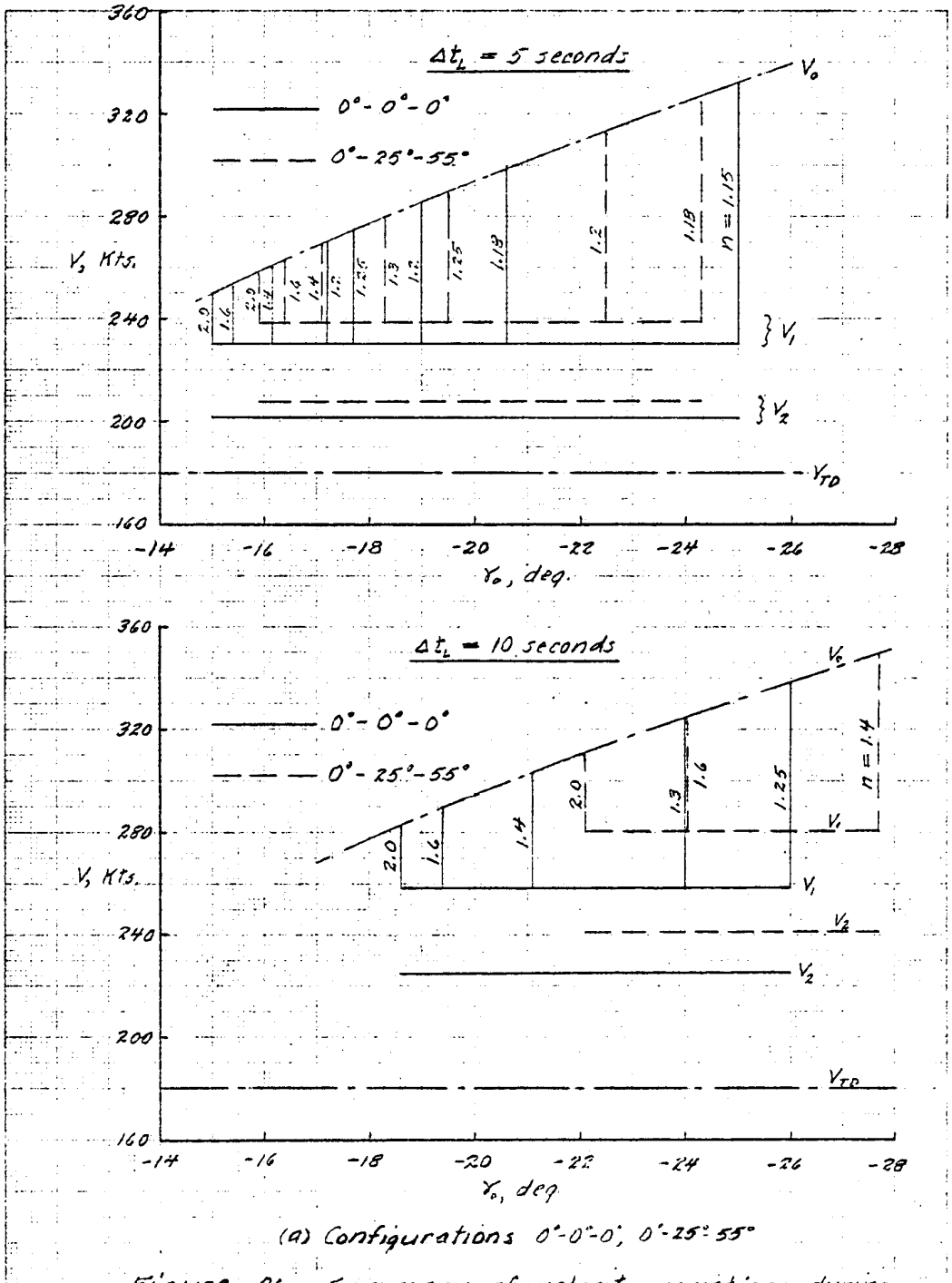

(a) Configurations 0°-0°-0°, 0°-25°-55°

Figure 26 Summary of velocity variations during the landing maneuver W/S = 54 psf

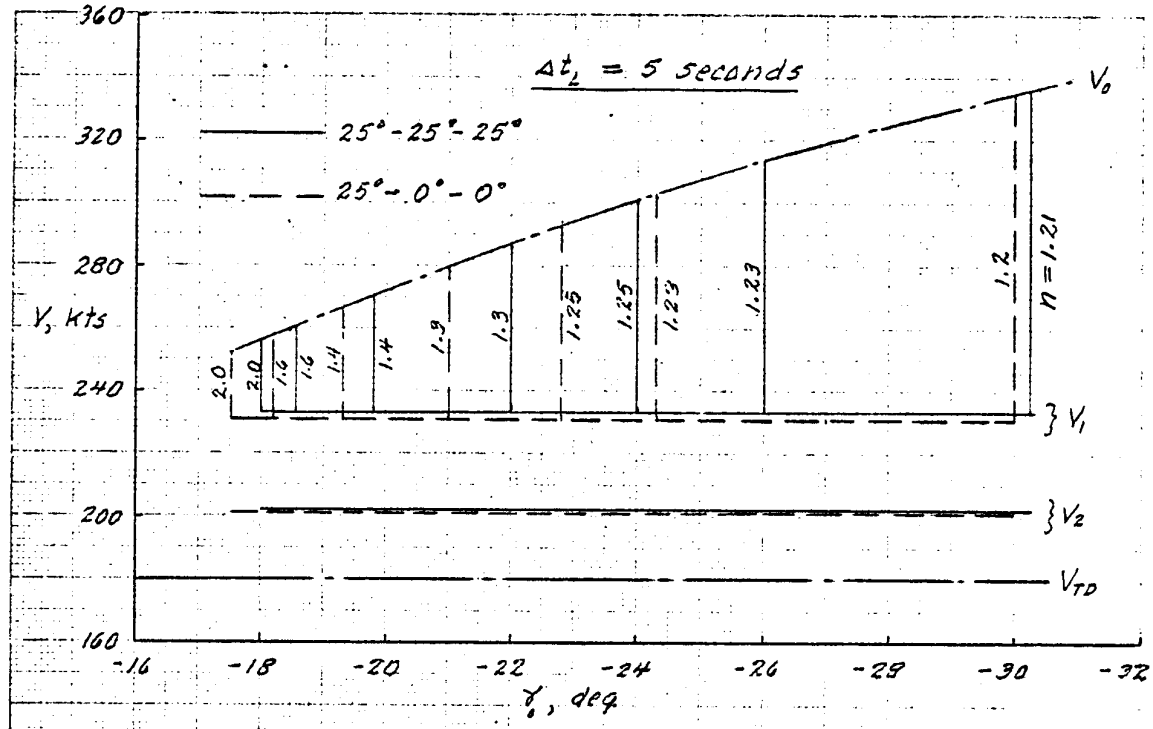

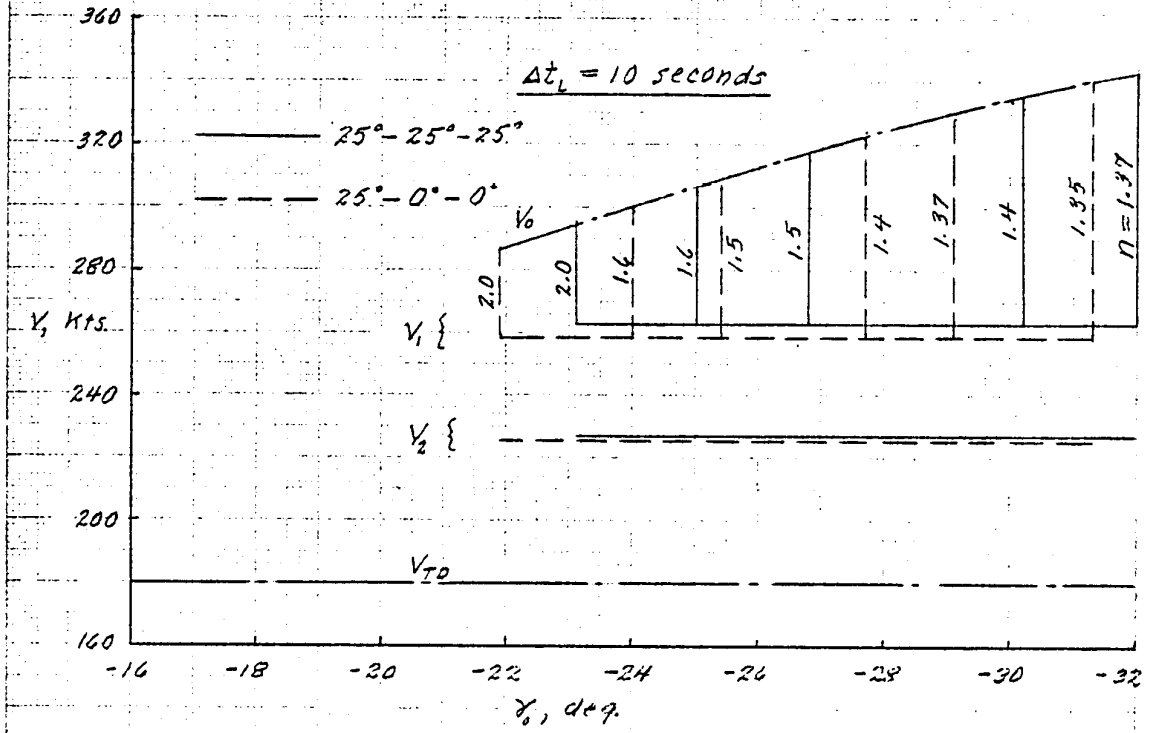

(b) Configurations 25°-25°-25°, 25°-0°-0°

Figure 24 Continued.

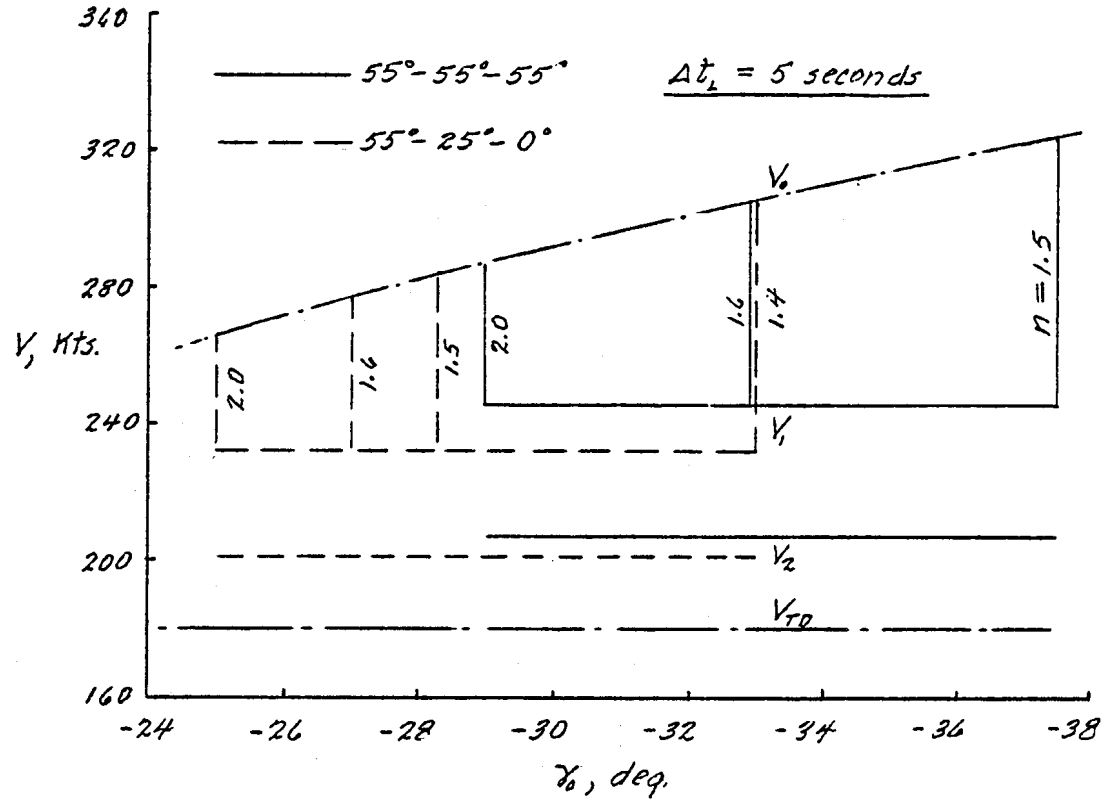

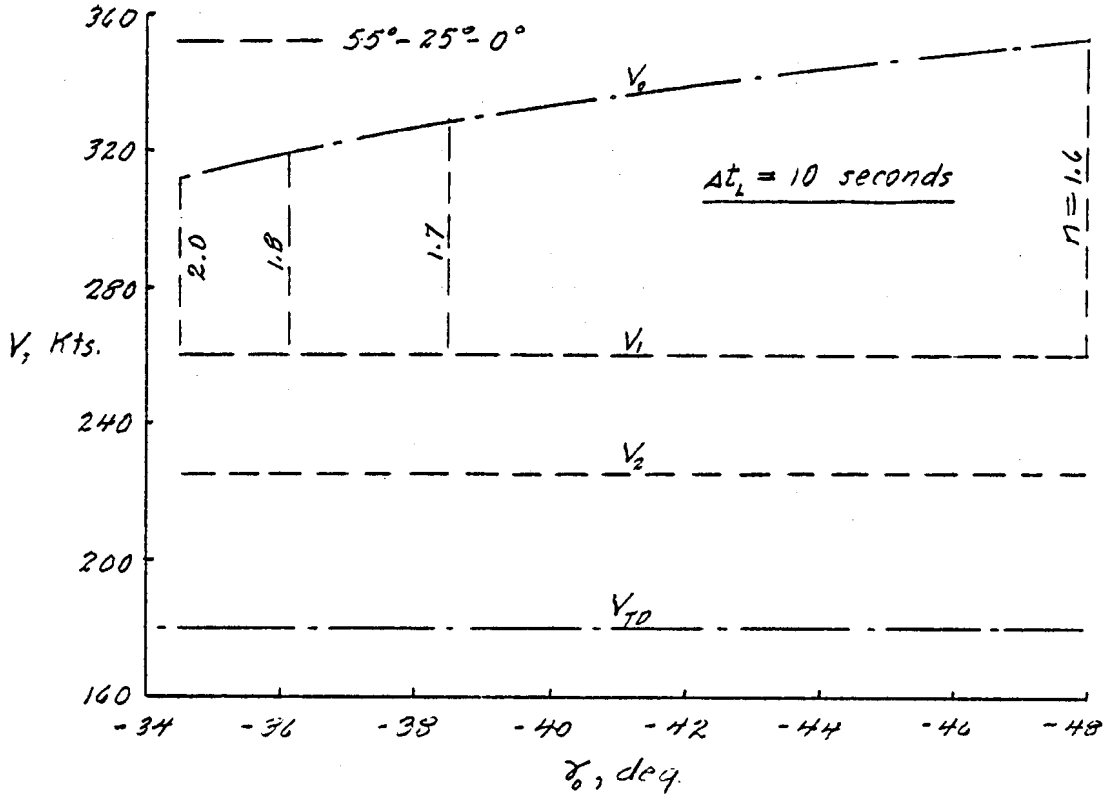

(c) Configurations 55°-55°-55°; 55°-25°-0°

Figure 26. Continued.

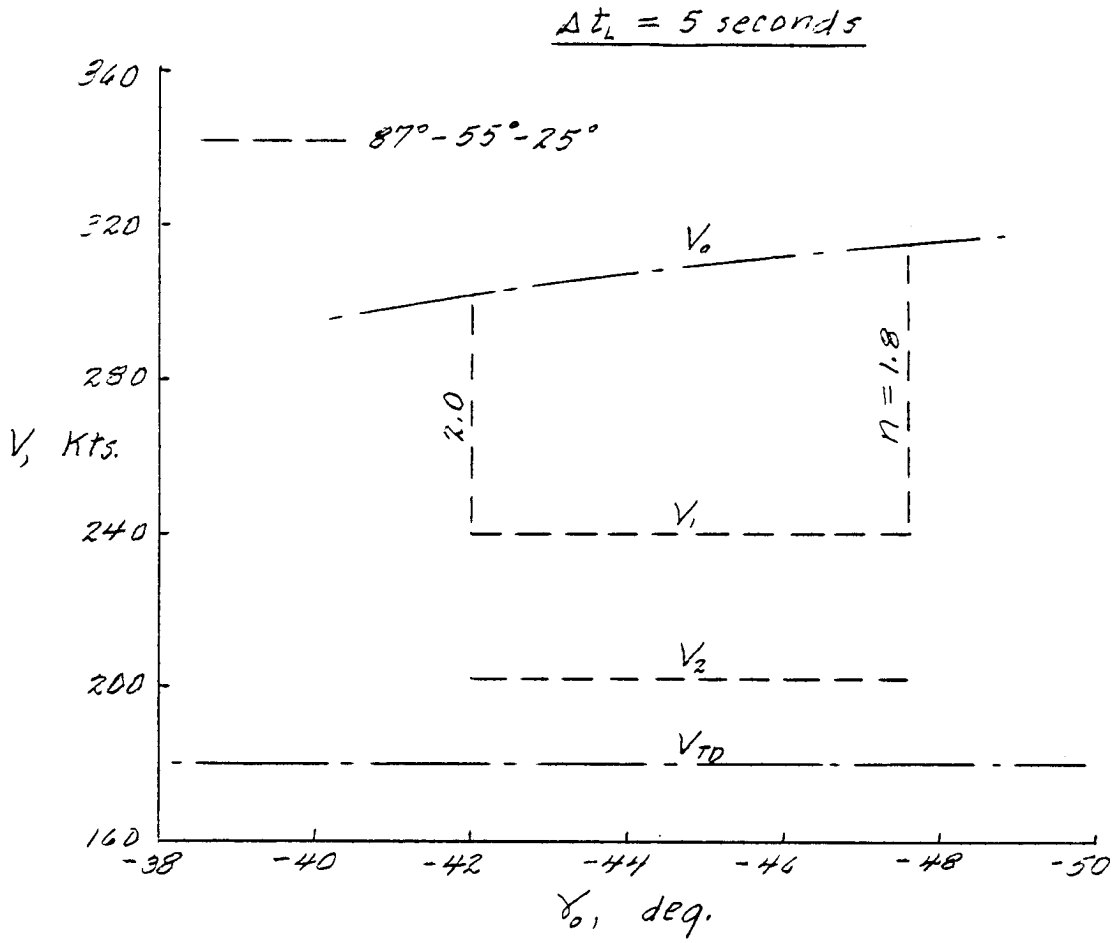

(d) Configuration 87°-55°-25°

Figure 26. Concluded.

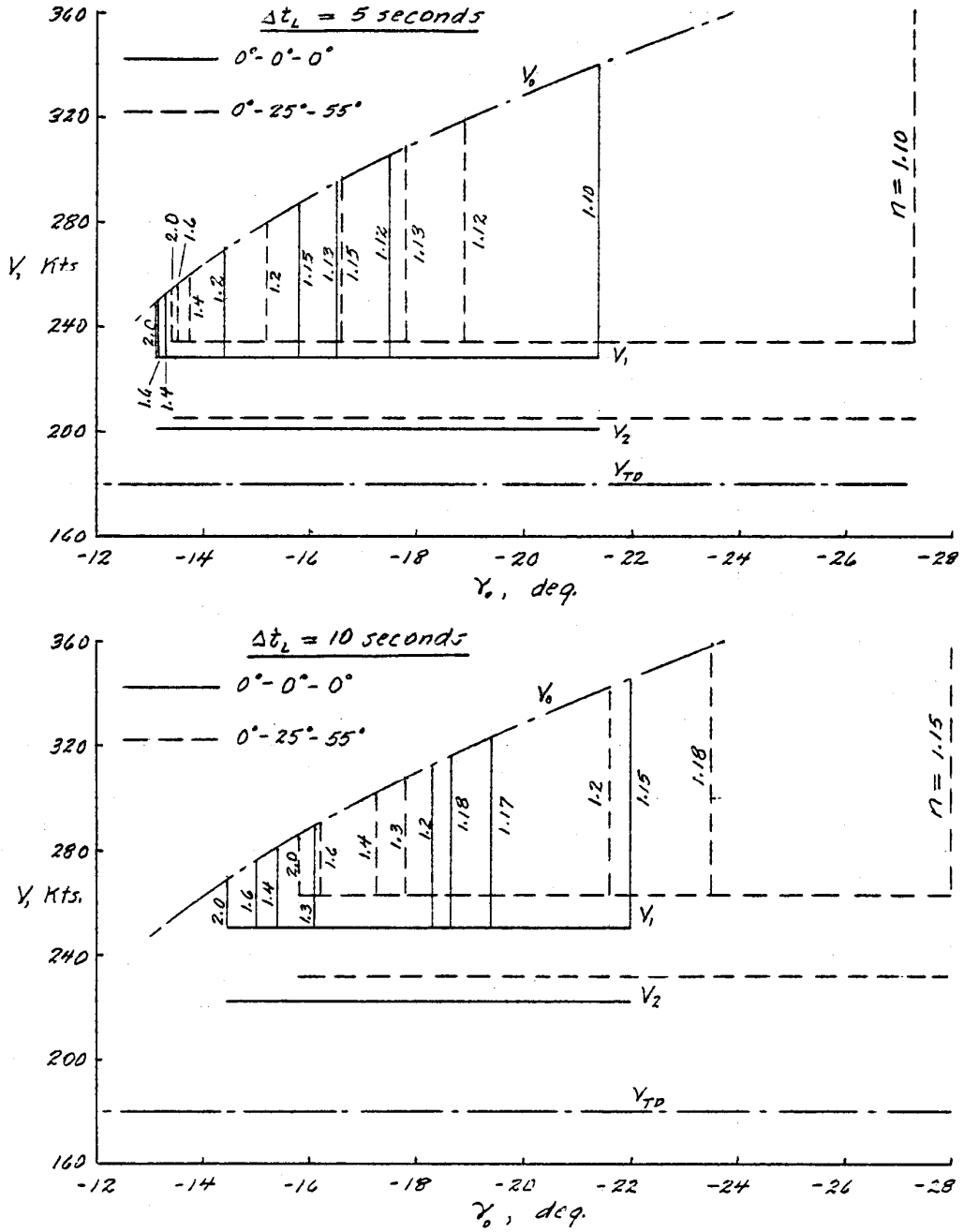

(a) Configurations 0°-0°-0°, 0°-25°-55°

Figure 27. Summary of velocity variations during the landing maneuver. W/S = 70.6 psf

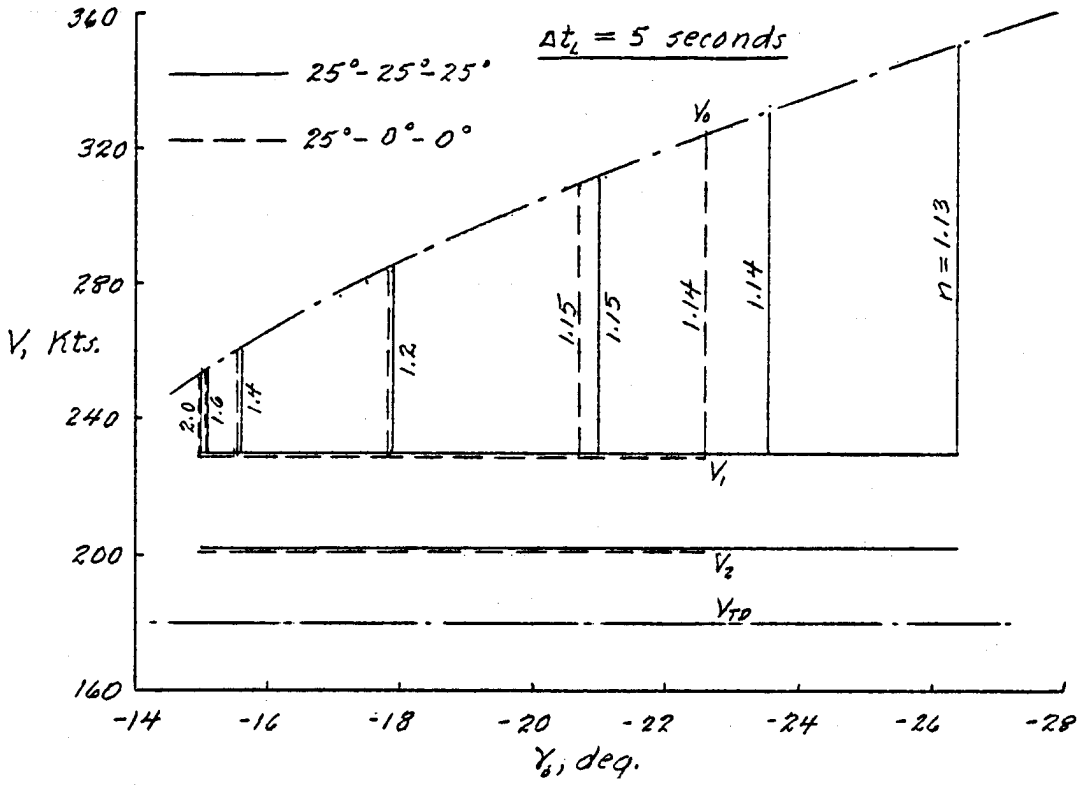

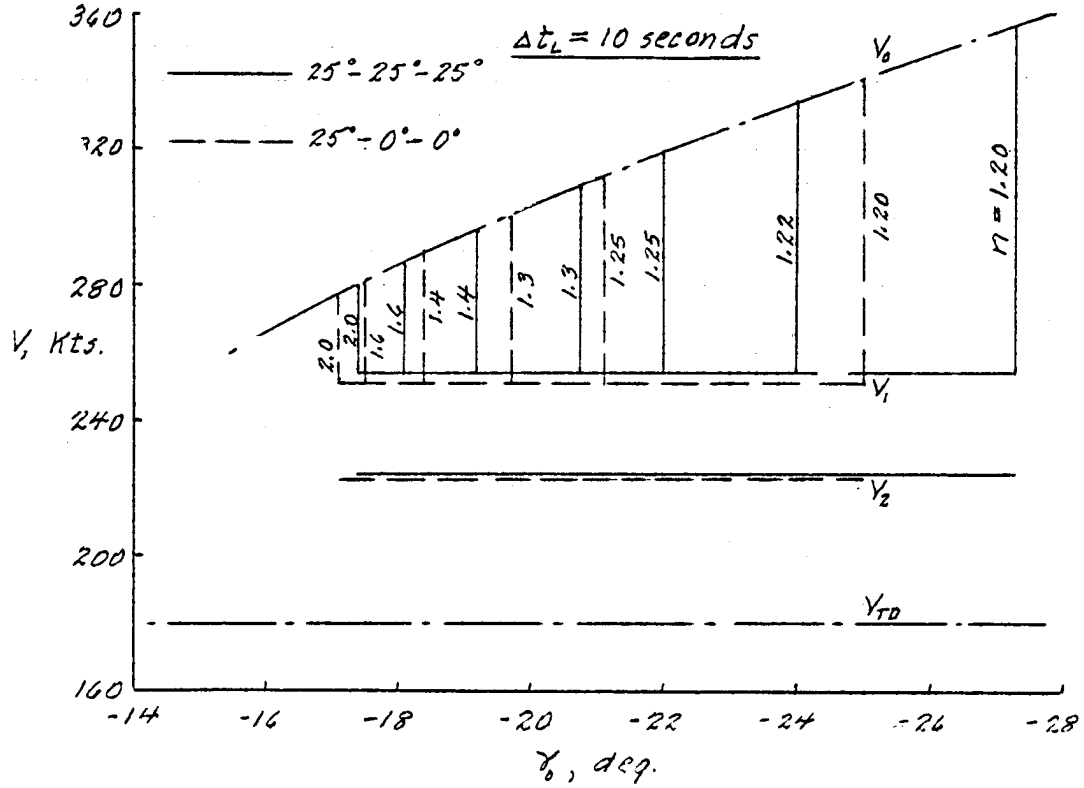

(b) Configurations 25°-25°-25°, 25°-0°-0°

Figure 27. Continued.

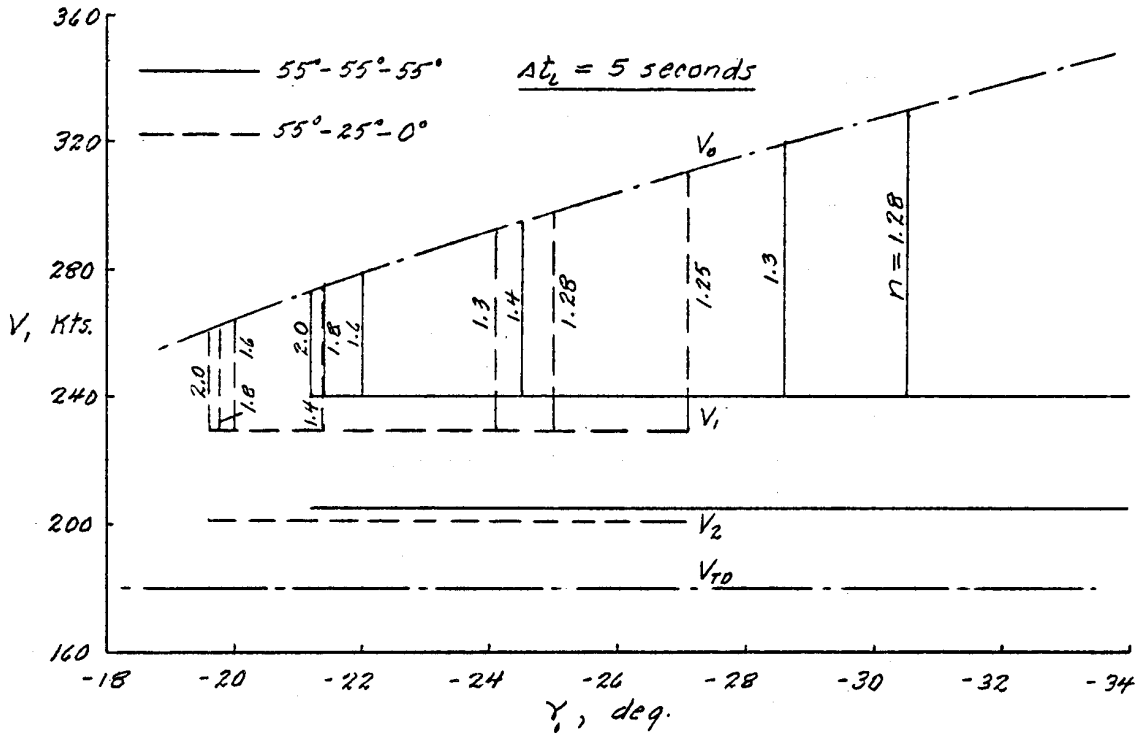

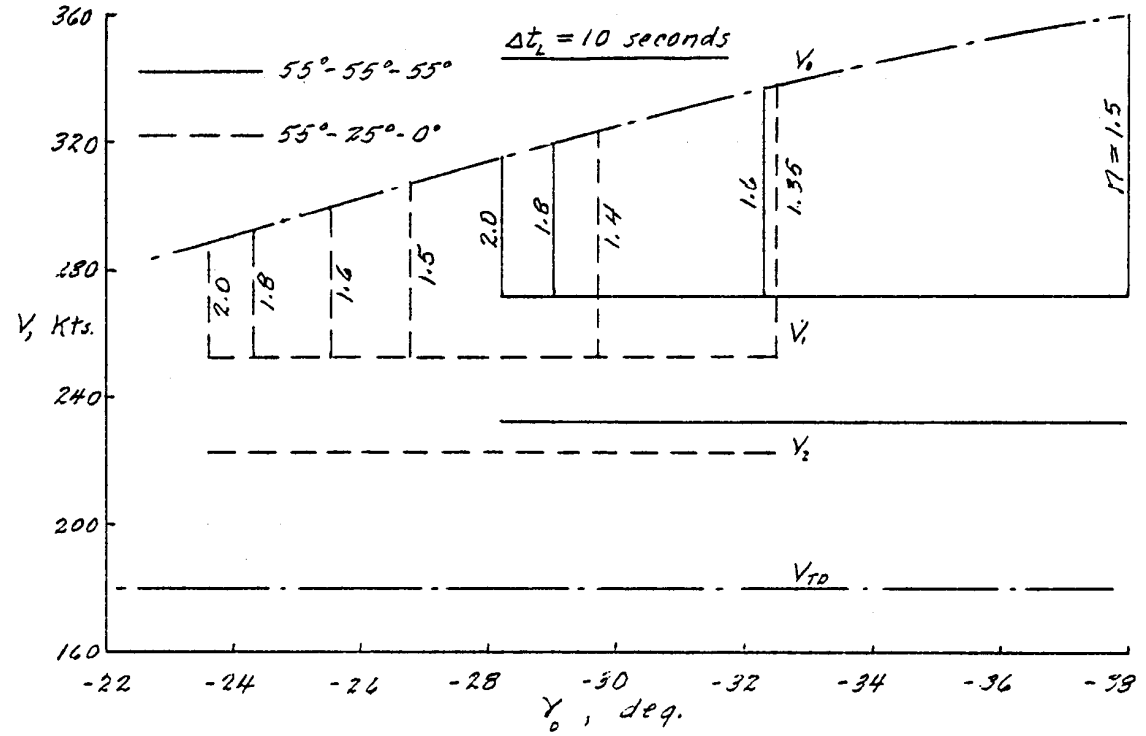

(c) Configurations 55°-55°-55°, 55°-25°-0°

Figure 27. Continued.

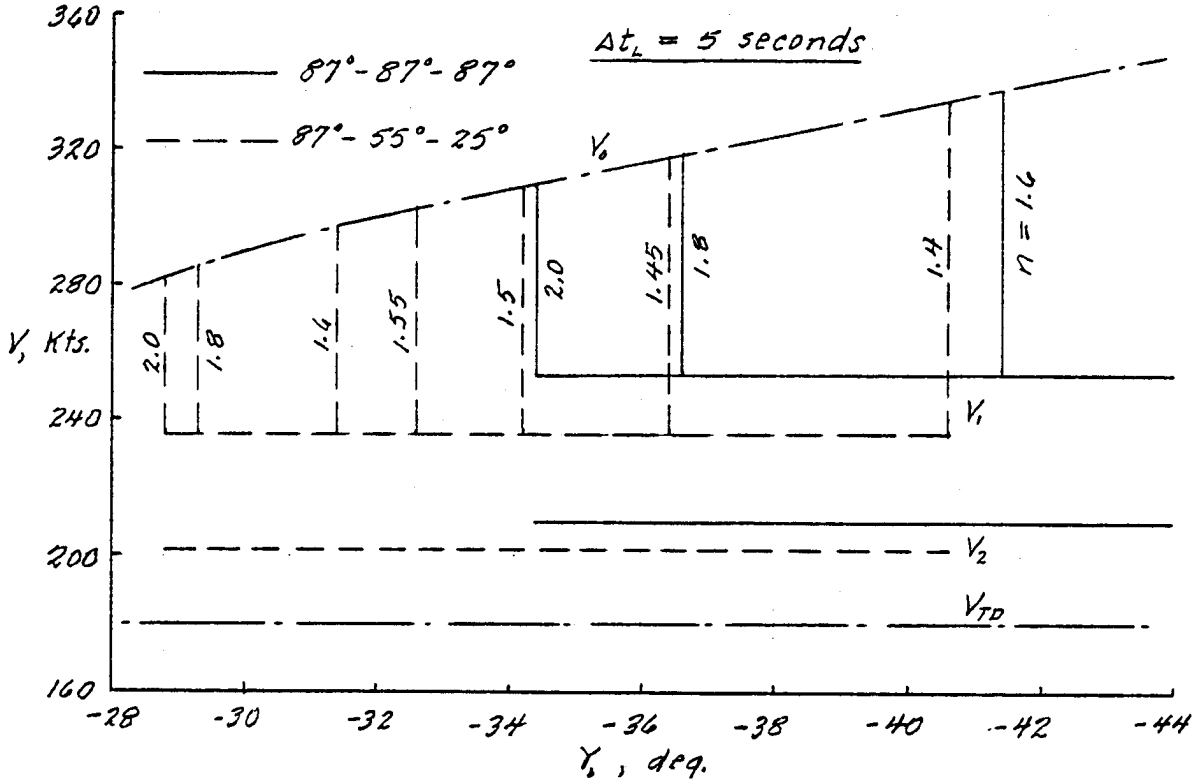

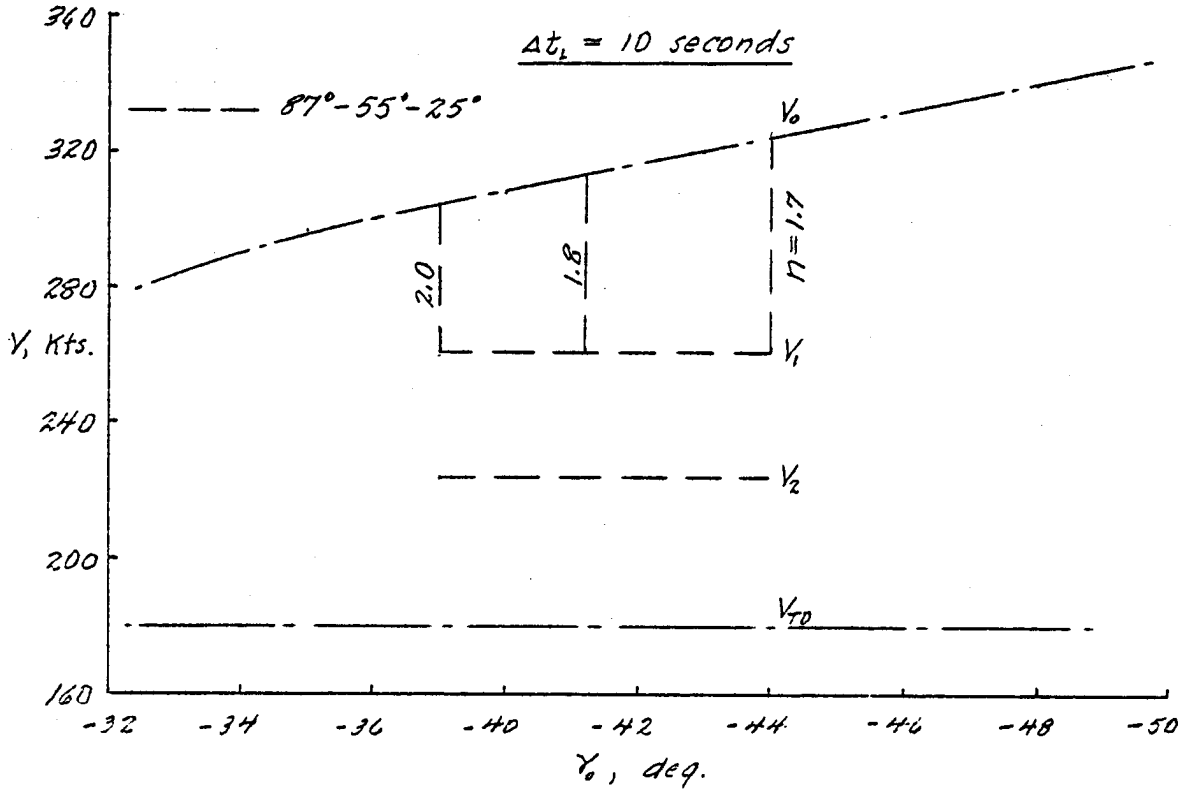

(d) Configurations 87°-87°-87°, 87°-55°-25°

Figure 27. Concluded.

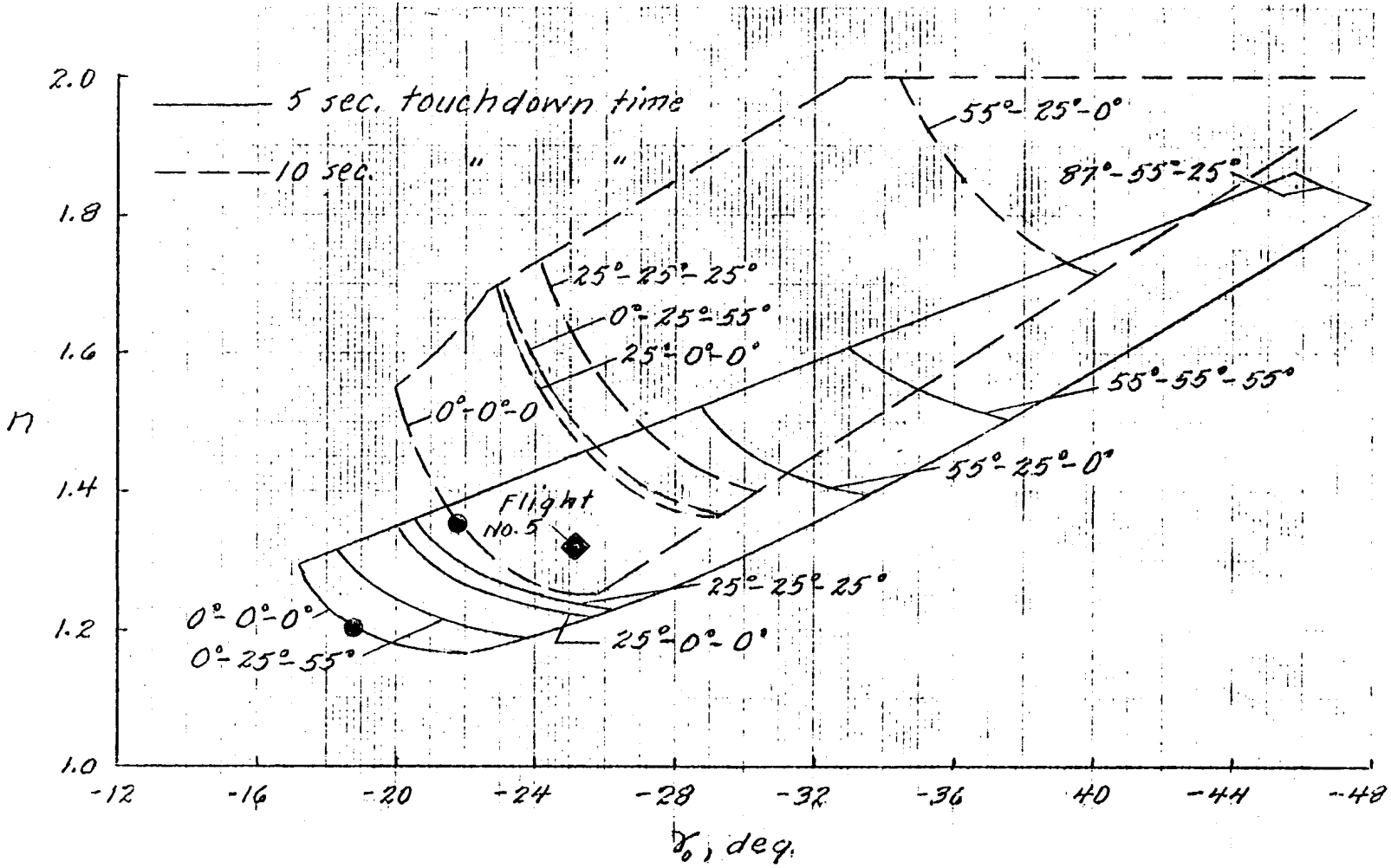

(a) Point locations.

Figure 28 Comparison of landing trajectories for orbiter flight numbers 5 and the representative points on the boundaries for 5 and 10 second touchdown maneuver times. W/S = 56 psf.

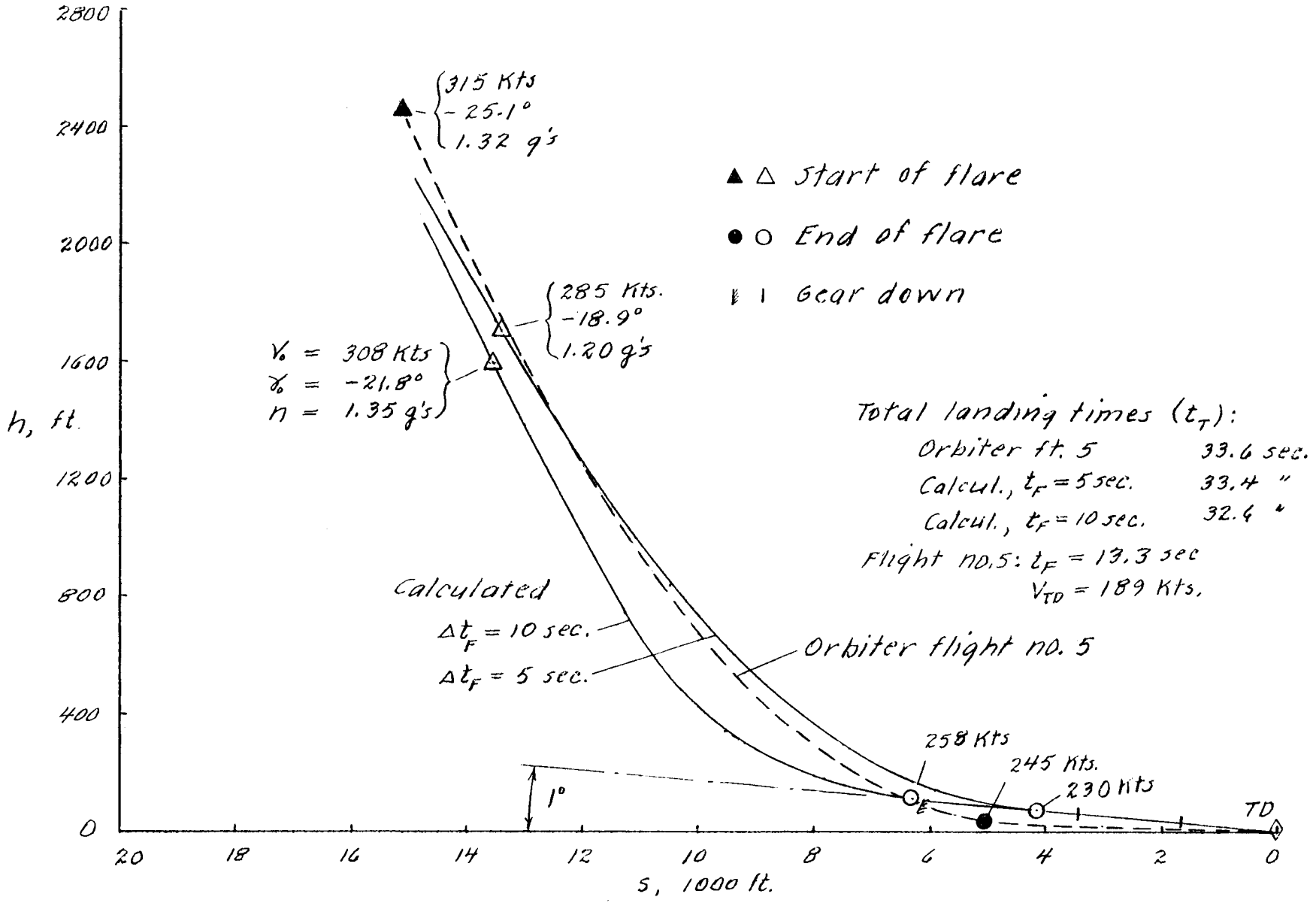

(b) Trajectory comparison

Figure 28. Concluded.

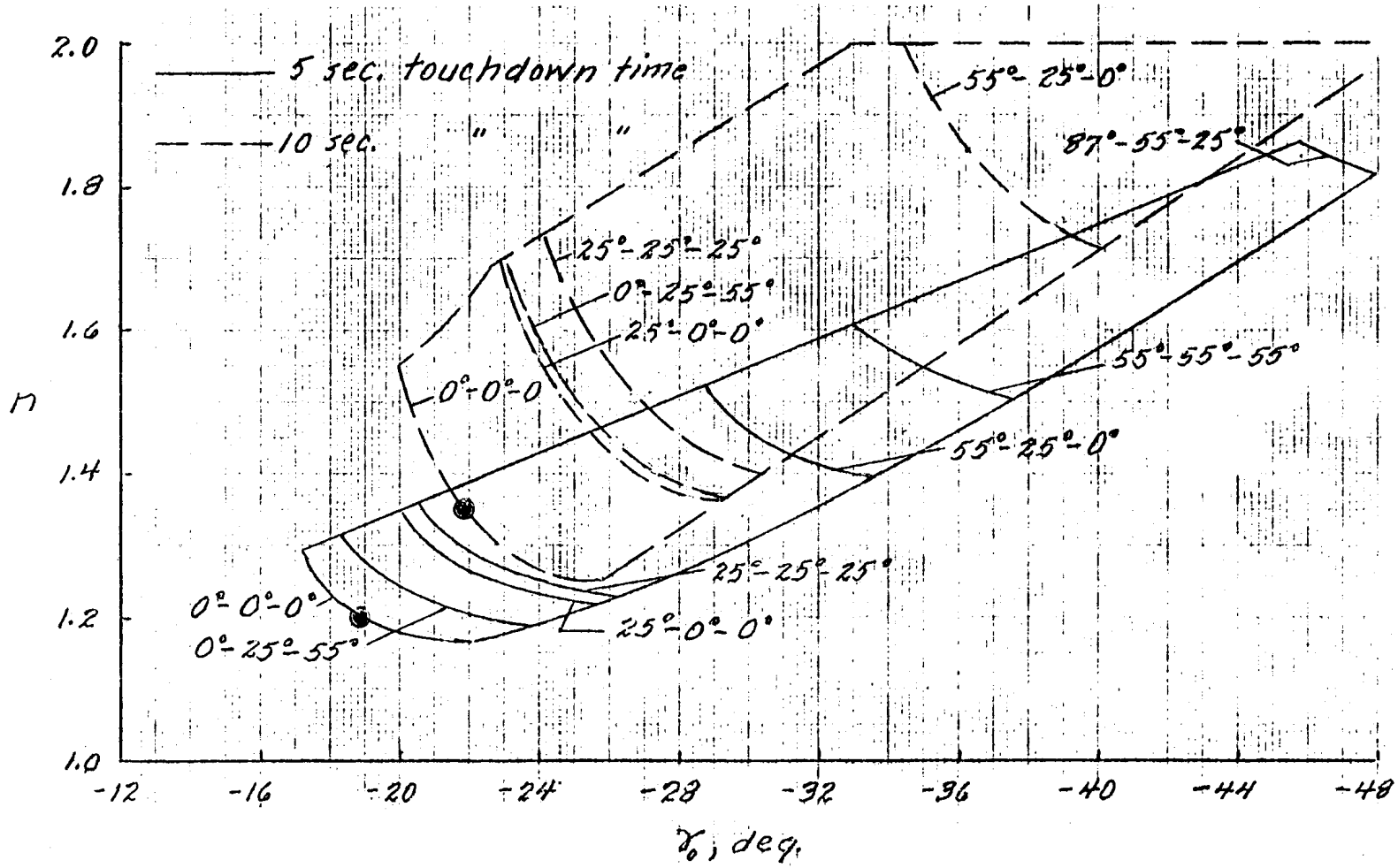

(a) Boundary points, $W/S = 56$ psf.

Figure 29. Comparison of trajectories for the mid points of the boundaries for the 0°-0°-0° configuration for vehicle loadings of 56 and 70.6 psf.

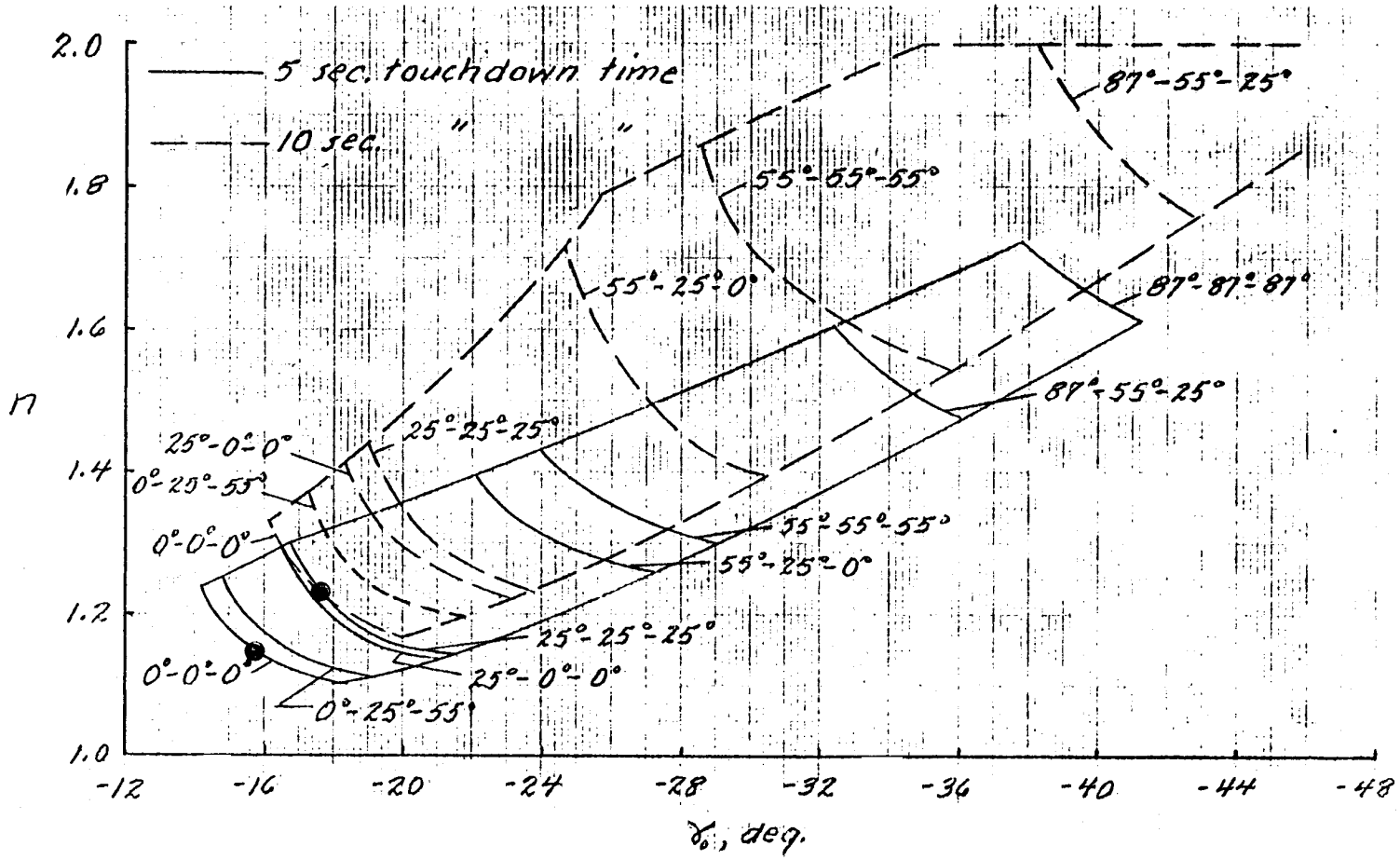

(b) Boundary points, W/S = 70.6 psf

Figure 29. Continued.

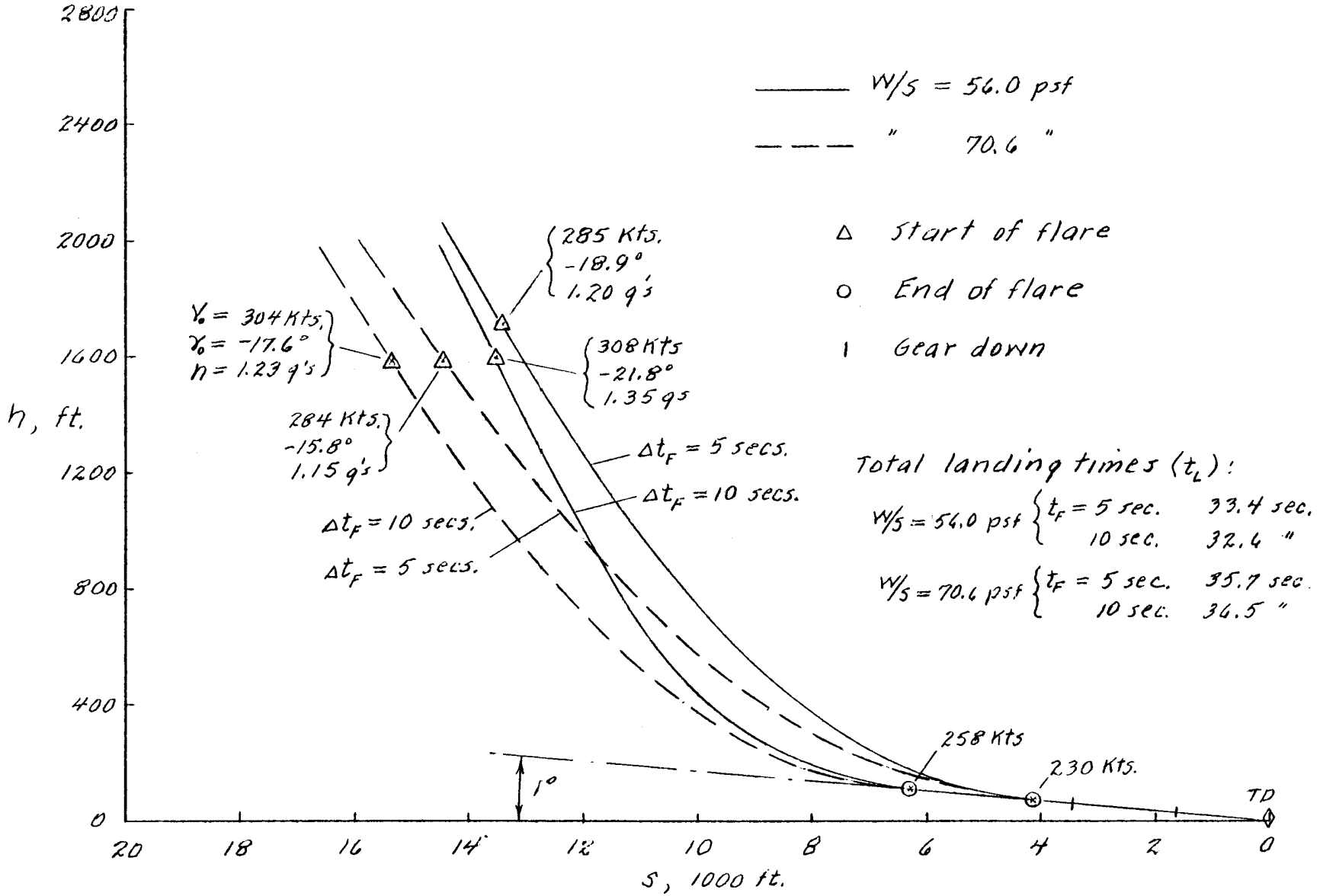

(c) Trajectory comparison

Figure 29. Concluded.

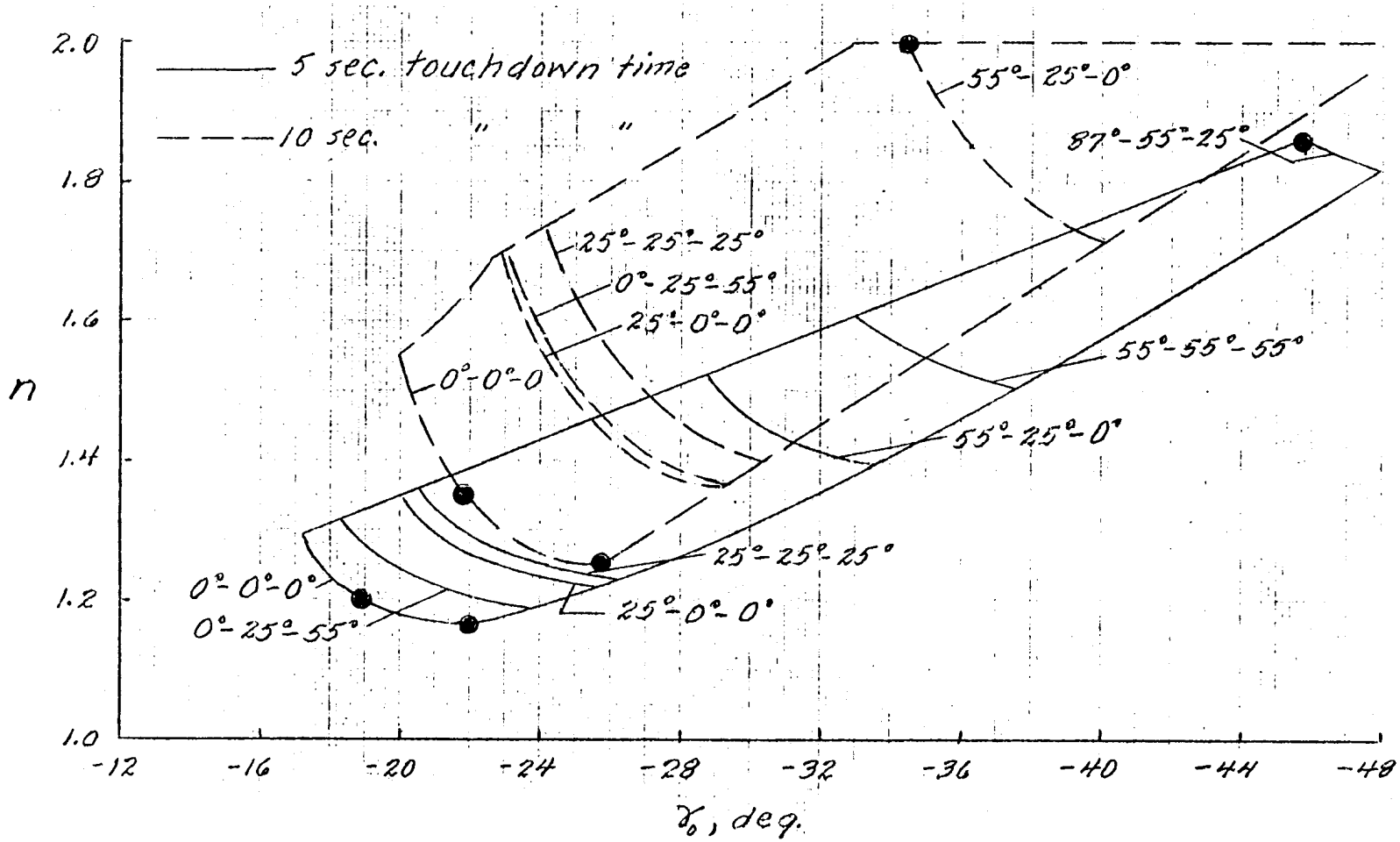

(a) Boundary points

Figure 30. Comparison of trajectories for extreme points on the landing maneuver boundaries for W/s = 56 psf.

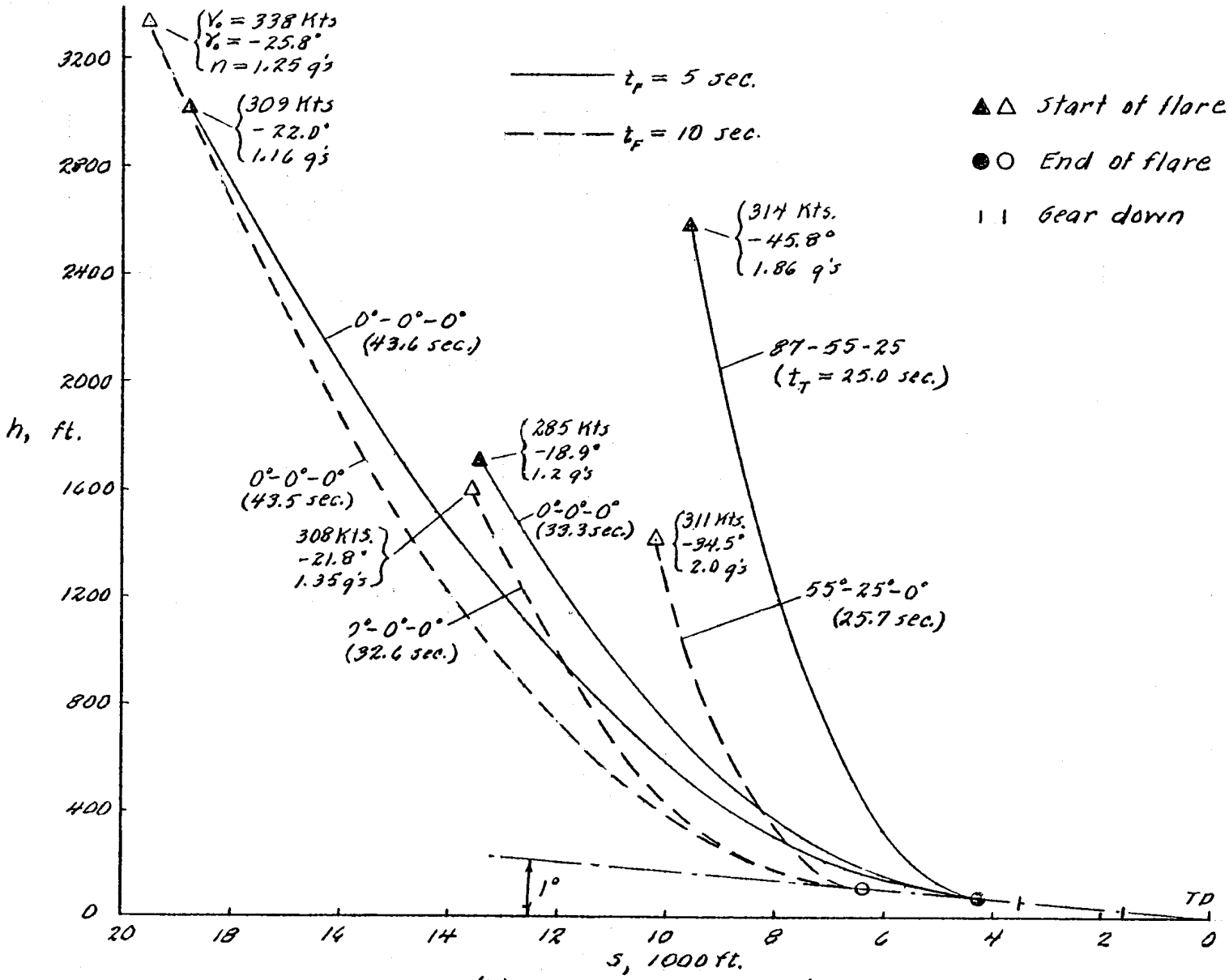

(b) Trajectory comparison

Figure 30. Concluded.

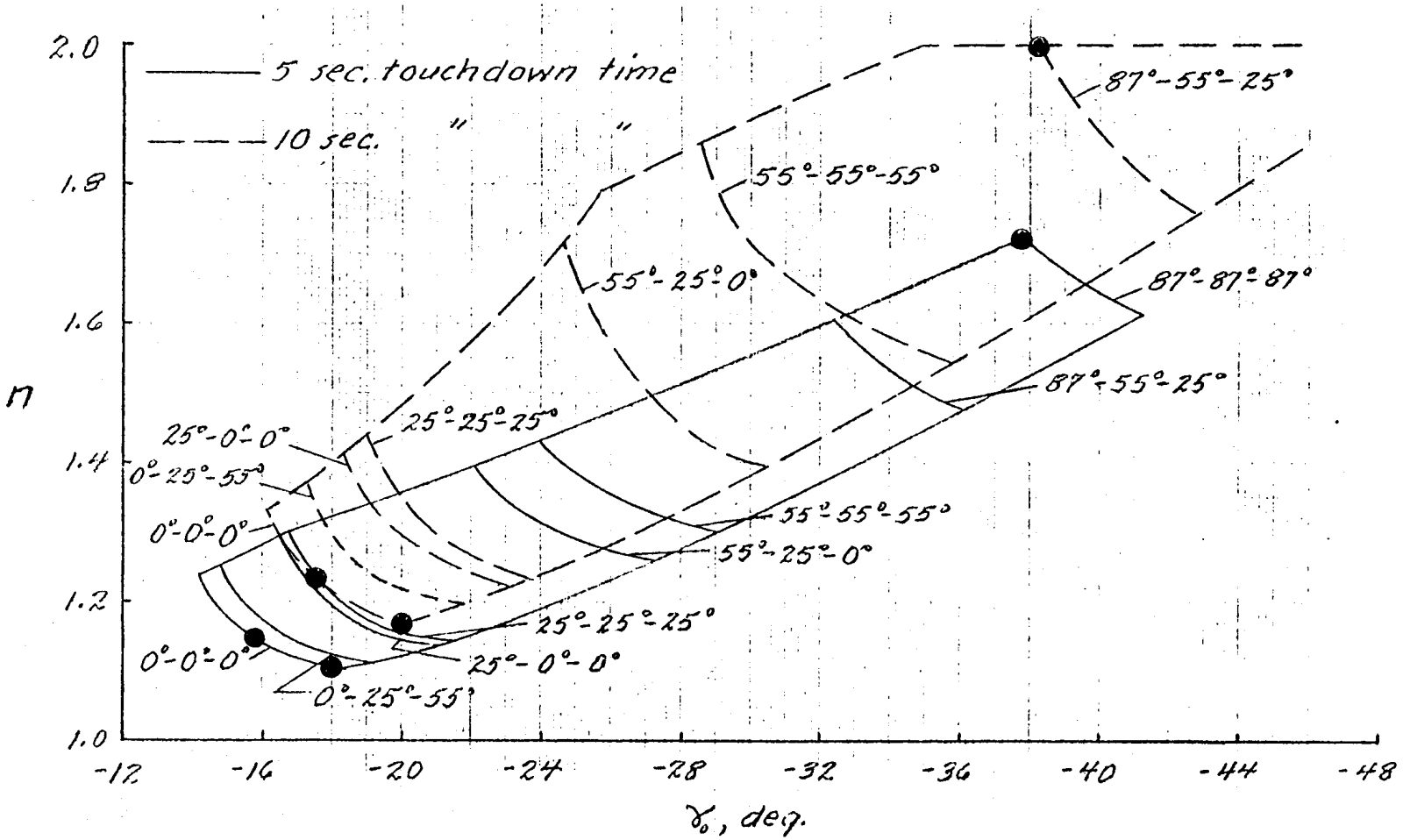

(a) Boundary points.

Figure 31. Comparison of trajectories for extreme points on the landing maneuver boundaries for $W/S = 70.6$ psf.

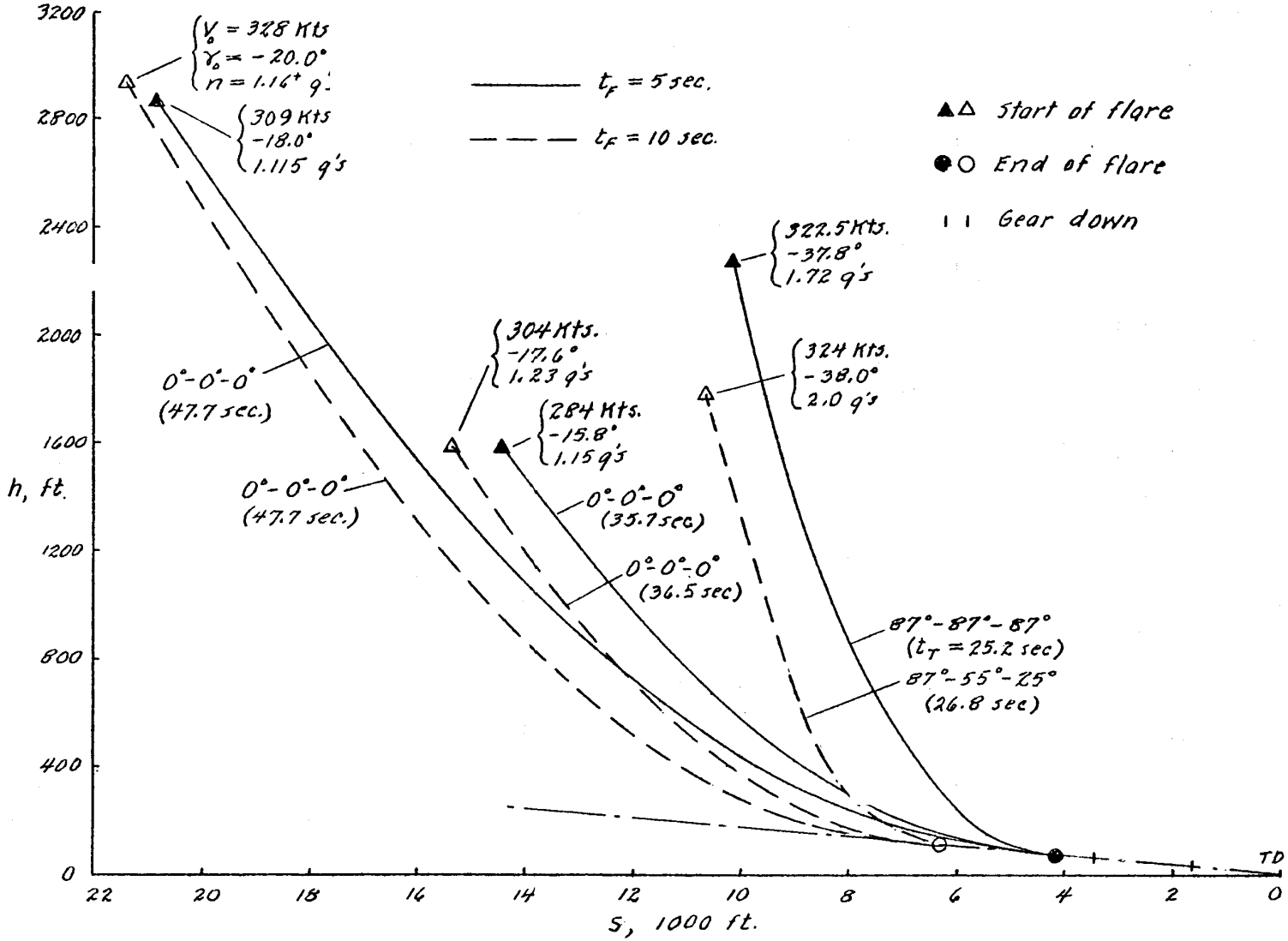

(b) Trajectory Comparison

Figure 31. Concluded.

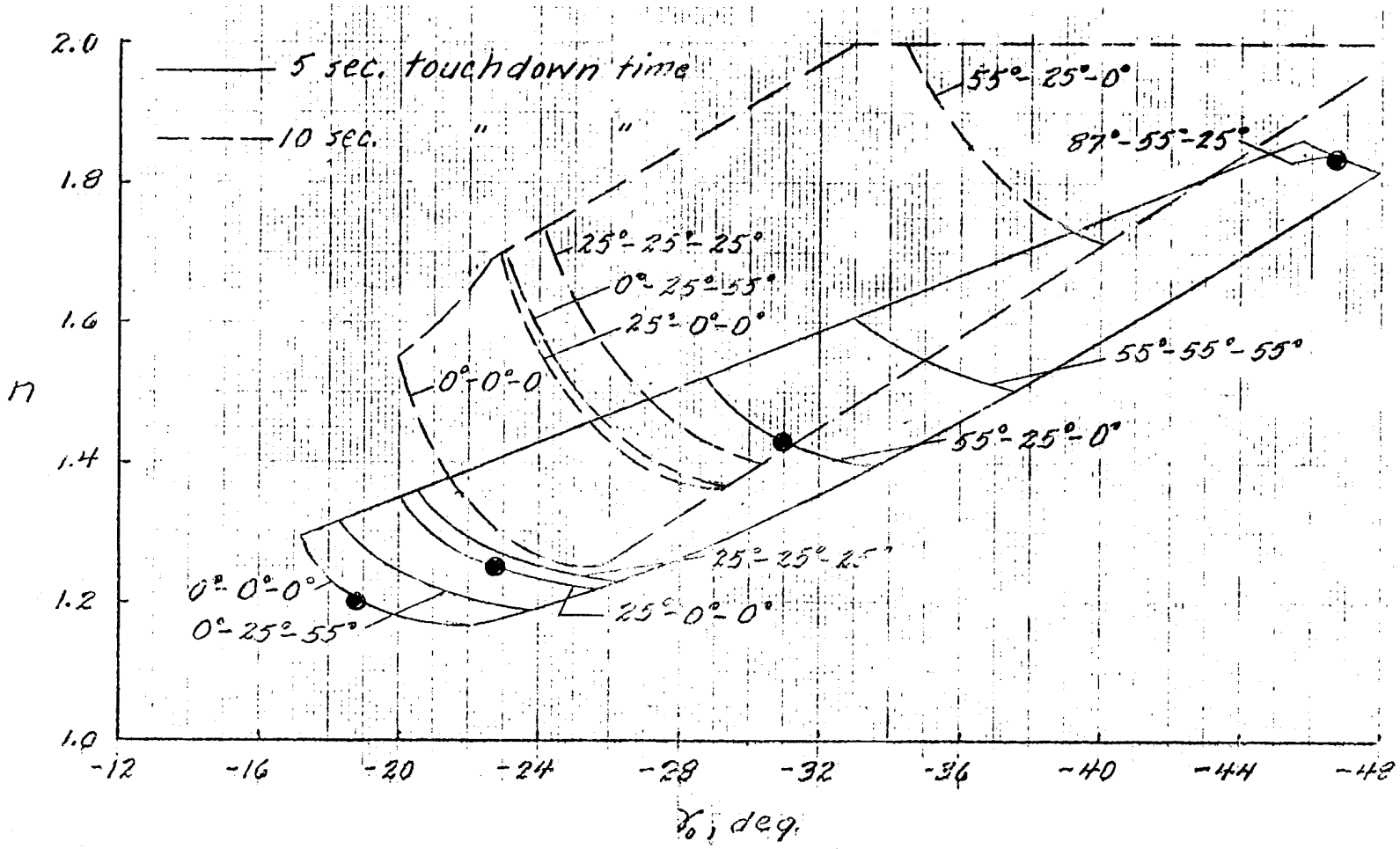

(a) Boundary points.

Figure 32. Effect of configuration changes on the landing trajectories at midpoints of the 5-second boundary for W/S = 56 psf.

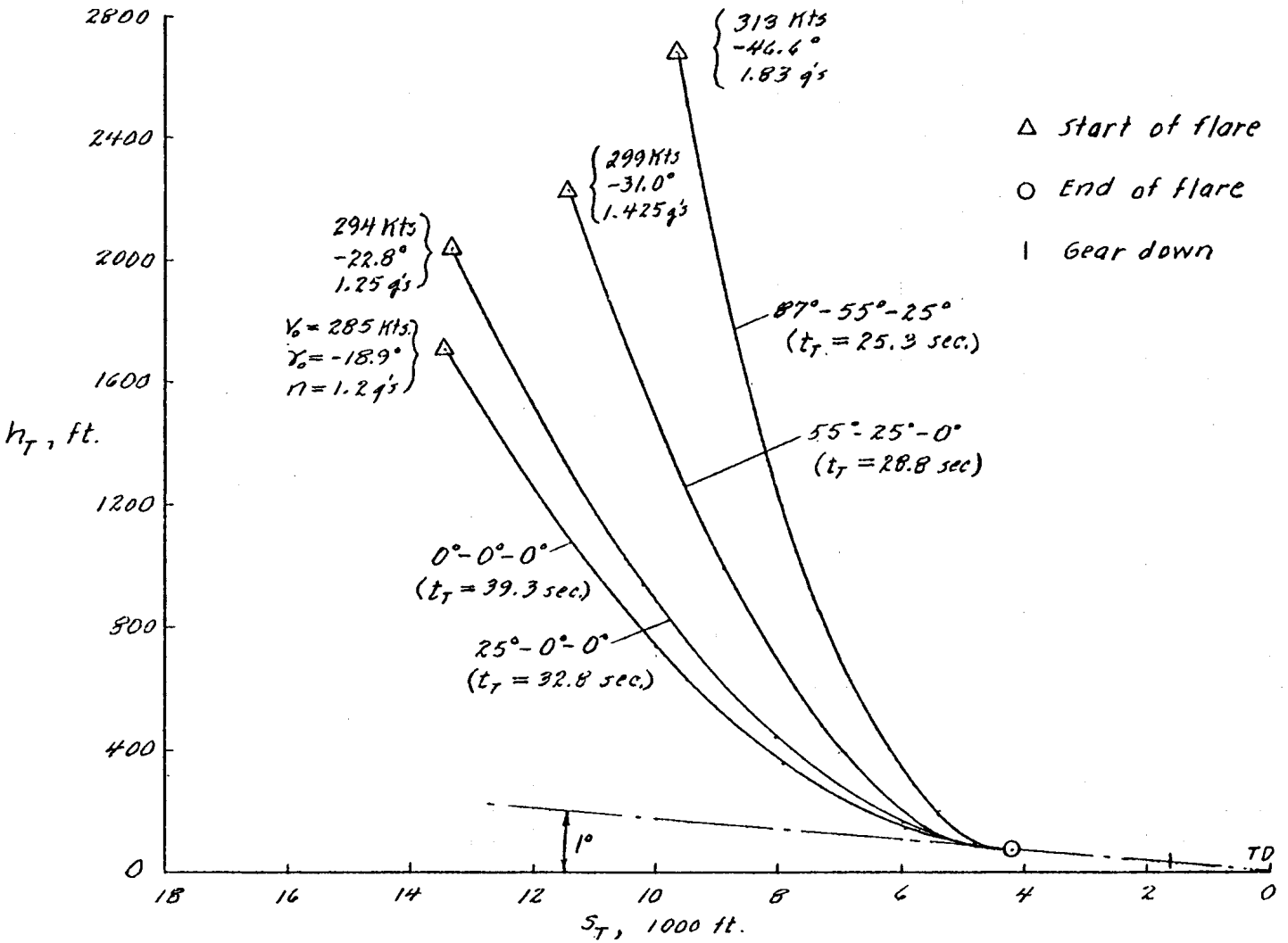

(b) Trajectory comparison

Figure 32. Concluded.

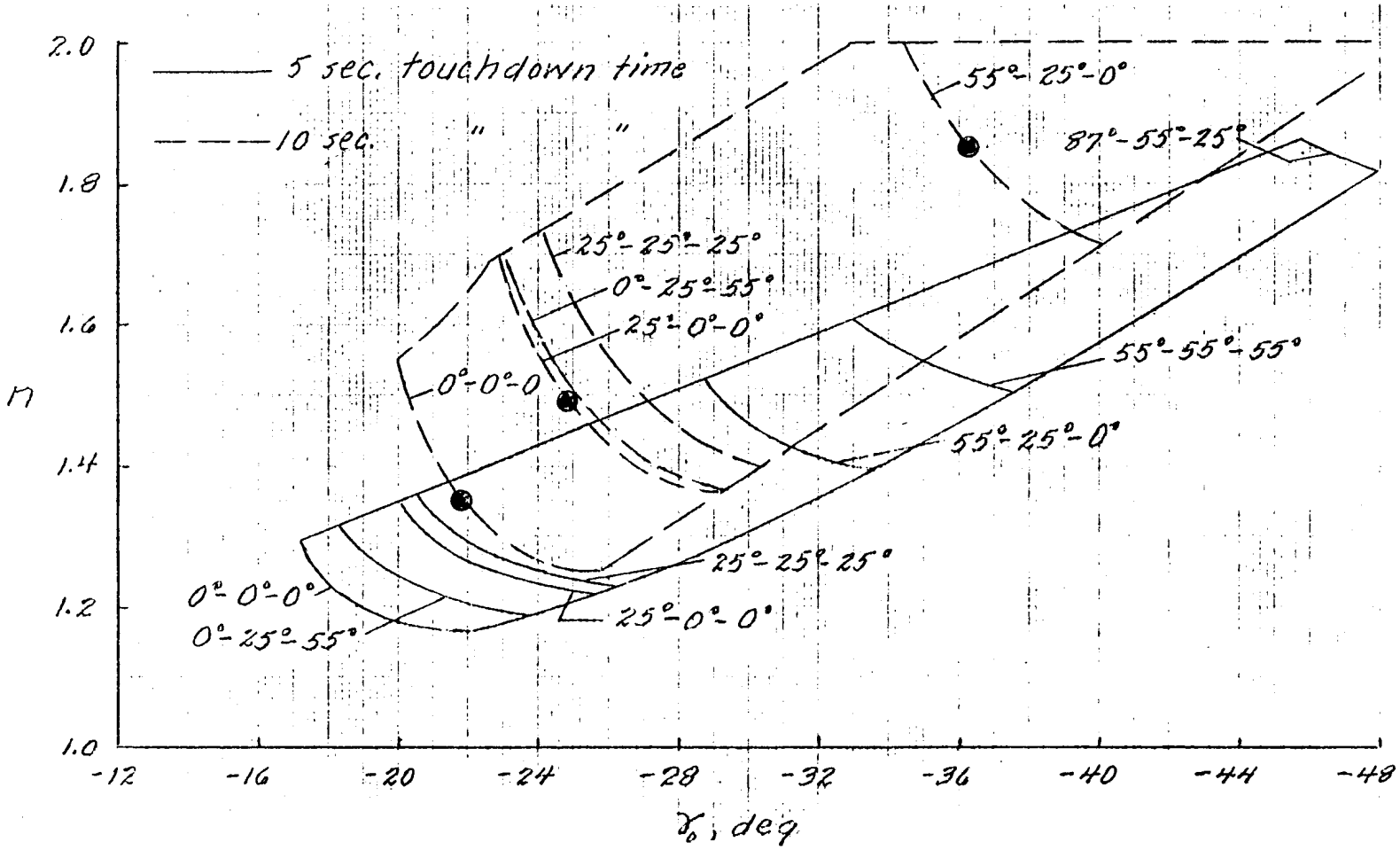

(a) Boundary points.

Figure 33. Effect of configuration changes on the landing trajectories at midpoints of the 10-second boundary for $W/S = 56$ psf.

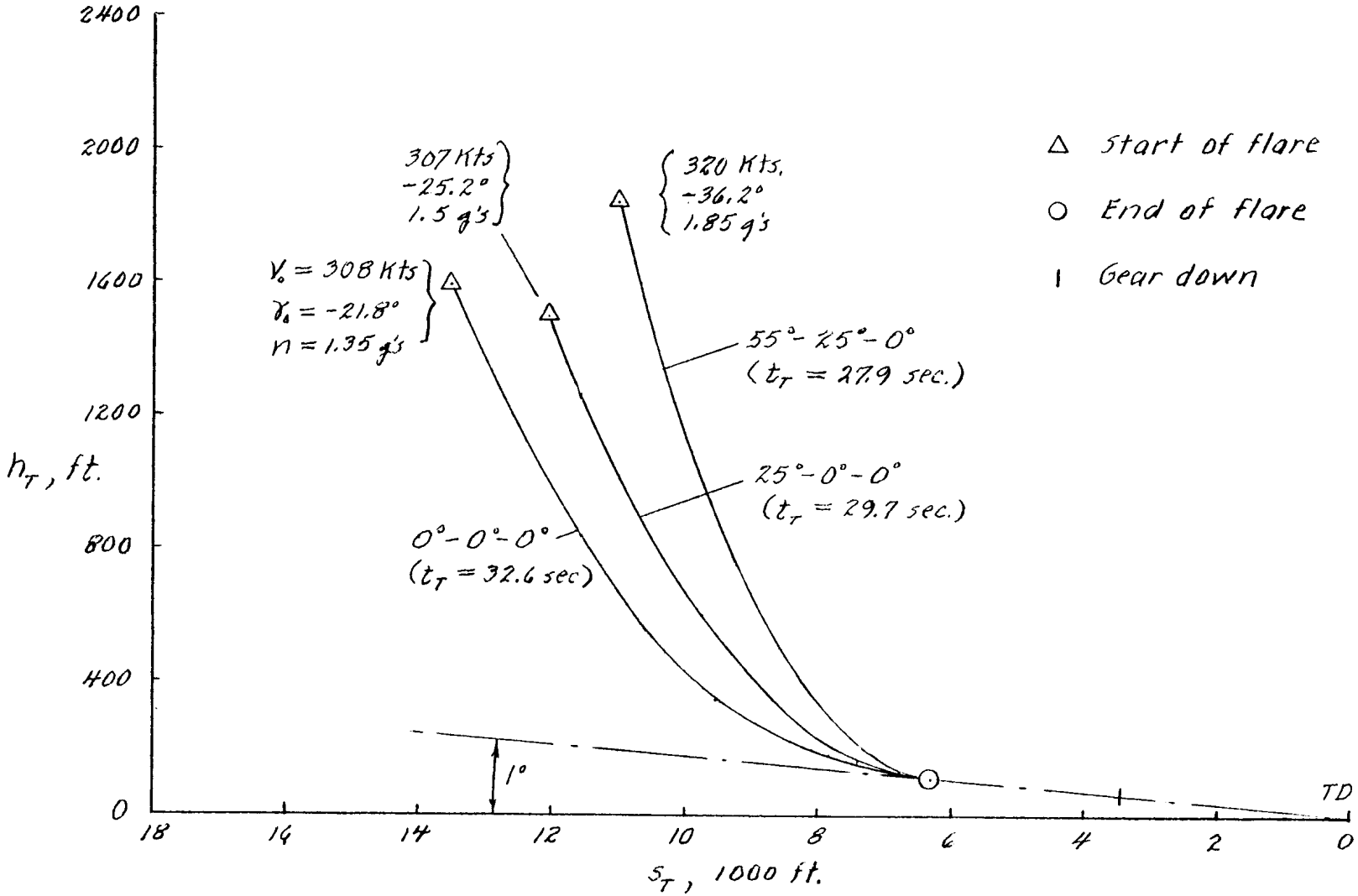

(b) Trajectory comparison

Figure 33. Concluded.

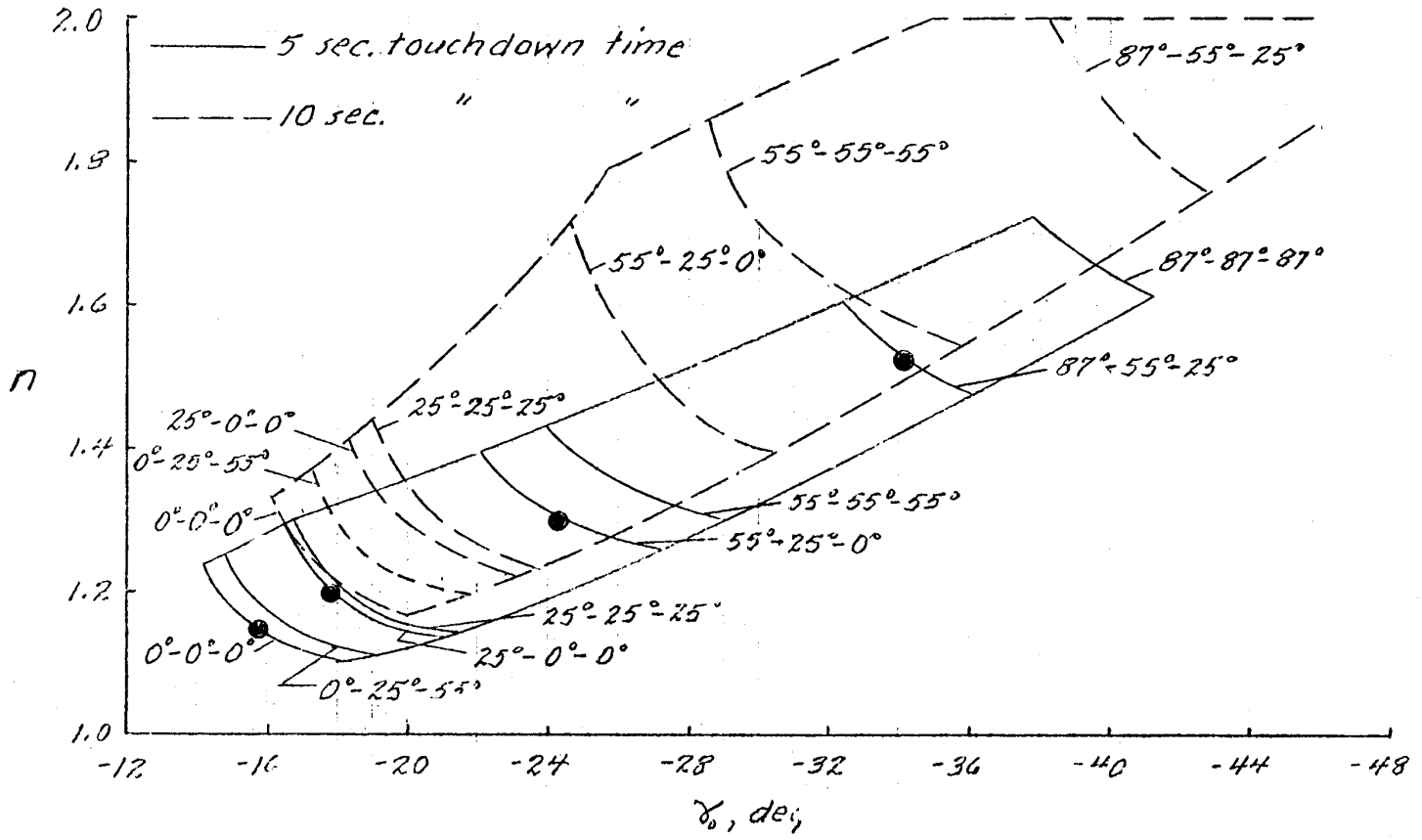

(a) Boundary points.

Figure 34. Effect of configuration changes on the landing trajectories at midpoints of the 5 second boundary for $W/S = 70.0$ psf.

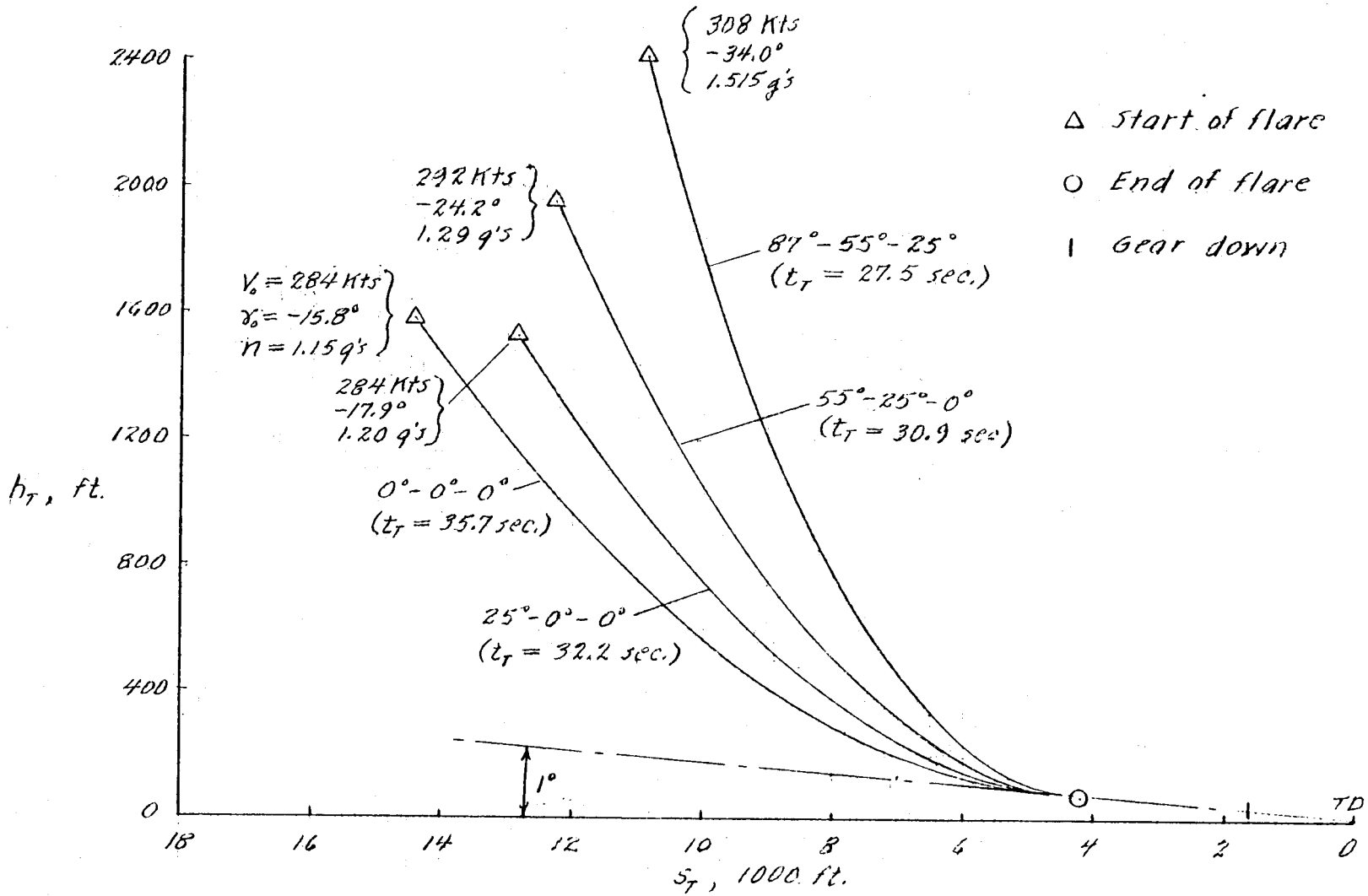

(b) Trajectory comparison

Figure 34. Concluded.

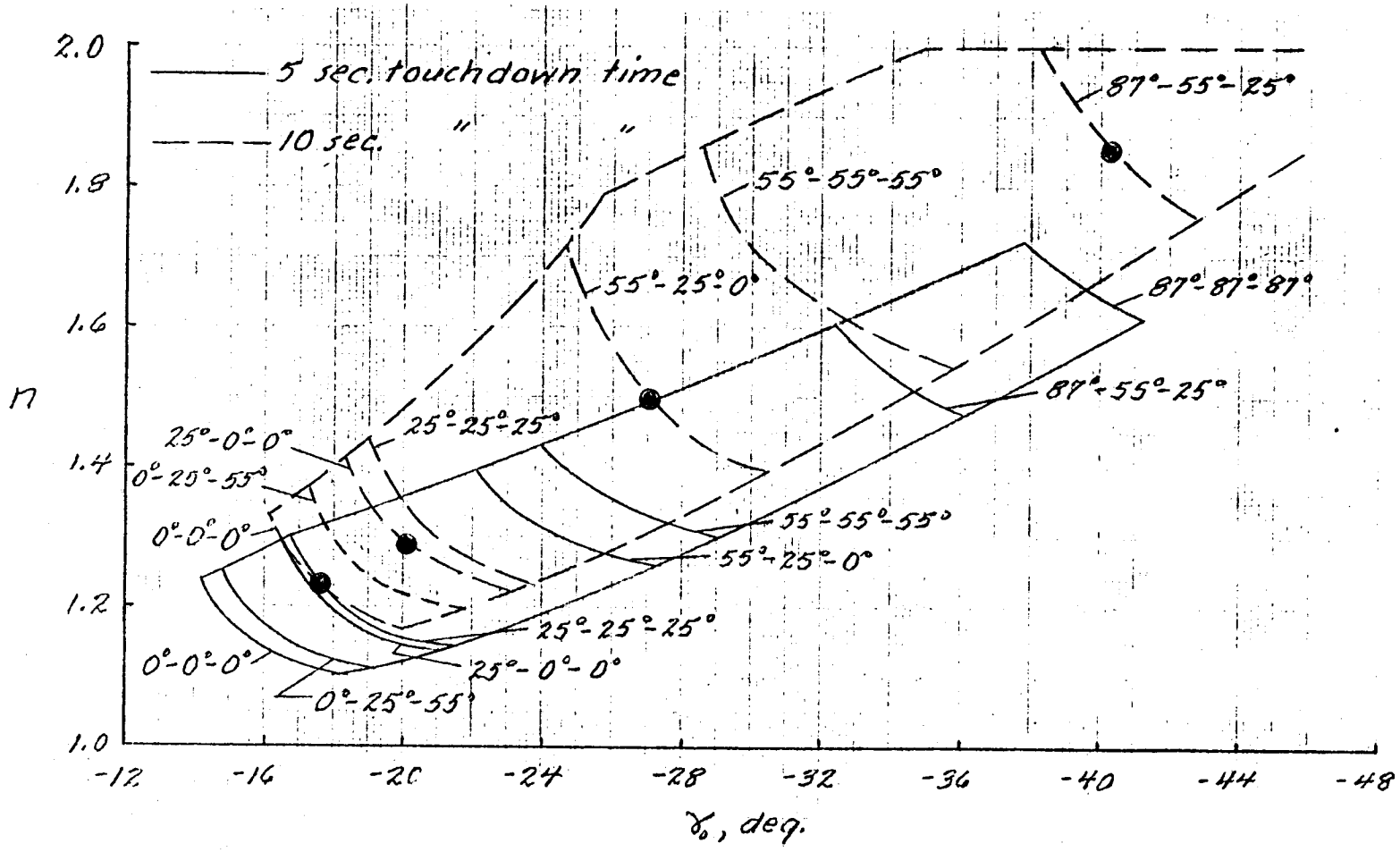

(a) Boundary points.

Figure 35. Effect of configuration changes on the landing trajectories at midpoints of the 10-second boundary for $W/S = 70.6$ psf.

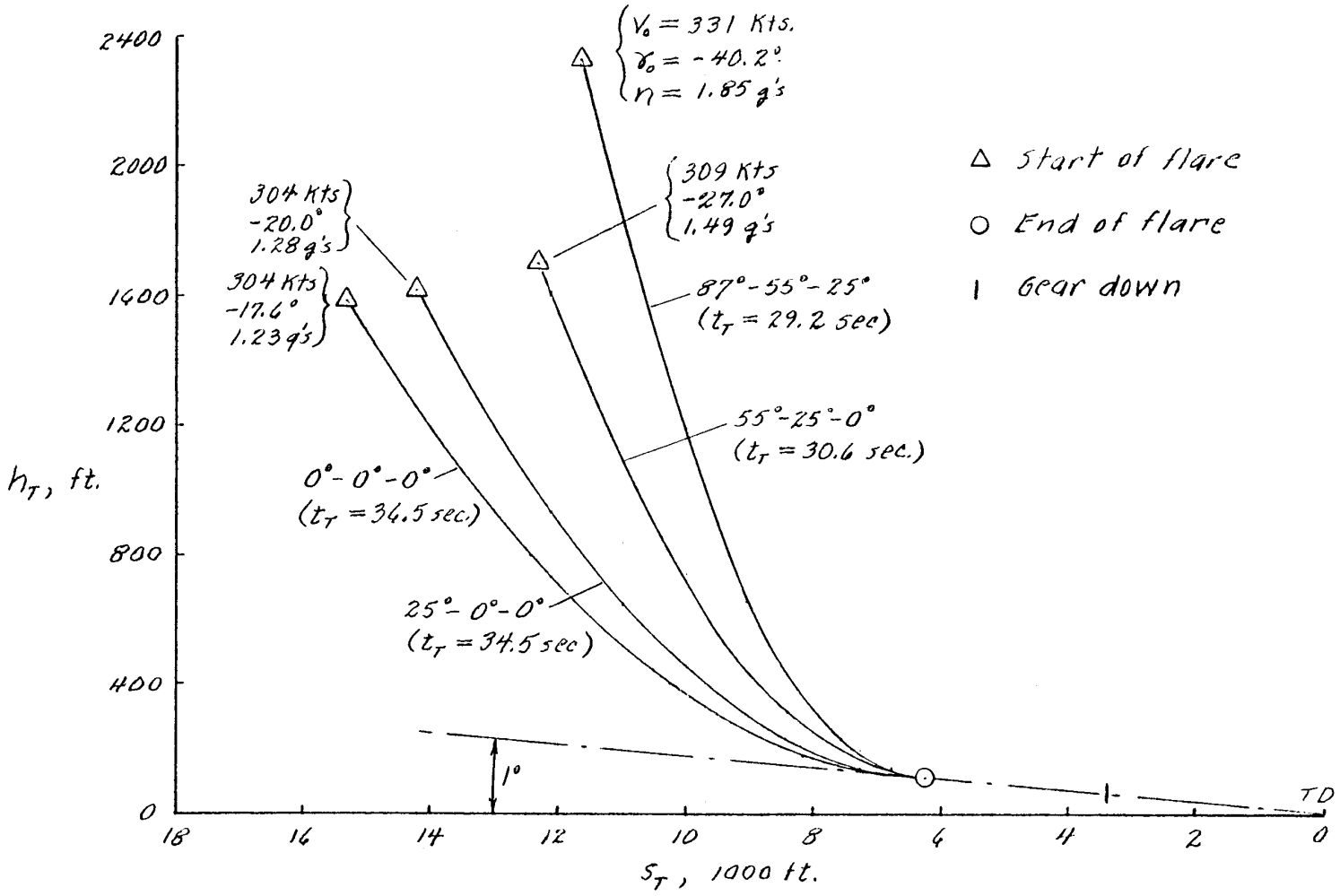

(b) Trajectory comparison

Figure 35. Concluded.

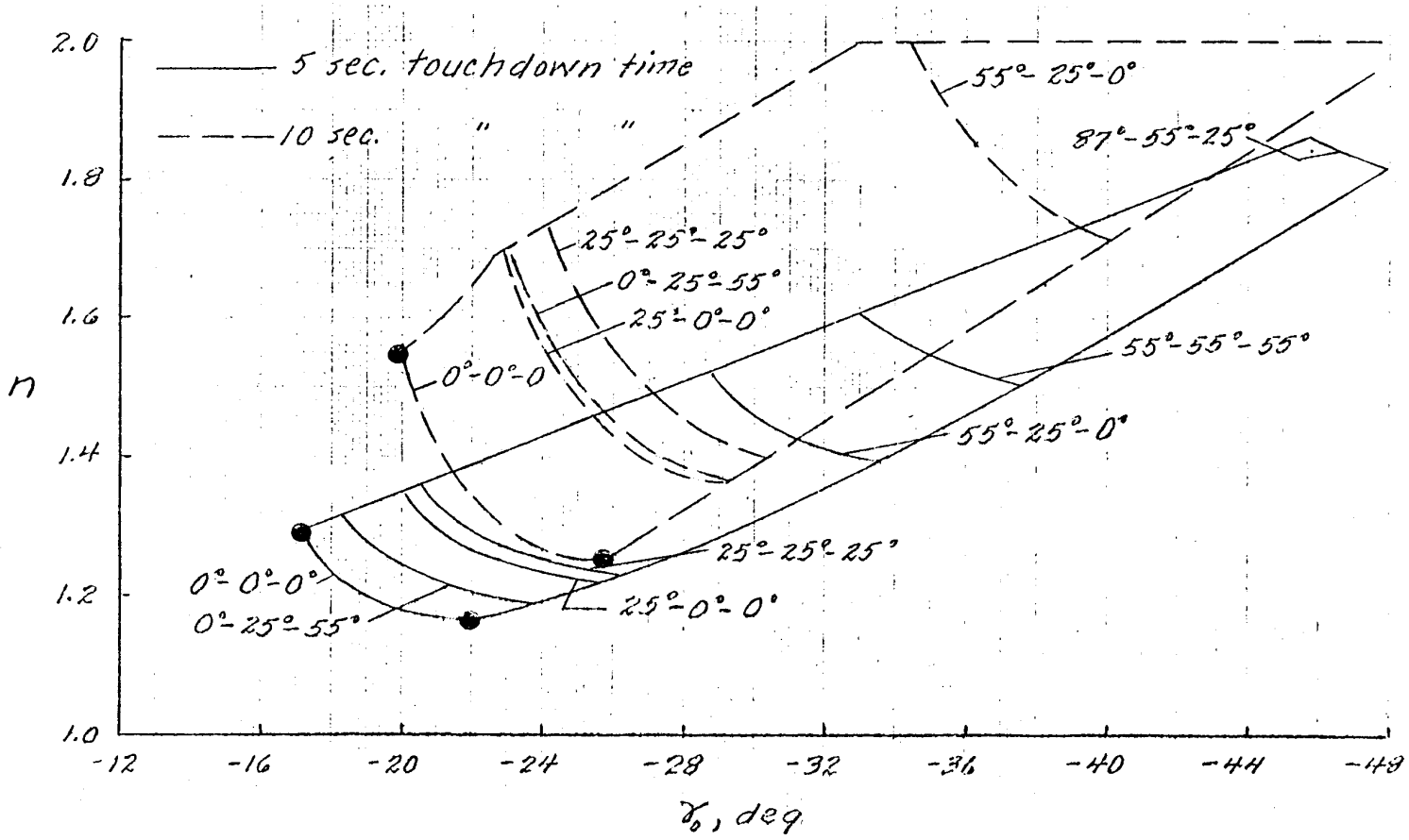

(a) Boundary points.

Figure 36. Range of landing trajectories for 0°-0°-0° configuration and touchdown maneuver times of 5 and 10 seconds. $W/S = 56$ psf.

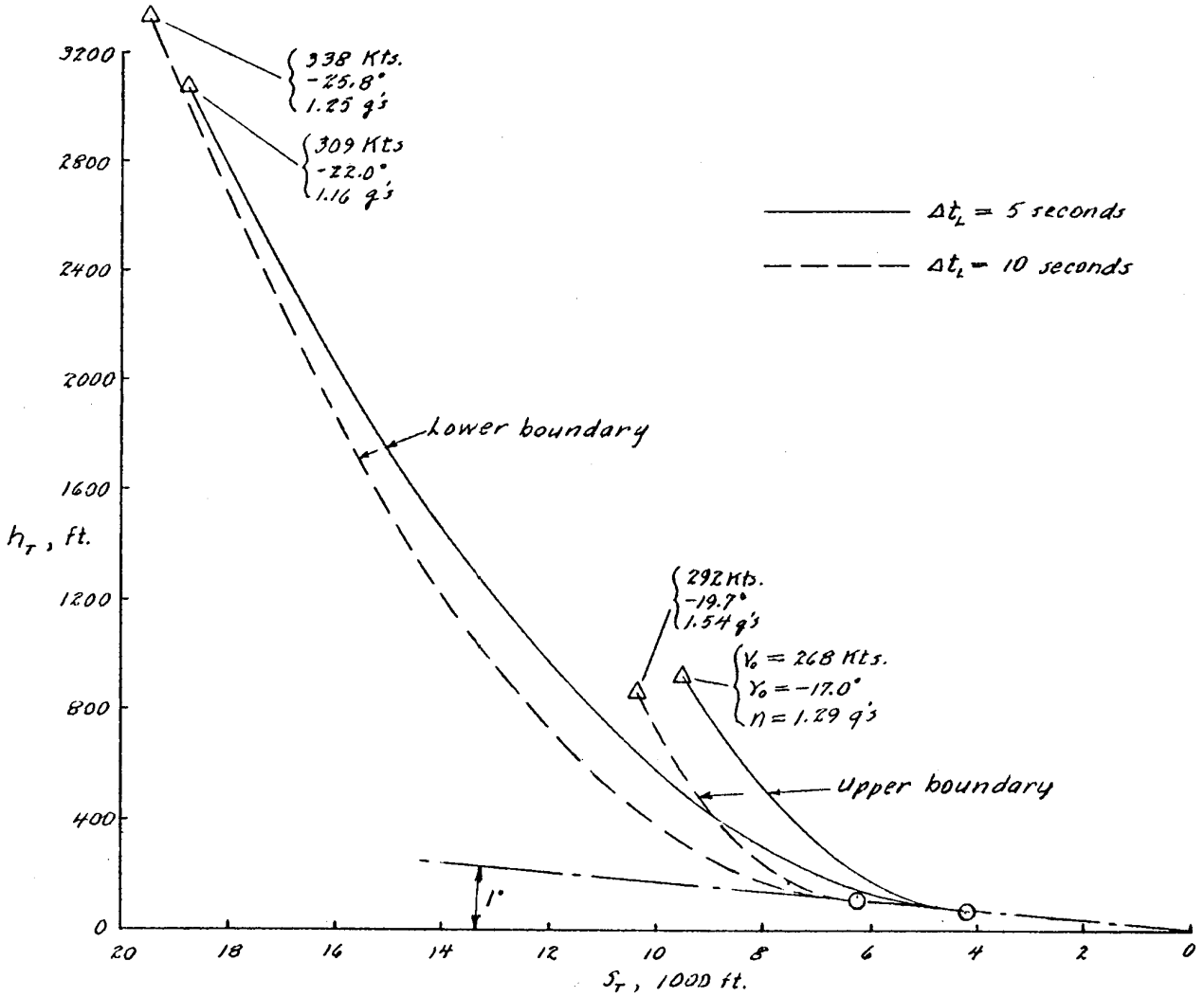

(b) Limit trajectories

Figure 36. Concluded.

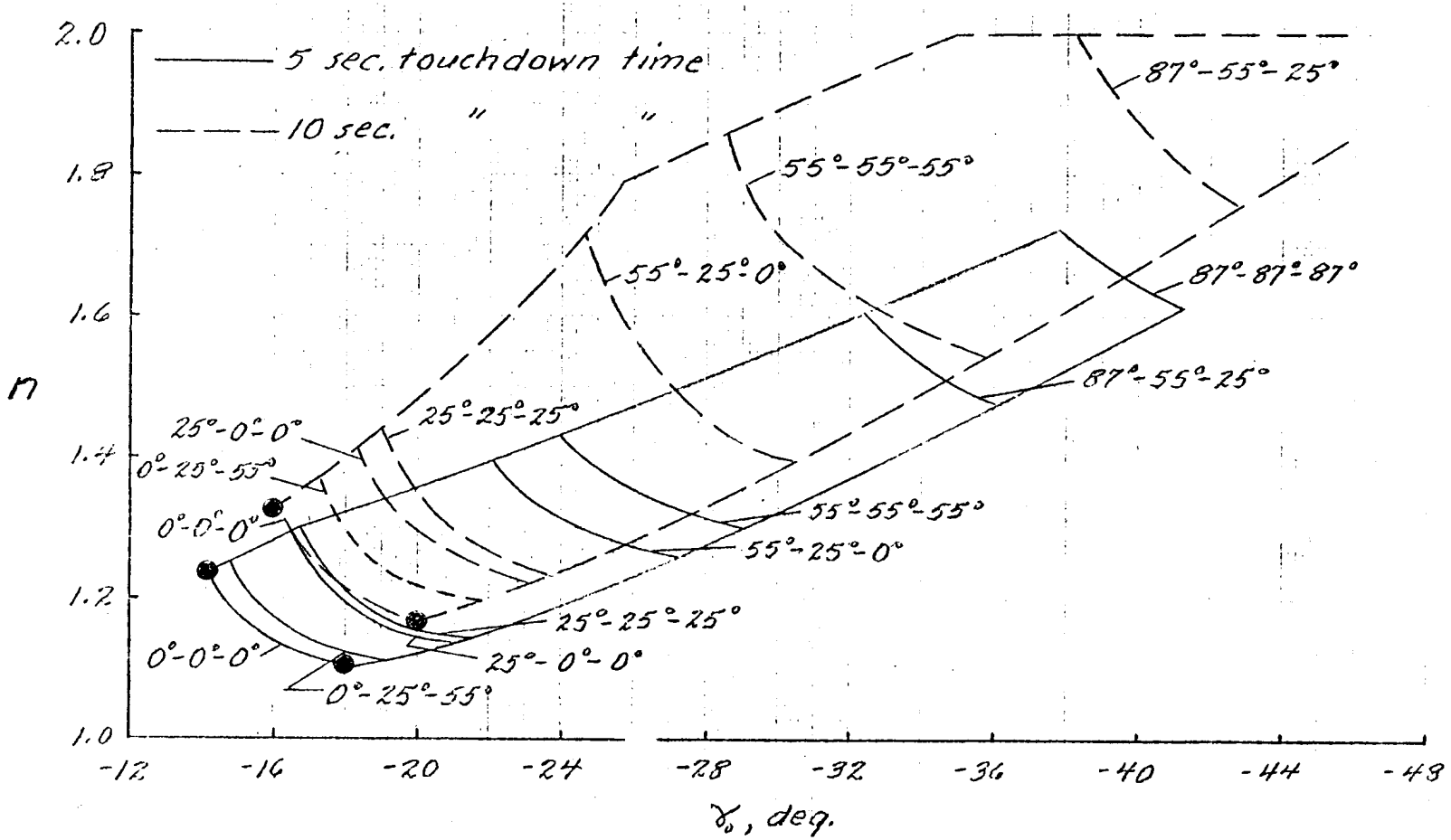

(a) Boundary points

Figure 37. Range of landing trajectories for the 0°-0°-0° configuration and touchdown maneuver times of 5 and 10 seconds. W/S = 70.6 psf.

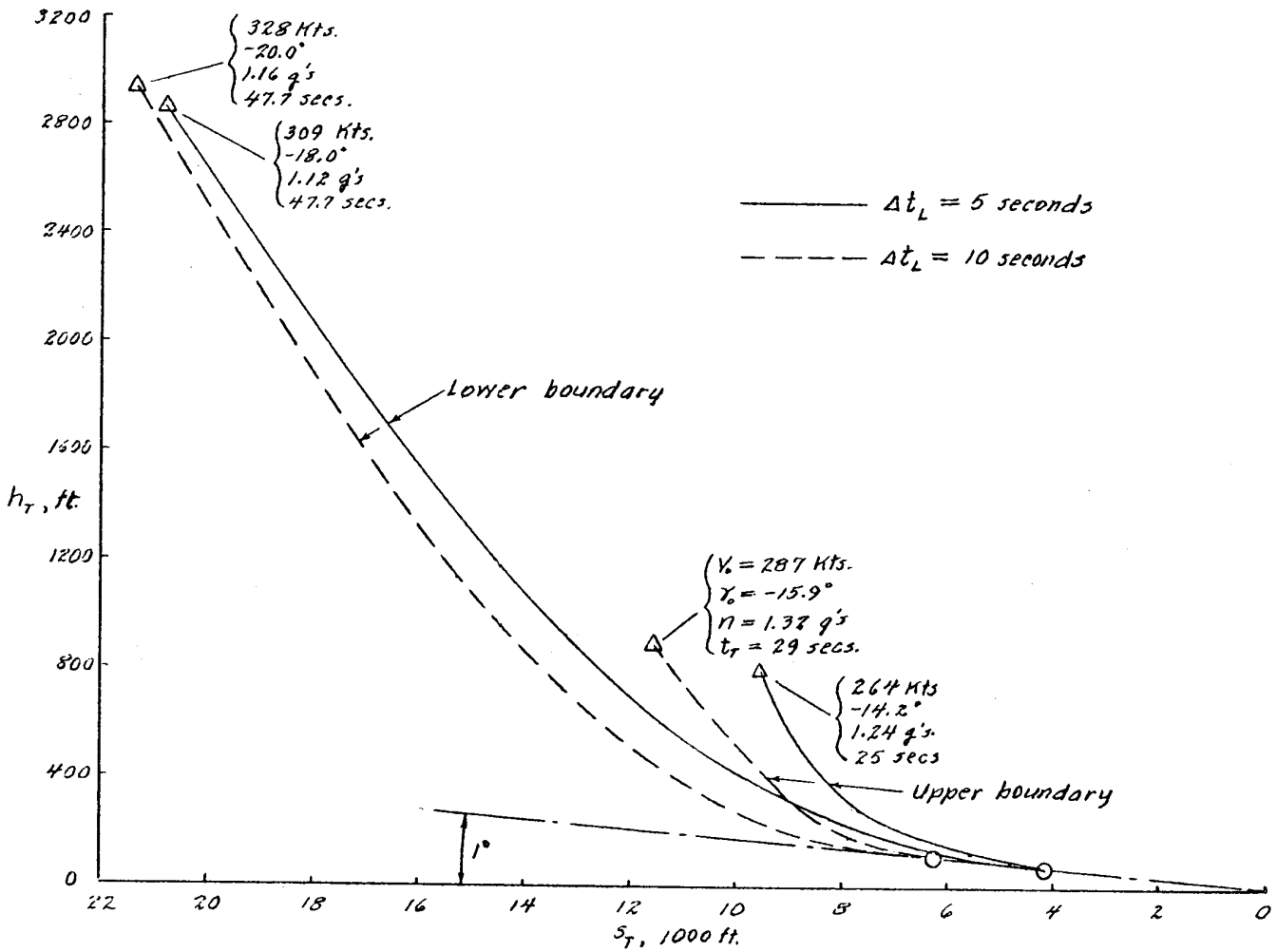

(b) Limit trajectories

Figure 37. Concluded.

1. Report No.	2. Government Accession No.	3. Recipient's Catalog No.
NASA TM-81365		

4. Title and Subtitle	5. Report Date
ANALYTIC STUDY OF ORBITER LANDING PROFILES	September 1981
	6. Performing Organization Code
7. Author(s)	8. Performing Organization Report No.
Harold J. Walker	H-1160
	10. Work Unit No.
9. Performing Organization Name and Address	
NASA Dryden Flight Research Center P.O. Box 273 Edwards, alifornia 93523	11. Contract or Grant No.
	13. Type of Report and Period Covered
12. Sponsoring Agency Name and Address	Technical Memorandum
National Aeronautics and Space Administration Washington, D.C. 20546	14. Sponsoring Agency Code

15. Supplementary Notes

16. Abstract

A broad survey of possible orbiter landing configurations was made with specific goals of defining boundaries for the landing task. The results suggest that the center of the corridors between marginal and routine represents a more or less optimal preflare condition for regular operations. Various constraints used to define the boundaries are based largely on qualitative judgments from earlier flight experience with the X-15 and lifting body research aircraft. The study results should serve as useful background for expanding and validating landing simulation programs.

The analytic approach offers a particular advantage in identifying trends due to the systematic variation of factors such as vehicle weight, load factor, approach speed, and aim point. Limitations of this study, such as a constant load factor during the flare and using a fixed gear deployment time interval, can be removed by increasing the flexibility of the computer program. This analytic definition of landing profiles of the orbiter may suggest additional studies, including more configurations or more comparisons of landing profiles within and beyond the corridor boundaries.

17. Key Words (Suggested by Author(s))	18. Distribution Statement
Low L/D power-off landings Shuttle orbiter Landing criteria	Unclassified-Unlimited STAR category 01

19. Security Classif. (of this report)	20. Security Classif. (of this page)	21. No. of Pages	22. Price*
Unclassified	Unclassified	115	A06

*For sale by the National Technical Information Service, Springfield, Virginia 22161